Spring 1998

Field Emission and Breakdown Processes in Vacuum Gaps with SiO(X)-Coated Cathodes

Raymond Jack Allen III
Old Dominion University

FIELD EMISSION AND BREAKDOWN PROCESSES IN VACUUM GAPS WITH SiO$_x$ COATED CATHODES

by

Raymond Jack Allen III
B.S.E.E. May 1992, Old Dominion University
M.S.E.E. May 1994, Old Dominion University

A Dissertation submitted to the Faculty of
Old Dominion University in Partial Fulfillment of the
Requirement for the Degree of

DOCTOR OF PHILOSOPHY

ELECTRICAL ENGINEERING

OLD DOMINION UNIVERSITY
May, 1998

Approved by: Γ_Λ ,

_____
Karl H. Schoenbach (Director)

_____
Hani E. Elsayed-Ali (Member)

_____
Gary E. Copeland (Member)

_____
Ravindra P. Joshi (Member)

ABSTRACT

FIELD EMISSION AND BREAKDOWN PROCESSES IN VACUUM GAPS WITH SiO$_X$ COATED CATHODES

Raymond Jack Allen III
Old Dominion University, 1998
Director: Dr. Karl H. Schoenbach

Field emission of electrons is the major cause of electrical breakdown in high voltage systems in vacuum. The highest hold-off electric field of the carefully polished and cleaned stainless steel cathodes was increased to 70MV/m. Thin silicon monoxide, SiO$_X$, cathode coatings reduced field emission and increased the hold-off field further. Coating the stainless steel cathodes with 2μm SiO$_X$ reduced the field emission current by at least two orders of magnitude at field of 50MV/m and increased the breakdown field to 140MV/m, doubling the breakdown voltage.

The increase in hold-off voltage with SiO$_X$ coatings is discussed in terms of electron transport within the coating. Measurements indicate that current in SiO$_X$ at high fields is controlled by Frenkel-Poole electron emission from deep centers located about 1eV below the conduction band. Field emission current is limited at the coating-vacuum interface due to an accumulation of filled electron traps. A figure of merit, γ, for SiO$_X$ cathode coatings is given by

$$\gamma = \frac{V_b(coated)}{V_b(uncoated)} = \frac{\beta_m \mathrm{E}_{C\,coating}}{\beta_c \mathrm{E}_{C\,metal}}$$

Based on this model the characteristics of an ideal cathode coating are described.

ACKNOWLEDGEMENTS

I would like to thank Dr. Karl H. Schoenbach for his guidance and support over the last seven years as well as for chairing my Ph.D. committee. I would also like to thank Dr. Hani E. Elsayed-Ali, Dr. Gary E. Copeland, and Dr. Ravindra P. Joshi for serving on my committee and for their valuable advice. I am indebted to Dr. Peter Kneisel for sharing his knowledge of field emission as well as the use of his facilities at Jefferson Lab. And, I would also like to thank Mike Adams for his help operating the SEM. Finally, I would like to thank Anja Müller for her support in completing this work.

TABLE OF CONTENTS

Page

LIST OF TABLES

LIST OF FIGURES

CHAPTER I

INTRODUCTION

Field emission is the limiting cause of electrical breakdown in high voltage (DC, AC, RF or pulsed) systems at high vacuum. Electrical breakdown between components at different potentials is defined as a transition into a self-sustained discharge where the current is limited only by the external circuit. The outcome is a visible arc and a sudden loss of the insulating properties of vacuum. The focus of this research is increasing the breakdown voltage of DC systems utilizing thin insulating cathode coatings. Since this involves reducing field emission, the research extends into RF, AC and pulsed fields as well.

Field emission and breakdown in vacuum with uncoated electrodes are described in the introduction. Previous research into electrode coatings is described in the second chapter. The possible benefits from cathode coatings are discussed in the third chapter. In Chapter IV the properties of our cathode coating material, silicon monoxide or SiO_x, and our deposition technique are discussed. The experimental setup and techniques used for measuring field emission current and breakdown voltage in vacuum are discussed in Chapter V. The results of experimental studies on cathodes with and without SiO_x coatings are presented in Chapter VI. Measurements of electron transport in SiO_x are presented in Chapter VII. In Chapter VIII the results from both the field emission measurements into vacuum and the electron transport measurements with SiO_x

---

The journal model of *Journal of Applied Physics* was used.

are discussed and a model for field emission from insulating coatings is presented. The dissertation concludes with a summary in Chapter IX.

The Paschen Law

In the pressure times gap spacing range of 10^{-3} to 10^3 torr·cm the DC breakdown voltage can generally be determined from the Paschen Law. A calculated Paschen curve in air with a gap of 0.1mm is shown in Fig. 1. The Paschen curve for this gap has a minimum at 125 torr. The Paschen Law, however, is undefined when the pressure drops below a certain value (47 torr in the above example). At higher vacuum there are few ionizing collisions within the electrode spacing, therefore, the electrodes instead of the gas are the primary source of charged particles. The sources of particles (charged and neutral) in a vacuum gap are illustrated in Fig. 2. Electrons are generated at the cathode by thermionic emission, field emission, and photoemission. Electrons, ions, and neutrals are created by ion bombardment of the cathode and electron bombardment of the anode. Electrons and ions are created in the gap by electron impact ionization.

Most of the charge generating effects depicted in Fig. 2 can be neglected in properly designed vacuum gaps. Thermionic emission is generally negligible from unheated metal electrodes. Photoemission is removed by operating in a dark chamber. Electron impact ionization and the subsequent ion bombardment of the cathode are negligible when operating in high vacuum where the mean free path for ionization is several times the electrode spacing.
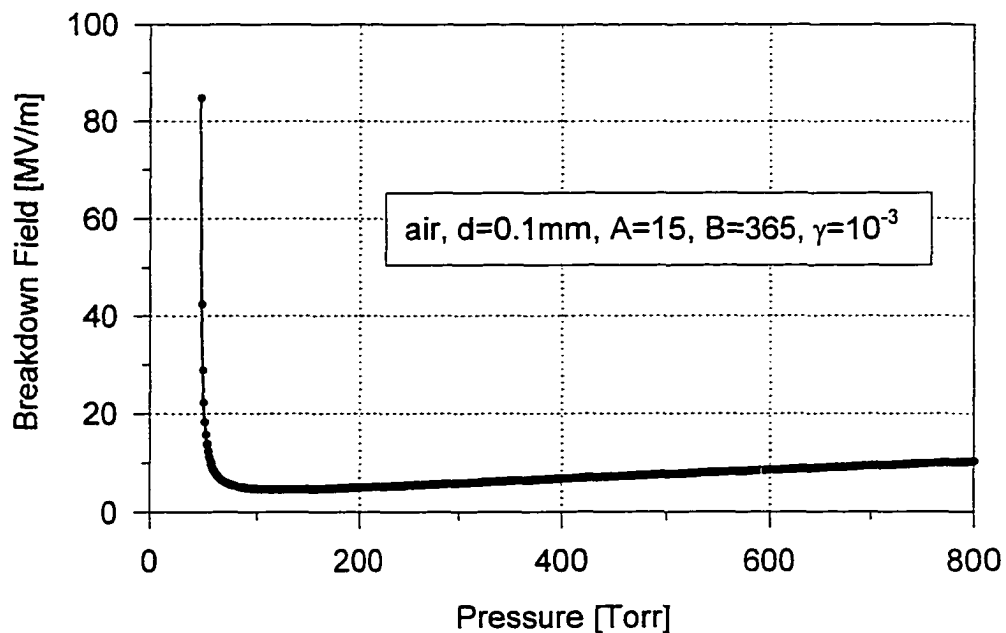
Figure 1. Calculated Paschen curve in air (d=0.1mm).
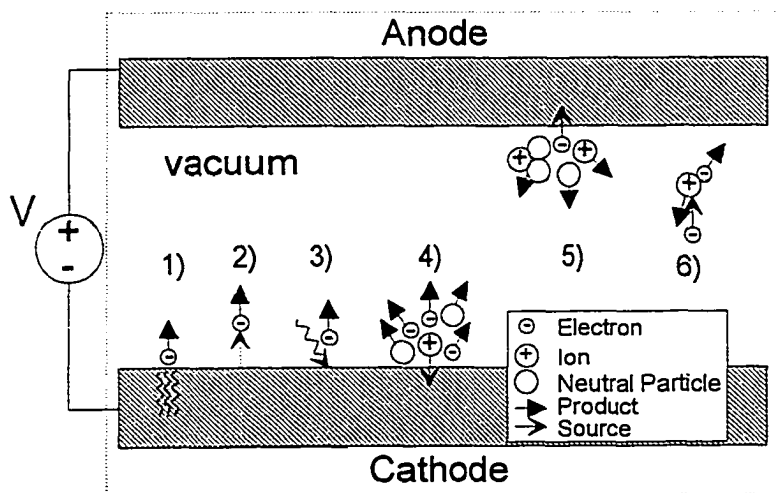
Figure 2. Sources of current in high vacuum: thermionic emission (1), field emission (2), photoemission (3), ion bombardment of the cathode (4), electron bombardment of the anode (5), and electron impact ionization (6).

The one electron source that is most difficult to control is field emission. Field emission is the primary failure mechanism of high voltage vacuum gaps. When high voltages are used the field emitted electrons strike the anode with high

energy and electron bombardment of the anode releases particles which add to the current.

General High Vacuum Breakdown Process

Breakdown in high vacuum gaps results from elevated field emission from the cathode. In systems with larger electrode spacing there are also anode interactions. Consequently, there are two regimes in high vacuum breakdown; the field controlled regime with gap spacing less than about 1mm and breakdown voltages usually less than about 200kV, and the voltage or electron energy controlled regime with gaps greater than 1mm and breakdown voltages greater than 200kV. The breakdown process in each regime is outlined in Fig.3.

Field Controlled, V_b<200kV, Small Gap, d <1mm	Voltage Controlled, V_b>200kV, Large Gap, d >1mm
E-Field applied	E-Field applied
Field emission	Field emission
Joule heating of cathode	Electron bombardment of anode
Evaporation of cathode	Particle bombardment of cathode
Ionization of metal vapor	Ionization of metal vapor
Vacuum arc / Breakdown	Vacuum Arc / Breakdown
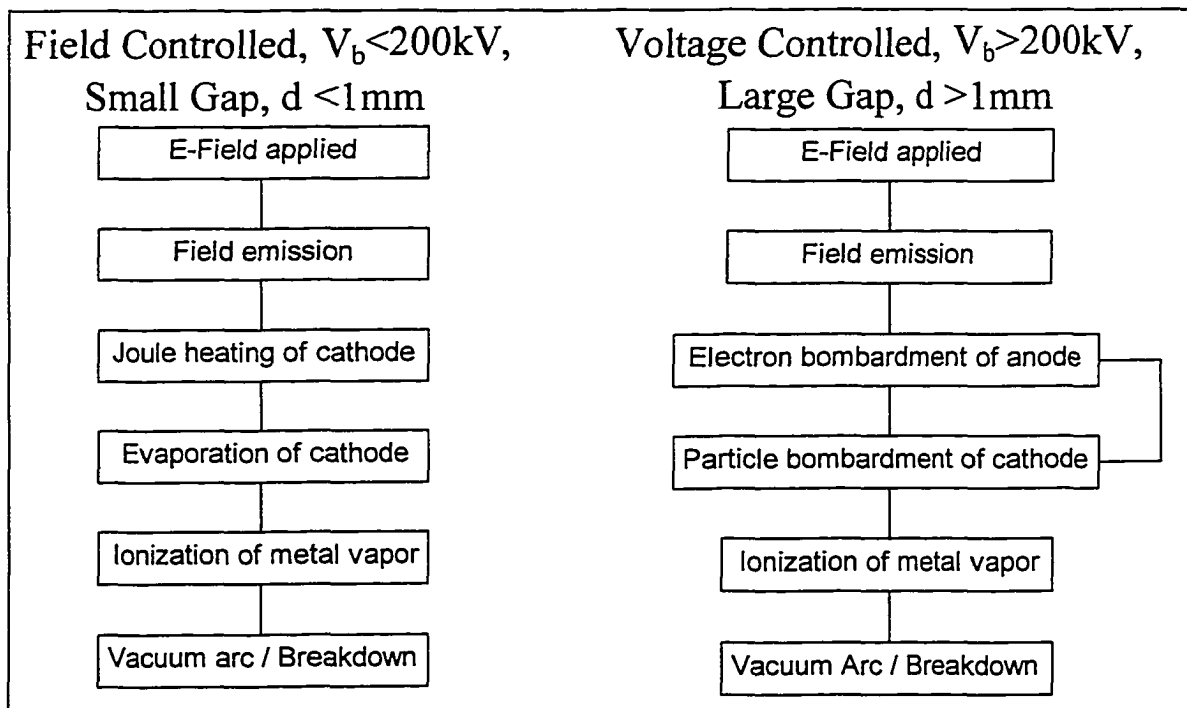
Figure 3. General breakdown process in field controlled gaps (left) and voltage controlled gaps (right).

In field controlled systems breakdown is initiated at the cathode. Field emission is known to evolve from a few, high field enhancement sites distributed over the cathode. Because these sites are very small, the current density at each site can be high. Joule heating, due to the current, raises the temperature of these sites. As the applied voltage is increased the emission site will eventually vaporize sending metal vapor into the gap. Calculations by Dyke[1] show that most metals vaporize when the current density reaches about 10^{12} A/m^2. This metal vapor becomes ionized and a gas discharge develops. This gas discharge is often called a *vacuum arc*, which is misleading because an arc is generally considered a high pressure phenomenon. However, during breakdown the local pressure is suddenly increased due to the metal vapor emission so the discharge is actually at high pressure. The breakdown voltage in this regime is independent of anode material. Breakdown in short gaps is *field* controlled because the breakdown field is independent of gap distance.

In voltage controlled gaps the breakdown field is reduced due to anode interactions. As with small gaps under electric stress, large numbers of electrons are emitted from small points on the cathode. Electrons from the cathode follow the electric field lines to a point on the anode where they deposit energy proportional to the gap voltage. This energy causes ion and neutral generation from the anode. These ions strike the cathode liberating many secondary electrons and causing a feedback effect. In these larger gaps, therefore, breakdown begins at the anode instead of the cathode. Davies and Biondi[2] showed this by monitoring the radiation from the discharge. Using an anode and

cathode of different materials they found that the discharge begins with radiation from atoms of the anode material.

There are various, subtlety different, views on how exactly the ionized anode material is generated. Anderson[3] assumes that the anode surface releases ions due to electron impact. Davies and Biondi's[4] model is based on the assumption that the electrons knock larger neutral particles loose from the anode. The large particles are vaporized and ionized in the gap leading to breakdown. Slivkov[5] suggested that the electron beam evaporates the anode surface and the vapor is then ionized.

In any case, the result of the anode interaction is that the breakdown voltage for large gaps no longer increases linearly with gap distance. For voltage controlled gaps the breakdown voltage is approximately constant, which has been called the "total voltage" effect. Breakdown in this regime could also be called *energy controlled* because it is the energy of the charged particles, determined by gap voltage, which determines breakdown. The actual dependence of breakdown voltage on gap distance has been measured to be approximately to the square root of gap distance or $V_b \propto d^m$ where m has values from 0.4 to 0.7.[6]

With pulsed voltages and large gaps the behavior depends on the pulse width.[7,8,9] For short pulses breakdown is initiated by the cathode with behavior similar to that of short gap systems. This behavior may be due to the finite "time of flight" of charged particles across the gap or the finite time required to deposit

energy into the anode such that vapor and ion emission occurs. With long pulses the behavior is similar to the DC voltage case.

Field Emission

All of the described breakdown scenarios have a common starting point in field emission. Field emission is defined as "the emission of electrons from the surface of a condensed phase into another phase, usually a vacuum, under the action of high electrostatic fields."[10] Field emission is easy to describe by considering the current between two metal electrodes in a vacuum as depicted in Fig. 4. When a voltage is applied between the electrodes, electrons emitted by the negative electrode, or cathode, will be accelerated towards the positive electrode, or anode, constituting a current. In a perfect vacuum, i.e., without ionization, electron emission from the cathode is the only contribution to the current. Field emission is one mechanism whereby electrons are emitted from the cathode, but there are several others including thermionic emission, photoemission and secondary electron emission. However, the current due to these other processes is for the most part independent of the applied electric field, whereas field emission, as the name implies, is strongly dependent on the applied field.

R.W. Wood made the earliest report describing field emission in 1897.[11] J.E. Lilienfeld[12] and W.D. Coolidge[13] continued studies of the phenomenon in the 1920's in the context of x-ray tube development.
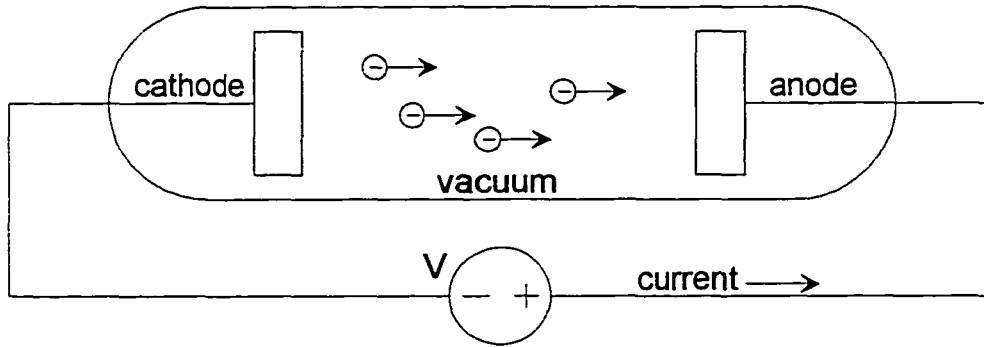
Figure 4. Depiction of electron emission from a metal cathode in vacuum.

Field emission is based on a quantum mechanical effect, the tunneling of electrons from the cathode into vacuum. R. Fowler and L. Nordheim first laid the theoretical foundations for field emission in 1928.[14] They developed the analytical expression for the field emission current density, J, known as the *Fowler-Nordheim equation* which can be written

$$J = \frac{1.541 \cdot 10^{-2}\, \mathcal{E}^2}{\Phi t^2(y)} \exp\left[\frac{-6.831 \cdot 10^9\, \Phi^{3/2} v(y)}{\mathcal{E}}\right] \qquad [\text{A/m}^2]$$

[1]

$$y = \frac{3.795 \cdot 10^{-3}\sqrt{\mathcal{E}}}{\Phi}$$

where Φ is the work function of the cathode, $\mathcal{E}$ is the electric field, and the functions $v(y)$ and $t(y)$ are due to the image force. A derivation of the Fowler-Nordheim equation is included in Appendix A. Tabulated values for $v(y)$ and $t(y)$ can also be found in the appendix. Note that $v(y)$ and $t(y)$ are often replaced with the constant value of one for simplification.

Field Enhancement

While experimental measurements followed the trend in eqn. (1) the absolute values did not agree at first.[15] For example, the field emission current

calculated for stainless steel is shown in Fig. 5 along with current levels for thermionic emission (independent of applied field). Measurements, however, while following the trend in Fig. 5, have electric field values ~100 times less than predicted. Also, field emission is found to occur primarily from a few isolated points on the surface. This caused some doubt in the validity of Fowler-Nordheim theory. The Fowler-Nordheim theory was, however, proven correct when properly adapted to include the effects of *field enhancement*.

Field enhancement occurs in almost all practical applications. Field enhancement is due to localized imperfections on the electrodes, where the electric field can be much larger than that calculated by dividing applied voltage by electrode spacing. There are two basic types of field enhancement; geometric and microscopic.
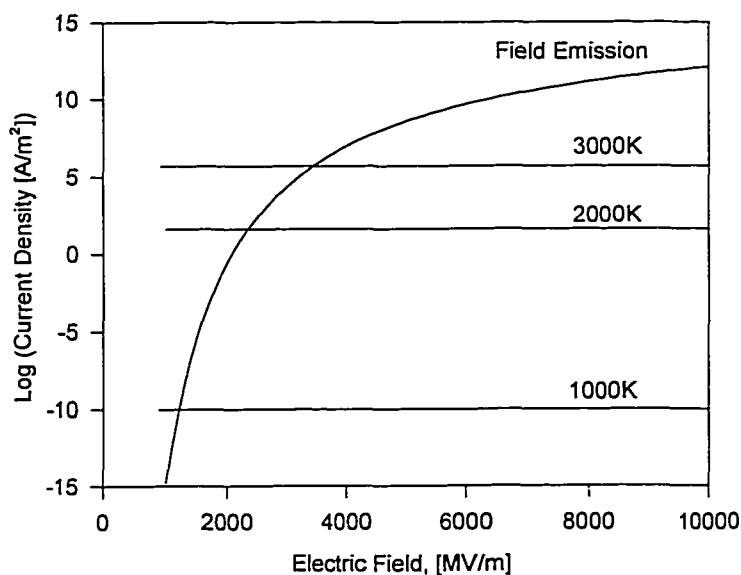
Figure 5. Field emission and thermionic emission from stainless steel (without field enhancement).

Geometric field enhancement is due to the gross shape of the electrodes. The relative increase in electric field is called the field enhancement factor, β_g, where the subscript refers to the geometry. Macroscopic tips and sharp edges generate electric fields that far exceed the average electric field.

The second type of field enhancement is microscopic field enhancement. Microscopic field enhancement occurs on all broad area electrodes even those polished to mirror-like finishes. Contributing to the microscopic field enhancement factor, β_u, are protrusions, inclusions, and contamination. Using a scanning electron microscope Little and Whitney[16] took pictures of protrusions on stainless steel and aluminum surfaces. Although these protrusions extend less than 5µm from the surface they were estimated to produce values of β_u of about 100.

More recent studies tend to point toward inclusions and contamination as the major source of field enhancement.[17,18,19] Inclusions are pieces of foreign material embedded into the surface. Inclusions are often the result of polishing when small pieces of the abrasive adhere to the metal surface. Contamination is foreign particles that come to rest on the surface of the metal. Particles of contamination can be loosely bonded to the surface due to van der Waals forces.

Geometric and microscopic field enhancement factors multiply to give the overall field enhancement factor

$$\beta = \beta_g \beta_u$$

Values of β for high voltage electrodes are usually found to vary between 50 and 500 depending of shape, polishing, cleaning, etc.

It was not until the invention of the field emission microscope by E.W. Müller[20] in 1937 that the Fowler-Nordheim equation was proven correct. With the field emission microscope the emission from the rounded tip of a thin wire is studied. The well defined, approximately hemispherical, shape of the tip can be viewed with an SEM to determine the radius of curvature from which the value of β can be determined with some precision. The heated tip is enclosed in an evacuated glass sphere with a phosphor screen. By measuring the current from the tip excellent correspondence with theory was found when β was included in the Fowler-Nordheim equation now given by

$$J = \frac{1.541 \cdot 10^{-2} (\beta\varepsilon)^2}{\Phi t^2(y')} \exp\left[\frac{-6.831 \cdot 10^9 \Phi^{3/2} v(y')}{\beta\varepsilon}\right] \qquad [\text{A/m}^2]$$

$$y' = \frac{3.795 \cdot 10^{-3} \sqrt{\beta\varepsilon}}{\Phi}$$

(2)

Due to the hemispherical shape of the emitter and the anode screen, the microscopic emission sites are greatly magnified on the screen and are visible due to the phosphor. In fact, the contributions to the current from individual atoms on the tip were made visible. This was the first device to provide images of individual atoms.

The Rogowski Profile

One of the simplest ways to reduce β and thereby increase the breakdown voltage is by shaping of the electrodes. Sharp edges result in high

values of geometric field enhancement, β_g. Curved electrodes often result in β_g ranging from 2 to 5. This is often acceptable for many applications. There are, however, special shapes which give zero field enhancement, i.e., β_g =1. One such shape is the Rogowski profile. A Rogowski profile electrode takes the form of a constant potential surface between two parallel plates.[21] Details about the Rogowski profile are given in Appendix B.
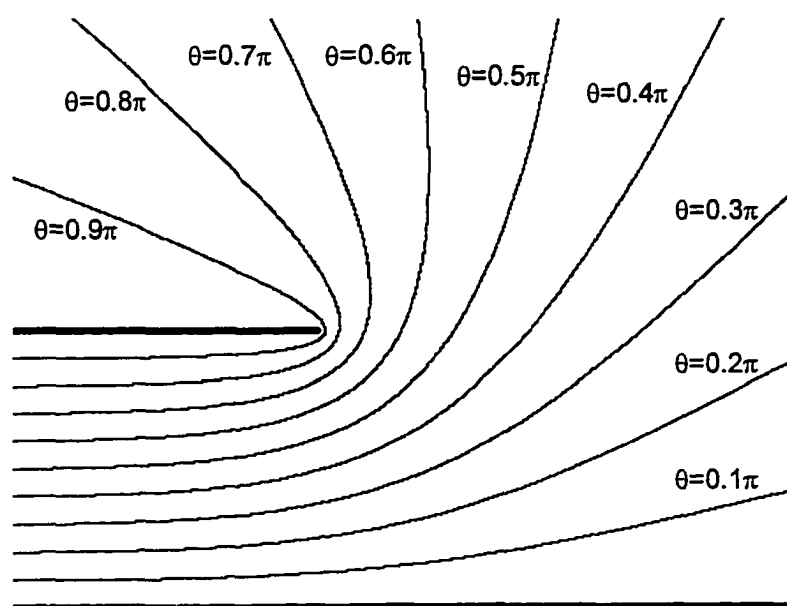
Figure 6. Equipotential lines at the edge of a plate above a ground plane.

From Fig. 6 we see that for $\theta > 0.5\pi$ there is a narrowing of the line spacing near the edge of the plate. Since the electric field is proportional to the distance between the equipotential lines there is field enhancement near the plate's edge. However, for $\theta \leq 0.5\pi$ the distance between equipotential lines increases monotonously. Therefore, the electric field is nowhere greater than in the center

of the plate. For a Rogowski profile electrode we simply construct electrodes with edges like that in Fig. 6 with $\theta \leq 0.5\pi$.

Fowler-Nordheim Plots

The prebreakdown current in vacuum gaps follows the Fowler-Nordheim equation when modified to include the effect of field enhancement. By measuring the prebreakdown current it is possible from eqn. (2) to determine the field enhancement factor for a cathode. The field enhancement factor is a good indicator of the quality of a cathode surface and can be used to predict the breakdown voltage. Note that with a large area cathode there are likely to be several emission sites contributing to the total current with an effective field enhancement factor, $\overline{\beta}$. The Fowler-Nordheim equation can then be rewritten in terms of the total current, I, and applied voltage, V, as

$$I = \frac{1.541 \cdot 10^{-2} \overline{A}(\overline{\beta}V)^2}{\Phi d^2} \exp\left[\frac{-6.831 \cdot 10^9 d\Phi^{3/2}}{\overline{\beta}V}\right] \qquad [\text{A}]$$

where $\overline{A}$ is the effective area of the combined emitting sites and d is the gap distance. The functions t(y) and v(y) resulting from the image force are ignored (set to unity) in eqn. 2 to ease calculation, the error being only a few percent.[22] Taking the logarithm base 10 we write

$$\log_{10}\left(\frac{I}{V^2}\right) = -\log_{10}\left(\frac{\Phi d^2}{1.541 \cdot 10^{-2} \overline{A}\overline{\beta}^2}\right) - \frac{6.831 \cdot 10^9 d\Phi^{3/2}}{\ln(10)\overline{\beta}V} \qquad [\text{A}] \qquad (3)$$

From eqn. (3) we see that plots of $\log_{10}\left(\frac{I}{V^2}\right)$ versus $\left(\frac{1}{V}\right)$ will form a straight line with a constant slope given by

$$slope = -\frac{6.831 \cdot 10^9 \, d\Phi^{3/2}}{\ln(10)\overline{\beta}} \tag{4}$$

Such plots are called Fowler-Nordheim plots. In practice excellent correspondence can be obtained and Fowler-Nordheim plots form straight lines over several orders of magnitude of current. A typical result is shown in Fig. 7 from which using eqn. (4) and knowledge of the work function, Φ, the field enhancement factor, $\overline{\beta}$, can be determined. The work function for most materials is well known through thermionic emission and photoemission measurements. The typical value of $\overline{\beta}$ ranges from about 150 to 500 for broad area electrodes (without extraordinary polishing and cleaning procedures).[23] There is often some deviation from theory observed at high current that has been attributed to either thermal or space charge effects.[24] The effective emitter area can be determined from the y-intercept of the Fowler-Nordheim plot given by

$$10^{-(y-intercept)} = \frac{\Phi d^2}{1.541 \cdot 10^{-2} \overline{A}\overline{\beta}^2} \tag{5}$$
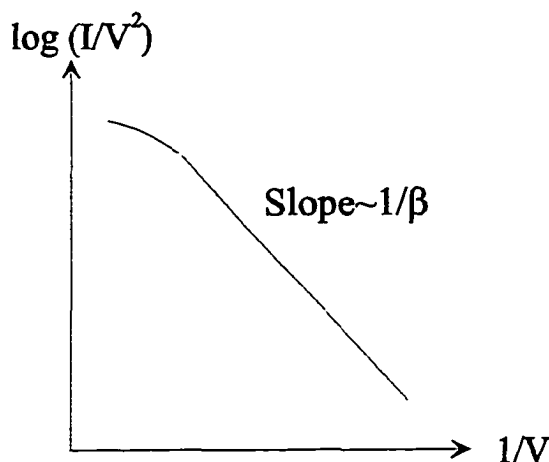
Figure 7. A typical Fowler-Nordheim plot from which the field enhancement factor can be determined from the slope.

Electrode Material

Nearly all common metals have been tested under high electrical stress in vacuum. For short gaps the cathode material determines the breakdown voltage and breakdown occurs when the critical field, E_C, is reached. The value of the critical field can be measured experimentally by measuring the breakdown voltage, V_b. The value of β, however, must be taken into account. β can be determined through the Fowler-Nordheim plot. We then have

$$E_C = \frac{\beta V_b}{d} \tag{6}$$

Values of E_C for several metals were collected by Lafferty[25] and are listed in Table 1. Note, however, that the value of β and hence E_C depends on the value for Φ used. (Lafferty indicates that the field value for Ni may be too high.) One material not listed in Table 1 is aluminum, which has a peculiar behavior. Although aluminum has a notably high Φ, it was found to be a poor electrode because under stress particles are torn from the electrodes initiating breakdown at relatively low fields.[26]

Table 1. Critical field values and assumed work functions for common metals

Metal	E_C [10^9 V/m]	Assumed Φ (eV)
Chromium	5.32 ± 0.1	4.6
Molybdenum	5.4 ± 1.0	4.37
Stainless Steel	5.9 ± 1.4	4.4
Gold	6.36 ± 0.63	4.8
Tungsten	6.5 ± 1	4.5
Copper	6.9 ± 1.0	4.5
Nickel	10.4 ± 1.3	4.6

For large gaps the anode material also determines the breakdown voltage. Rosanova and Granovskii made an extensive study comparing anode materials.[27] The breakdown voltage of several common anode materials was measured with a fixed cathode material and gap spacing in the range from 0.25 to 2.0mm. Their breakdown experiments were performed in sealed glass tubes with a spherical cathode above a flat anode. The breakdown voltage was considered that voltage that produced 10 discharges every minute. The order of increasing breakdown voltage for anode material was found to be C(graphite), Al, Cu, Fe and Ni, Mo, then W. This order corresponds to arranging the metals by their Young's modulus. The conclusion is that the breakdown strength increases with the mechanical strength of the anode material where the mechanical strength is given by the Young's modulus.

Conditioning

By "conditioning" one refers to any method, prior to application of high voltage, which reduces field emission and improves the dielectric strength of a vacuum gap. There are several types of conditioning including heat treatment, ion etching, acid etching, ultra-pure water rinsing, and electrical conditioning.[28] The types of conditioning employed depend on the application. Heat treatment involves simply heating up to cathode sometimes to 900°C to remove emitting sites. Ion etching is commonly performed by adding ~1 torr of argon or hydrogen to the chamber and starting a DC glow discharge with ~100 volts applied to the cathode with a current density ~1mA/cm^2. This has the effect of sputtering away high β spots. In RF cavities acid treatments and ultra-pure water rinsing have

been found effective at reducing field emission.[29] Electrical conditioning is perhaps the most effective and widely used type of conditioning.

The goal of electrical conditioning is to remove the worst of the field emission sites through controlled breakdown. At high fields, field enhanced tips vaporize which usually initiates a full breakdown causing damage to the electrodes. If, however, a large resistor is used to limit the current, the damage is controlled. Gruszka and Musicka-Grzesiak[30] studied conditioning of several types of metals with varying degrees of polishing. They found that there is an ideal conditioning current that is a function of both the material and the surface roughness. They also found that lower currents work better for rougher surfaces and that rougher surfaces show the greatest improvement after conditioning. There is a wide variety of conditioning currents and times found in the literature. Most values of current seem to be in the μA range for a time of about 15 minutes. Conditioning is generally required to obtain a reproducible current-voltage relationship and breakdown voltage. The beneficial effects of electrical conditioning, however, have a limited lifetime which may last anywhere from a few hours to months.

During conditioning some interesting effects can be observed when measuring the current. When applying voltage to "virgin" cathodes Latham[31] observed that the initial current is very low, $<10^{-12}$ A. Then at a certain voltage there will be sudden "activation" or "turn-on" and the current will rise several orders of magnitude. At this point if the voltage is varied the current follows the Fowler-Nordheim equation. When the voltage is raised further at some point

there will likely be another activation event and the current will again suddenly rise. Again the current follows Fowler-Nordheim but with a different β value. The typical sequence is shown in Fig. 8. Latham gives no explanation for this effect.

log I
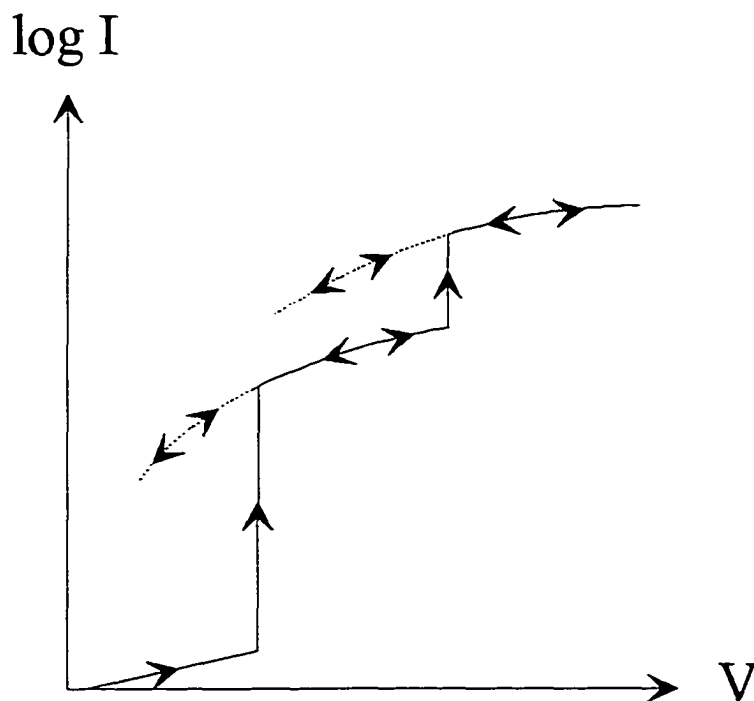
Figure 8. Typical current-voltage characteristics of a "virgin" cathode.

Residual Gas Effects

Residual gas in the vacuum chamber will affect the breakdown voltage. At high pressures Paschen breakdown will occur. Below this point there are two major effects to consider; modification of the work function of the metal by absorbed gas and sputtering of the metal surface. There is some question about the influence of these effects on breakdown when the surface is well conditioned. Hackam and Salman[32] measured the breakdown voltage for stainless steel gaps of 0.76, 0.50, and 0.30mm over the hydrogen pressure

range from $3 \cdot 10^{-9}$ to 10^{-2} torr and observed a near constant breakdown field. The effect of Paschen breakdown is seen only in the larger gap at the highest pressures where the breakdown voltage drops rapidly with increasing pressure.

Although Hackam and Salman observed little residual gas effects in their experiment with hydrogen, others have found that the type of residual gas and level of conditioning are important. Bloomer and Cox[33] found that adding oxygen to their system with a field applied increased the breakdown voltage while adding argon had no effect. Since the ionization cross section and sputtering properties of argon and oxygen are similar they concluded that an increase in the work function of the molybdenum electrodes by 1.7eV due to oxygen chemisorption was responsible.

At higher pressures the level of conditioning may also determine the effect of residual gas. With non-conditioned stainless steel electrodes with various gap lengths Cooke[34] measured a sixfold increase in the breakdown voltage with nitrogen pressures in the millitorr range compared to the breakdown voltage at 10^{-4} torr. The effect, which was reduced for partially conditioned electrodes, was attributed to ion bombardment and sputtering of emitter sites.

Emission Site Microprobes

Many recent studies use microscopic probes to localize the individual emission sites on the cathode. One goal of this technique is to determine the exact nature of the emission process. Two techniques have been used; the first uses an anode with a small hole, and the second uses a needle-like anode.[35] In the first system the anode hole is scanned over the cathode.[36] When an

emission site is crossed, electrons pass through the hole and are collected to register as a current. In this way the cathode emitters can be localized and the I-V characteristics of individual emitters can be measured. Similarly, in the second system the needle anode is scanned over the surface of the cathode and emission sites are detected directly as anode-cathode current.[37] Both of these systems incorporated a SEM with x-ray detector to image and analyze the emitter. The anode hole type system can also be used with an electron energy spectrometer to measure the energy content of emitted electrons.

Results from these experiments show that the emitters are usually inclusions or cracks at grain boundaries rather than microprotrusions as earlier thought. The inclusions were either insulating or conducting but insulated from the cathode. They also determined that carbon placed on the surface is a strong emitter and hypothesize than carbon, known to exist at grain boundaries, could be responsible for the large emission observed from grain boundaries.

Other studies using the needle-like anode configuration have demonstrated that high fields can be obtained with little or no emission through advanced cleaning procedures.[38,39,40] Fields of up to 200MV/m scanning over a large area of Nb were obtained with little field emission. Two techniques were used; UHV heat treatment and ultrapure water rinsing. Heating the samples to 1400°C for 30 min. in vacuum followed by a fast cool down was found very effective in removing field enhancing sites. Heating to only 400°C was found to create emission sites. Ultrapure water rinsing was also investigated was for applications where heat treatment is impractical. It was found that a high

pressure, ultrapure water rinse followed by an N_2 blow dry was also effective at removing field enhancing sites. The emitters were found to be either micron sized foreign particles, scratches, or pits.

Hot-Electron Model

Based on the observation that emission sites can usually be associated with dielectric inclusions rather than metallic protrusions, Latham and his coworkers proposed the "hot-electron model". According to this model there is a switch-on transition when the applied field is large enough for electrons to tunnel from the metal into the dielectric inclusion. At this point there is a conducting channel formed in the dielectric. The field in the conducting channel is low, however, there is a high field region at the dielectric-vacuum interface resulting from field penetration. It is in the high field region where the hot electrons gain kinetic energy. These electrons are then emitted either over or through the potential barrier into vacuum. The hot-electron model is supported by electron energy spectra from retarding potential measurements of the emission.

CHAPTER II

THE EFFECT OF ELECTRODE COATINGS ON BREAKDOWN IN VACUUM:
PREVIOUS RESEARCH

There are many ways of reducing field emission and increasing the hold-off voltage in vacuum gaps. Most of these are collectively called conditioning and usually involve removing field-enhanced imperfections on the electrode surface. Conventional conditioning, however, has limited effectiveness, can take a long time, and the surface has been found to degrade over time. Another method of reducing field emission and increasing the breakdown voltage utilizes thin electrode coatings. Several studies have been made in the last thirty years on a variety of electrode and coating materials. Insulating, conducting, and semiconducting conducting coatings have all been used with varying degrees of success. Most of the research described in this chapter involves DC fields although some work with AC and RF fields is discussed.

Insulating Coatings

Jedynak[41] published the first comprehensive study of electrode coatings, one that is often cited in the literature, in 1964. Using aluminum and stainless steel electrodes Jedynak measured the pre-breakdown current and breakdown voltage of nine types of insulating coatings. Some of them, such as epoxies and tapes, are not compatible with modern UHV systems either because they outgas or because they cannot be baked. Jedynak found that a few of the cathode

coatings suppressed field emission sometimes by 2 to 4 orders of magnitude and increased breakdown strength up to 70%.

The system used by Jedynak was a cylindrical aluminum chamber enclosing opposing electrodes with 15cm diameter and a Rogowski profile. A diffusion pump was used to generate a vacuum of $\sim 1\cdot 10^{-6}$ torr. The high voltage source was a 500kV Van de Graaff generator with a maximum current of 35μA. The general experimental technique was to raise the voltage in 10kV steps every five minutes until a spark occurred. After a spark the voltage was kept constant until sparking subsided for five minutes before again raising the voltage. The experiment ended when the voltage could no longer be raised (defining the breakdown voltage). Small gap currents were measured with a current integrator circuit with $2\cdot 10^{-10}$ A resolution.

The cathode coatings that showed an improvement over bare electrodes were MgF$_2$ (2.5, 3.5, 10 and 18μm thickness), epoxy (25 and 130μm), silicon monoxide (3μm), Mylar tape (2.5μm), Formvar (2μm) and titanium dioxide (130μm). Coatings with a negative effect on breakdown voltage were cerium oxide, iron oxide, and tin oxide. A few anode films were tested with and without a coated cathode and in all cases the anode film proved detrimental to performance. Of all the cathode films, the best performers were MgF$_2$, epoxy, and silicon monoxide.

With the MgF$_2$ coating there was little improvement in the breakdown voltage compared to uncoated electrodes, however, there was a 2 to 4 order of magnitude decrease in pre-breakdown current. No dependence on film

thickness was observed with the 3.5, 10, and 18μm films. By varying the gap distance from 1 to 5mm the breakdown voltage was found to increase steadily with the gap.

The highest breakdown voltages were achieved with epoxy coatings. With a thick epoxy coating (130μm) and a 5mm gap a final voltage 340kV with an average current of 10^{-9}A was achieved after over 100 sparks. This is a great improvement over his results with uncoated aluminum electrodes with 6.3mm gap giving a breakdown voltage of 220kV and an average current of 10^{-5}A after several sparks. Thinner epoxy coatings (25μm) allowed him to reach 300kV without a single spark and then he achieved 340kV after several sparks.

The breakdown voltage of a gap with a silicon monoxide coated cathode reached 260kV after a few sparks in a 5mm gap with an average current $<10^{-9}$ A. Jedynak found the peak voltage to be well defined because an increase in voltage causes a violent but nondestructive spark. By varying the gap distance the breakdown voltage only increased by 25% in the range from 3mm to 8mm. The resistivity of the silicon monoxide film was measured to be $5 \cdot 10^{13} \Omega \cdot \text{cm}$.

Jedynak attributed the reduction in field emission current to a smaller density of electrons in the insulator compared to that in metal, although the potential barriers are similar. He assumed that breakdown was caused by field enhancing sites either at the insulator surface or at the insulator-metal interface. In his discussion Jedynak stated his criteria for a good cathode film as follows:

- resistivity>$10^{11}\Omega$·cm
- dielectric constant from 1.5 to 4
- dielectric strength > 10^6 V/cm
- film thickness 10 to 25μm
- hard and smooth w/ high abrasion resistance and adhesion strength
- no gas bubbles (or bubbles much smaller than film thickness)
- low vapor pressure and moisture absorption
- chemically resistant to water and solvents
- cathode surface should be a mirror polish

Jedynak and Towliati[42] later followed up this work with a similar experiment using an epoxy-coated cathode with thickness of 30-35μm. They found the pre-breakdown currents to range from 10^{-10} to 10^{-8} A. By varying the gap from 1 to 5mm they observed a linear increase in breakdown voltage, similar to the earlier work with MgF_2. Thus, the breakdown voltage is not limited by the total voltage effect as found in earlier studies with bare electrodes.[43] The breakdown voltage of epoxy coated cathodes increased with gap distance at a rate of 64kV/mm, which is much higher than the 36kV/mm measured with MgF_2. Taking the dielectric constants into account, the fields inside the films are similar with 213kV/cm for epoxy and 180kV/cm for MgF_2. At those fields a field enhancement of only about five is required to exceed the insulation strength of the film. They believed that breakdown is initiated by the field-enhancing site on the cathode, which exceeds the dielectric strength of the film thereby initiating a full breakdown. The required field magnification is easily possible for mechanically polished electrodes.

In 1986 Latham and Mousa[44] studied the electron emission from the tip of a thin tungsten wire coated with epoxy. The purpose of their study was to support the "hot-electron" model, described in Chapter I, and to investigate

coated tips as field emitters for electron guns. The 0.1mm wire was prepared in a similar way as the tips of the field emission microscope, i.e., etched in NaOH for a final tip radius of ~30nm. The hemispherical shape of the tip was verified with TEM so that the field enhancement can be calculated exactly. Dipping in epoxy then coated the tip. Each dip produced a layer ~0.04μm thick. Using multiple dips the final thickness was varied from 0.04 to 0.20μm. The results show a "switching process" occurring at relatively low fields, 10-20MV/m, where the current increases rapidly. Interestingly, the current then saturates and remains constant until the breakdown voltage, which was about twice the saturation voltage. A comparison of coated and uncoated results is shown in Fig. 9. The initial current from the coated tip (up to about half of the saturation current) also follows Fowler-Nordheim. Comparing coated and uncoated tips on a Fowler-Nordeim plot, the slope of the coated tip is ¼ that of the uncoated tip as shown in Fig. 10. Comparing tips with varying coating thickness, they found that both the saturation voltage and current are relatively independent of epoxy thickness with values of 1·10^9 V/m and 5μA.
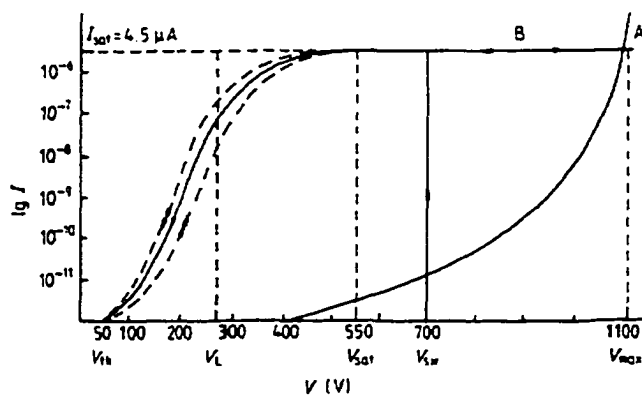
Figure 9. Comparison of emission from an uncoated W tip (curve A) and a 150nm epoxy coated tip (curve B) (reproduced with permission from R.V. Latham).
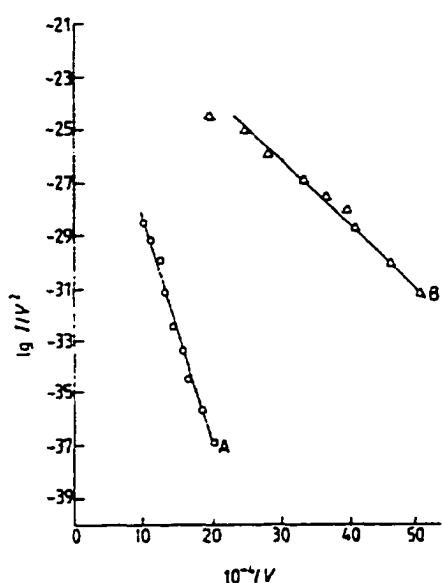
Figure 10. Fowler-Nordheim plots of the emission from an uncoated W tip (line A) and the initial current from a 150nm epoxy coated tip (line B). The slope of line B (coated) is ~1/4 as steep as that of line A (uncoated) (reproduced with permission from R.V. Latham).

Semiconducting Coatings

Both a CaF_2 insulating coating and a silicon semiconducting coating were tested by Smith.[45,46] The cathodes substrates were 50mm diameter stainless steel disks polished to a mirror-like finish. The anode was a 1cm stainless steel sphere. Electrode spacing was varied from 200 to 400μm and measured with a microscope with crosshairs. The films were deposited on only half of the cathode. With the anode off-center from the cathode, the cathode is rotated so that several spots on the cathode can be tested.

The CaF_2 and Si films were deposited by molecular-beam epitaxy. The thickness of the CaF_2 films was 0.2 and 0.4μm and the thickness of the Si films was 0.45 and 1.1μm, measured using surface profilometry. High voltage measurements were made at a vacuum of 10^{-9} torr. The breakdown voltage for

uncoated stainless steel was found to be ~50MV/m. With the CaF$_2$ coating the breakdown voltage increased by 50% to 75 to 85MV/m. Si coating only gave a slight improvement of 15%. Pre-breakdown currents were reduced by 6 orders of magnitude at 0.5MV/cm with the 0.4μm CaF$_2$ coating. There was less reduction with the 0.2μm CaF$_2$ coating compared to the 0.4μm coating, which is attributed to incomplete trapping since the electron path through the film is shorter. The 1.1μm Si coating reduced pre-breakdown currents by 2 to 3 orders of magnitude with less effect from the 0.45μm coating.

Smith also made some other interesting observations. After arcing the beneficial effects of the coating were gone. Also, the virgin cathode pre-breakdown current stayed below 10^{-12} A up to 2/3 of the breakdown voltage at which time there was a microbreakdown with the currents rising to from 10^{-8} to 10^{-6} A. After the microbreakdown reproducible I-V curves were measured.

The slopes in Fowler-Nordheim plots of the pre-breakdown current stayed constant with coating especially for the Si coating suggesting a constant value of β. From this Smith formulated an emission model considering the reduction in the electric field at the metal proportional to the dielectric constant and the transmission probability through the dielectric-vacuum barrier. He writes

$$ I = I'D(\Phi, \mathcal{E}) = 1.54 \cdot 10^6 A \left(\frac{\beta \mathcal{E}}{\varepsilon_r} \right)^2 \frac{1}{\Phi_{B1}} \exp\left[-\frac{68.3}{\beta \mathcal{E}} \left(\varepsilon_r \Phi_{B1}^{3/2} + \Phi_{B2}^{3/2} \right) \right] \quad \text{[A]} $$

where A is the emitter area in cm^2, Φ_{B1} and Φ_{B2} are the barriers at the metal-dielectric interface and dielectric-vacuum interfaces respectively, and ε_r is the dielectric constant. Smith uses the electron affinity, χ, of the dielectric for Φ_{B2}.

The value of $\Phi_{B1}=\Phi_m-\chi$ is the difference between the work function of the metal and the electron affinity. Using this model Smith found excellent agreement between theory and experiment. Based on this a criteria for improved coatings is a large ε_r and an χ on the order of or less than ½ of Φ_m.

Conductive Coating

Conductive coatings have also been demonstrated to reduce field emission. Ping He and Sinha[47] measured the pre-breakdown currents from Mo coated Mo cathodes. Mo films of 10, 30, 100 and 300Å were sputter deposited on high polished Mo substrates at a rate of from 37.5 to 60Å/min. The current-voltage was then measured with a 1.0mm gap. The pre-breakdown current was reduced in some cases by factors from 55 to 3000. From Fowler-Nordheim plots a reduction in both β and the effective area was observed. Poor performance was found with the 300μm coating, which is believed to be due to stresses in the film which increase with film thickness. It was assumed that the improvement is due to the increased smoothness of the cathode surface.

Insulating Coatings with Alternating Voltage

With low frequency AC voltages similar behavior to DC is expected. Of course, both electrodes have to be coated since both are cathodes for a half cycle while the other electrode is the anode. Anode coating are expected to give poor results (see Jedynak ref. [11] for example), however, an improvement with coated aluminum electrodes was measured by Opydo, Grzybowski and Kuffel[48] with low frequency (50Hz) AC voltage. Both electrodes were made of aluminum tested with and without Al_2O_3 coatings. The Al_2O_3 coatings were

created by electrolytic oxidation of the aluminum electrodes in a 10% NaOH solution. One possible problem with Al_2O_3 films grown in this way is the formation of many pores in the surface, which can lead to electron multiplication. This problem was partially solved in this experiment by coating with a silicon-based varnish with a 3-5μm thickness. The breakdown voltage with gap spacing of 3 and 5mm was measured with film thickness from 6 to 37μm. The electrodes were conditioned at a current 0.5μA. The breakdown voltage was increased for all coatings except for the thinnest 6-9μm films. The best improvement was with films of from 12 to 16μm thick. Comparing the breakdown voltage with and without this coating, the 3mm gap V_b increased from 91.0 to 132.2KV$_{peak}$ and with the 5mm gap V_b increased from 133.1 to 174.2KV$_{peak}$. The reason for the improvement was believed to be a lowering of the electric field in the film by the dielectric constant which is ε_r=9 for Al_2O_3. Breakdown was believed to be caused by an electron avalanche at unfilled pores in the Al_2O_3 surface as diagrammed in Fig. 11.
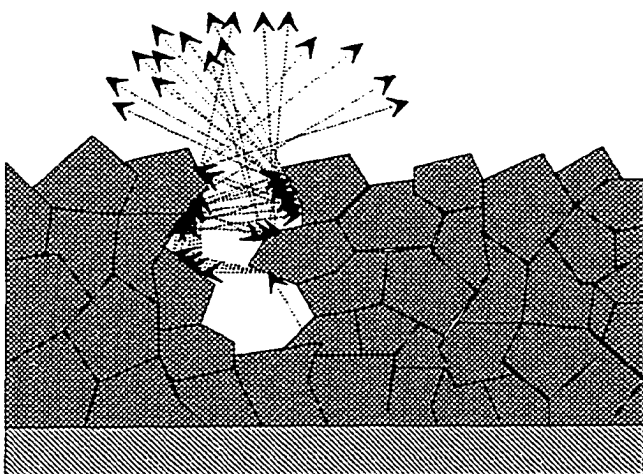
Figure 11. Schematic diagram of believed failure mechanism with Al_2O_3 coatings; electron avalanche within micropore with secondary electron coefficient>1.

Insulating Coatings for RF Cavities

Field emission has also been found to be a major problem in RF cavities. Instead of breakdown, however, the problem is loading whereby the RF energy in the cavity is absorbed by field emitted electrons from the cavity interior surface. Sayag, Viet, Bergeret and Septier[49] investigated the possibility of using insulating coatings inside superconducting RF cavities. Oxidizing the Nb substrates produced a Nb_2O_5 layer of thickness' 40, 80, and 160nm giving the dielectric layer. Oxidation was performed in a 14% NH_3 solution at a current density of $5A/m^2$. Film thickness was approximated using the empirical relationship of 2nm/V applied and verified by the visible color changes according to the Newton scale.

Although the film is to be used in RF cavities, tests of the field emission current were carried out in a DC gap with a coated cathode in a similar method to the others in this section. The electrodes were identical pure Nb with $1cm^2$ area and rounded edges. The gap used was 0.25mm set using a micrometer screw and view with a sighting tube with crosshairs. Experiments were performed at room temperature and at 4.2°K with Nb in the superconducting state in another chamber. Prior to measurements the chamber was baked at 200-250°C for 30-40 hours. Conditioning was performed by raising the voltage three to four times to a point where a current of ~1μA would flow.

Their results show a steady decrease in β with film thickness. The breakdown voltage also increased with film thickness. From the chamber designed for the liquid helium tests no change in emission was observed when

the temperature was lowered from 300°K down to 4.2°K. To test whether the coating is affected by electron bombardment the polarity of the gap was reversed for 10min, bombarding the film with 8keV electrons. Subsequent testing showed no change in behavior.

Recently, Peter[50,51] has tested several film for application in RF cavities using the same general experimental technique as Smith. The purpose of the film is to suppress multipacting. Multipacting is an electron avalanche process in RF cavities where electrons follow electric field lines back and forth inside the cavity impacting the cavity walls at either end. If the product of secondary emission coefficients at these two locations is >1 then the number of electrons can increase with each RF cycle. In the past titanium and carbon based coatings have been used to suppress secondary emission. The concept of Peter was to use insulating or semiconducting coatings to trap electrons from both field emission from field enhancing spots and secondary emitted electrons striking the film surface. Peter looked for films with a low secondary emission ratio for both electrons and ions. He suggests that a good RF cavity coating does not contaminate cathodes, is bakeable to 500°C, is radiation resistant, is mechanically stable, and does not affect the Q-factor of the cavity.

In order for the coating not to perturb the RF field requires coatings with a field diffusion time, $\tau_d <<$ ½ the cycle time of the field. For a dielectric τ_d is given by

$$\tau_d = \frac{nL}{c}$$

where n is the index of refraction, c is the speed of light, and L is the film thickness. As an example, with a frequency of 50MHz the thickness for most insulators must only be less than several meters. For conductors τ_d is given by

$$\tau_d = \frac{4\pi\sigma c^2}{L^2}$$

where $\sigma = 1/\rho$ is the conductivity. With carbon material ($\rho = 375\mu\Omega cm$) the thickness must be much less than $830\mu m$.

The experimental setup consisted of an OFHC copper cathode with a 5cm diameter and a stainless steel ball anode with a 1cm diameter. The gap was adjusted with a micrometer feedthrough to $100\mu m$ and $200\mu m$. The "zero" gap was detected by resistance (no coating) or capacitance (w/ coating) measurements. Rotation of the cathode allowed measurements on several areas of the cathode. The chamber vacuum was in the high 10^{-9} torr range. Several cathode coatings were tested including CaF_2, TiN, Si, and three proprietary coatings.

The best results were obtained with a $5\mu m$ CaF_2 coating and proprietary coating #1. Peter found eight orders of magnitude reduction in the field emission and DC breakdown strengths up to 120MV/m which is ~3 times better than bare copper. The secondary emission coefficient and radiation resistance were measured and found to be acceptable.

Coating Thickness

For most applications the thickness of the film should be such that it does not increase the electric field in the vacuum space, ξ_{vacuum}. The electric field

inside the coating, $\mathcal{E}_{coating}$, is reduced by the dielectric constant of the film, ε_r. The increased electric field in vacuum is given by

$$V = \int \mathcal{E} \cdot dl = \mathcal{E}_{vacuum}(d-t) + \mathcal{E}_{coating}(t) \quad \Rightarrow \quad \mathcal{E}_{vacuum} = \frac{V}{d - t(1 - 1/\varepsilon_r)}$$

where d is the gap spacing and t is the coating thickness as shown in Fig. 12. A thin film also reduces out-gassing, prevents stressing and cracking of the film, reduces overall cost, and lowers deposition time. Previous research described in Chapter I by Smith and by Sayag, et.al., with varying film thickness of less than 2μm indicated that the hold-off voltage increases with film thickness. Opydo, Grzybowski and Kuffel found peak effectiveness in the 12-16μm range.
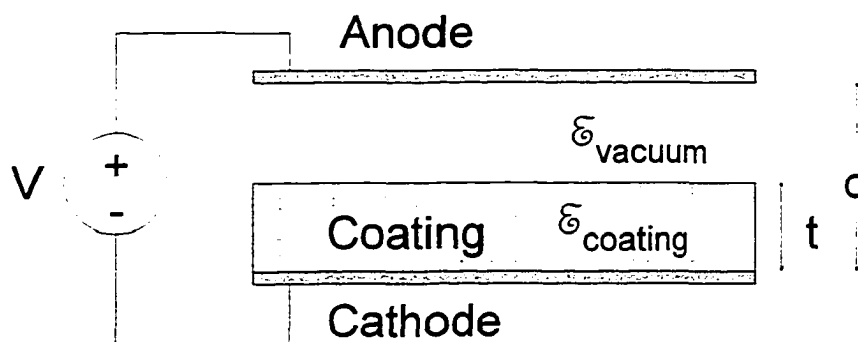
Figure 12. Effect of coating thickness on electric field.

The dielectric strength of the film is critical according to the analysis by Latham. The breakdown field for most dielectric thin films in the thickness range from nm to μm is nonlinear. There are three breakdown mechanisms possible in this range. For thick films, >10μm, electron avalanche is the usual mechanism. For thinner films, approx. 1-10μm, where the thickness is less than the mean

free path for ionization, the breakdown strength is highest, limited by thermal runaway. For very thin films, <1μm, the breakdown field is reduced by defects in the film. For our experiments we have chosen to operate with SiO_x coatings in the thickness range from 2 to 3μm where the dielectric strength is expected to be near maximum.

CHAPTER III

FIGURES OF MERIT FOR COATED ELECTRODES

When analyzing electron emission from a coated cathode there are three processes to consider: emission at the metal-coating interface, transport through the coating bulk, and emission from the coating-vacuum interface. Generally, one of these will limit emission. For what is considered here to be a "perfect" dielectric coating emission will be limited at the metal-coating interface. At the other extreme is conducting or semiconducting coatings where the emission will be limited at the coating-vacuum interface. For semi-insulating or "imperfect" dielectric coatings, the limiting interface may be the coating-vacuum interface at low current densities and then shift to either bulk transport or the metal-coating interface as the current density increases.

Figure of Merit: Metal-Coating Interface Limited Emission

We first consider electron emission with a cathode coated by a "perfect" dielectric. By "perfect" in this sense we mean one with a large bandgap, high resistivity, few electron traps, low electron affinity, and high electron mobility. The energy diagram for such a coating with an applied field is shown in Fig. 13. With no electron traps and high electron mobility the bands will be flat inside the coating. With a low electron affinity there will be little barrier for electron emission from the film into vacuum, therefore, no charge accumulation at the coating surface. With such a film, electron tunneling from the metal into the dielectric will control emission. Emission from the metal into the dielectric

coating can be considered similar to tunneling from the metal into vacuum. The major difference (and benefit) is that the electric field is reduced at the metal by the dielectric constant of the film. This is seen in Fig. 13 as the change in slope of the vacuum level. Also, the barrier height is reduced since electrons need only tunnel to the conduction band rather that all the way to the vacuum level. However, this difference is small if the electron affinity, χ, is low. If we consider the flat-band case with a uniform electric field inside the coating then the Fowler-Nordheim equation, eqn. (1), can still be used with following substitutions:

$$\mathcal{E}' = \mathcal{E}/\varepsilon_r$$
$$\Phi' = \Phi - \chi$$

where $\mathcal{E}'$ is the electric field at the cathode surface and Φ' is the effective barrier height for electron tunneling. The Fowler-Nordheim equation can then be written

$$J = \frac{1.541 \cdot 10^{-2}(\mathcal{E}')^2}{\Phi'} \exp\left[\frac{-6.831 \cdot 10^9 (\Phi')^{3/2}}{\mathcal{E}'}\right] \qquad \left[\text{A/m}^2\right] \qquad (7)$$

where the correction terms for the image force (v(y) and t(y)) are ignored. There is some evidence that the image force should be ignored for tunneling into thin films for quantum mechanical reasons.[52]

E

→ x

Metal   Coating   Vacuum

E_{vac}

E_f

E_C

E_V
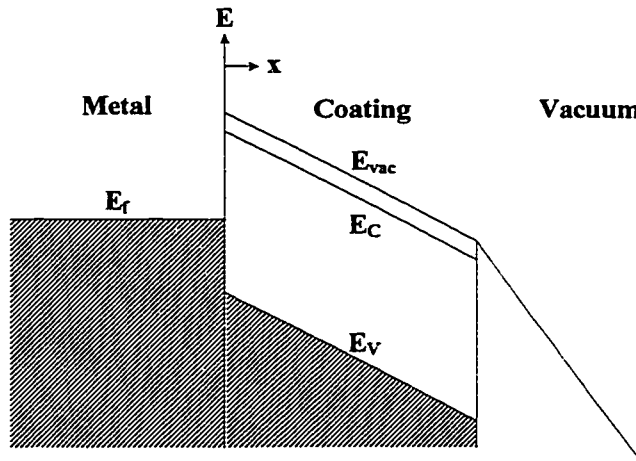
Figure 13. Energy diagram for a "perfect" insulator coated metal cathode with applied field.

For metal-coating limited emission one can derive a figure of merit for the coating as the increase in breakdown voltage with the coating compared to with no coating. It is assumed that the coating does not modify the field enhancement across the metal surface. It is further assumed that breakdown will occur at some critical current density at which point the metal will evaporate in keeping with the theory of Dyke.[53] This requires that the breakdown strength of the insulator is greater than the critical field for the metal. Also, the insulator must be able to handle the high temperatures of the metal as it becomes critical. In eqn. (7), we note that the exponential term will dominate at high current densities. The current density for the uncoated and coated cases can be expressed as

$$J(uncoated) = C \exp\left[\frac{-6.831 \cdot 10^9 (\Phi)^{3/2}}{\mathcal{E}}\right] \qquad [A/m^2]$$

$$J(coated) = C \exp\left[\frac{-6.831 \cdot 10^9 (\Phi')^{3/2}}{\mathcal{E}'}\right]$$

where C is a constant representing the pre-exponential terms. At the critical current density, assumed identical for coated and uncoated cases, the exponents can be equated yielding

$$V_b(uncoated) = \mathcal{E}d = \frac{-6.831 \cdot 10^9 (\Phi)^{3/2} d}{\ln(J_{critical}/C)} \qquad [V]$$

$$V_b(coated) = \mathcal{E}d = \frac{-6.831 \cdot 10^9 \varepsilon_r (\Phi - \chi)^{3/2} d}{\ln(J_{critical}/C)}$$

noting that the electrode spacing is much greater than the coating thickness and hence the gap voltage with a coating is closely approximated by the electric field in vacuum times gap distance, i.e., ignoring the voltage drop across the coating. The improvement factor or figure of merit, γ, for the coating is then found by taking a ratio of the breakdown voltages

$$\gamma = \frac{V_b(coated)}{V_b(uncoated)} = \varepsilon_r \left(\frac{\Phi - \chi}{\Phi}\right)^{3/2} \qquad (8)$$

For the "perfect" coating described above, γ is approximately just the dielectric constant of the coating. For this type of coating then a large dielectric constant is desirable. For coatings with electron traps or a large electron affinity the situation may change. Trapping of electrons in the film will reduce the electric field at the metal-coating interface reducing the current. The presence of traps also allows for trap assisted tunneling from the metal into the coating that would increase current. Field ionization of deep traps and Frenkel-Poole emission from shallow traps would also increase current. With a larger electron affinity some electrons will be reflected from coating-vacuum interface. This may generate an

accumulation of electrons at the coating surface reducing the field throughout the coating.

Figure of Merit: Coating-Vacuum Interface Limited Emission

At the other extreme of coatings are the conducting or semiconducting coatings where emission is limited by the coating-vacuum interface. The breakdown voltage can be increased with a conducting coating by reducing the field enhancement factor of the surface. This is done by smoothing over projections, filling pits, covering inclusions, etc. Additionally, emission could be reduced if the work function of the coating is greater than that of the cathode metal. Also, the critical field, E_C, of the coating could be higher than the metal yielding a larger breakdown voltage. This type of coating may also be applied to the anode. Anodes with large mechanical strengths have been linked to higher breakdown voltages. A figure of merit for this type of coating can be easily derived if the critical field, E_C, is known for the metal and the coating. The breakdown voltage for the uncoated and coated cases are given by

$$V_b(uncoated) = Ed = E_{C\,metal}\,d/\beta_m \qquad [V]$$
$$V_b(coated) = Ed = E_{C\,coating}\,d/\beta_c$$

where β_m, β_c are the field enhancements for the bare metal and coated cathodes, respectively. The figure of merit in this case is simply

$$\gamma = \frac{V_b(coated)}{V_b(uncoated)} = \frac{\beta_m E_{C\,coating}}{\beta_c E_{C\,metal}} \qquad (9)$$

The figure of merit could be high if the coating has a smooth surface such that β_c is much smaller than β_m.

It is believed that semiconducting coatings behave in a similar manner as conducting coatings. When a large field is applied an accumulation layer of electrons forms at the coating-vacuum interface as is illustrated in Fig. 14. This is well known from photoemission measurements with silicon.[54] The accumulation layer will be degenerate n-type regardless of the bulk doping of the semiconductor. The formation of the accumulation layer is aided by the comparatively large electron affinity of semiconductors as this usually means a high value of work function. This accumulation layer also occurs when the semiconductor is coated with an insulator, as is well know from metal-oxide-semiconductor, MOS, device physics. There will be some potential drop at the metal-semiconductor junction due to the Fermi level difference that will depend on bulk doping and the type of metal. There will also be some voltage drop across the bulk of the coating due to ohmic losses. The consequence of the accumulation layer is that the emission from the semiconductor with be similar as that from a metal with a work function given by the difference between E_{VAC} and E_C.
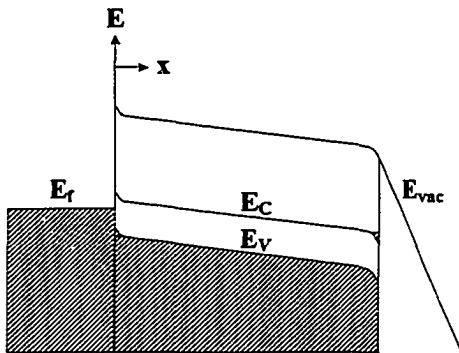
Figure 14. Energy diagram of a semiconducting coating on a metal cathode with an applied field. A degenerate n-type accumulation layer forms at semiconductor-vacuum interface.

CHAPTER IV

SiO$_x$ COATING: PROPERTIES AND DEPOSITION TECHNIQUE

Coating Selection

Insulating and semiconducting coatings were considered for our studies. Some of the properties of coating materials (mostly oxides) are listed in Table 2. The source for Table 2 was ref. [55] except where otherwise noted. Detailed information about the large ε_r materials Ta$_2$O$_5$ and TiO$_2$ could not be found. Specific information about SiO$_x$ is also difficult to specify, as the stochiometry of the material is variable as will be discussed in detail later.

Table 2. Properties of some coating materials.

Material	ε_r	E$_g$[eV]	χ [eV]	Thermal Conductivity [cal/cm-s-K]	Dielectric Strength [V/mil]	Young's Modulus [ksi]	Ave. Z	Density [g/cm^3]
Diamond	5.70	5.47[56]	~1	4.78	25-3000	152,000	6	3.515
Si	11.8	1.107*	4.05[57]	0.354	50-500*	23,560	14	2.33
SiO$_x$	~5			0.00359	100-10^4	72,000	11	2.125
SiO$_2$ (fused quartz)	3.75	9**	.9[60]	0.0033	700-1000	10,500	10	2.203
Ta$_2$O$_5$	25				17,000	44,800	26.6	8.0
TiO$_2$	86*			0.0156**			12.7	4.23*
Al$_2$O$_3$	10.3	~10[58]		0.110	1200	60,000	10	3.99

*from ref. [59]   **from ref. [60]

One very important property, which is not listed, is adhesion. Many films crack from internal stresses as a thick film is applied which would be detrimental for this application. For this and other reasons the deposition method is critical.

The growth rate and costs must also be considered for large scale applications. A 2 to 10μm film seems to be required to effectively coat mechanically polished electrodes. For coating large areas a deposition rate of 10Å/sec or greater is desirable. This is one reason why the deposition method is important.

Diamond films are usually deposited by some sort of chemical vapor deposition, CVD, process. Most other materials can be deposited by evaporation, CVD, or sputtering processes. Almost any material can be deposited by sputtering, however, deposition rates are usually low and costs are high. Ta_2O_5 and Al_2O_3 are routinely grown by anodic oxidation, which is perhaps the least expensive growth method. Anodic oxidation may be a poor method for this application, however, due to poor quality and a porous surface. SiO_2 can be grown by thermal oxidation, CVD, and sputtering. Thermally oxidized SiO_2 films are very high quality, but this would only work on a Si substrate. CVD growth of SiO_2 uses toxic gasses and is not environmentally friendly. Silicon monoxide, SiO_x, is usually deposited by thermal evaporation with high deposition rates, low costs, and no toxic by-products.

Silicon Monoxide

We have used silicon monoxide, SiO_x, as a cathode coating material. SiO_x was used in the past for optical coatings, thin film capacitor dielectric, mirror coatings, and electrically insulating layers. Silicon monoxide is easily deposited by thermal evaporation and the source is very inexpensive, currently about $3 per gram. Silicon monoxide not in widespread use today due to the development

of RF sputtering which allows deposition of a wide range of insulators, many with superior properties. For our application, however, SiO_x, is attractive because of high deposition rates, inexpensive costs of equipment and materials, high dielectric constant, and high dielectric strength.

Blevis has detailed many of the properties and techniques involved with silicon monoxide.[61] Evaporation of SiO_x is somewhat different to other materials because it sublimates instead of melts. A special Ta boat developed specifically for SiO_x is used to heat the SiO_x source. If placed on a normal, open-faced boat the source tends to bounce around once sublimation begins and will eventually jump out of the boat. Films deposited from open-faced boats also contain defects and pinholes. Boats used for depositing SiO_x use a baffling design similar to that shown in Fig. 15. The SiO_x source pellets are trapped inside the boat. The SiO gas escapes through the baffling and a hole in the top of the boat where it travels to the substrate and condenses to form a film.
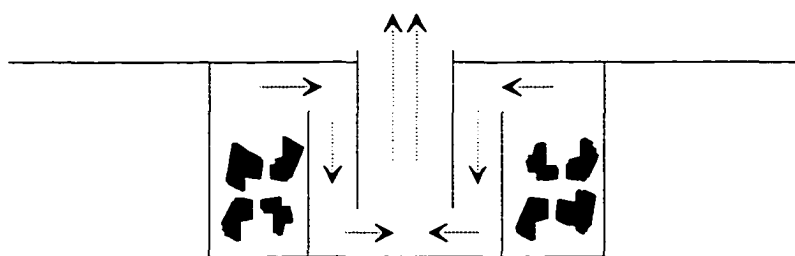
Figure 15. Baffled boat design used for evaporating SiO_x.

As the abbreviation suggests SiO_x has a variable stochiometry where x varies in the range from 1 to 2. The value of x depends on several factors including rate of evaporation, oxygen partial pressure, and substrate

temperature. A great deal of care is required to get reproducible results, which is one reason why SiO_x is not often used. The properties of the film vary with x from those of SiO_2 (x=2) to those associated with SiO_1 (x=1). It is important to note that SiO, silicon monoxide, only exists as a gas although the term 'silicon monoxide' is used in practice to describe SiO_x. The evaporation source is SiO_1, but it is believed to actually be an amorphous mixture of Si and SiO_2.

Normal rates for evaporation of SiO_x are in the range from 10 to 60Å/sec with boat temperatures from 1200 to 1350°C in which the properties vary from more like SiO_2 (low rate, temp.) to more like SiO_1 (high rate, temp.). It should be noted that the exact relationship between boat temperature, deposition rate and density has several dependencies including boat dimensions, boat to substrate distance, angle between the boat and the substrate, and residual gas pressure. The background pressures of water vapor and O_2 during deposition also affect the value of x. For high pressures the film will approach SiO_2 while at low pressures the deposition rate decides film properties.[62]

As described above the properties of SiO_x are variable. The dielectric constant can vary from 4 for SiO_2 to 6 for SiO_1.[63] The index of refraction varies from 1.4 for SiO_2[64] to 1.6 for SiO.[65] In the range from $SiO_{1.0}$ to $SiO_{1.5}$ there is absorption of wavelengths from UV to blue resulting in a dark appearance. This absorption declines and vanishes linearly over the x=1.0 to 1.5 range. In the infrared range there is an absorption peak which shifts approximately linearly from 9 to 10μm as x varies from 2 to 1. This effect can be used to determine value of x for a particular film.

It was partially because of these variable properties of SiO_x that it was chosen for use in our experiments. Varying the coating properties allows us to test some of our theories about metal-coating interface limited and possibly coating-vacuum limited coating described earlier. If we assume that the emission is metal-coating limited then we should see a change in the field emission currents consistent with the change in dielectric constant of the film. However, it is also known that films closer to SiO_1 have higher leakage currents. The bandgap in SiO_1 may also be smaller (as evident by the UV-blue absorption) resulting in a higher value of χ. Higher leakage currents and χ increase the likelihood of an accumulation layer and coating-vacuum limited emission. In that case we would expect very different behavior in the field emission currents as x is varied.

Silicon Dioxide Coatings

Although many of the details about SiO_x such as the band structure are not known exactly due to variability in composition and limited research, most properties of SiO_2 are well known since it is an integral substance in fabricating metal-oxide semiconductor, MOS, devices. Although no data concerning SiO_2 coatings of cathodes in vacuum could be found, the properties of MOS capacitors are well known. Based on the current-voltage relationship of MOS capacitors and knowledge of the energy band structure we can predict the behavior of SiO_2 cathode coatings in vacuum. From this we gain insight into the behavior of SiO_x coatings.

The basic differences between conduction in MOS capacitors and through a SiO_2 coated vacuum cathode are the boundary conditions at the coating-vacuum interface. In a MOS capacitor there is no barrier to electrons entering the anode. At a SiO_2-vacuum interface, however, there is a small barrier to electron flow. Additionally, hole injection is possible from the anode of a MOS capacitor but not vacuum.

The current-voltage relationship of an insulating film between conducting contacts, like in a MOS capacitor, gives valuable information about the conduction mechanisms inside the insulator. Although other insulators have space-charge-limited, Frenkel-Poole, or other bulk related currents, SiO_2 is normally limited at the cathode-SiO_2 interface due to wide bandgap, low trap density, and a high electron mobility.

Lenzinger and Snow showed that the current in MOS capacitors with a thin SiO_2 film is limited by the cathode-SiO_2 interface and is due to Fowler-Nordheim tunneling from the cathode.[66] Evidence of limiting by the cathode-SiO_2 interface is observed in current measurements that were found to be independent of the oxide thickness in the range from 640 to 5000Å. Dumin, et.al.[67], measured the trap (localized state in the forbidden gap) density and found that the leakage current was proportional to the number of traps. Also, the traps were distributed throughout the film not just at one interface. Scott and Dumin[68] later examined the time dependence of the excess current. It was found that the current decays over at time period of several minutes and is assumed to eventually fall to zero. Also, after removing the voltage a discharge

current in the opposite direction was measured indicating that the excess current is actually due to trapping and detrapping of stress generated traps rather than trap assisted tunneling at the cathode. Schuegraf and Hu[69] examined hole injection by separately measuring the currents for electrons and holes in a special configuration. They found that although electron current is dominant there is hole injection due to tunneling from the anode and this current can be linked to breakdown. It was shown that hole injection damages the oxide leading to breakdown.

With a SiO_2 coated cathode in vacuum the situation is slightly different. The energy diagram for the metal-SiO_2-vacuum system is deduced from optical measurements[70] to have a form similar to Fig. 16. There is a 0.9eV barrier to electron flow at the SiO_2 surface that is small compared to a cathode-SiO_2 junction. With few traps, as in the case of MOS gate oxides, we can be fairly certain that emission would be limited by field emission at the metal-SiO_2 barrier. However, for thick films with trap-assisted tunneling at the cathode the limiting may shift partially or completely to the SiO_2-vacuum interface where an accumulation of electrons would reduce the field inside the SiO_2 film. A shift could also occur due to field enhancing spots on the metal surface stimulating electron injection into the film.
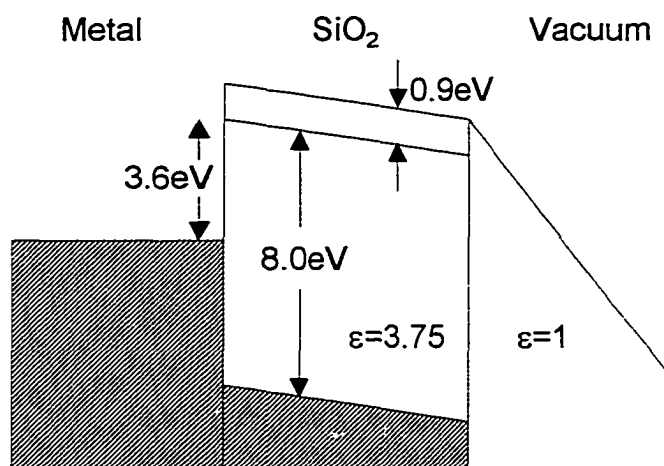
Metal   SiO₂   Vacuum

Figure 16. Band diagram of the metal-SiO₂-vacuum system without traps showing the 0.9eV barrier at the coating surface.

To better gauge the possibility of an accumulation layer the transmission coefficient, the transmission probability through a 0.9eV barrier was calculated using eqn. (25) in Appendix A. The transmission coefficient for electric fields ranging from 100 to 1000MV/m is listed in Table 3. The calculated transmission probability is very low until very high fields, >500MV/m, is reached when the image force reduces the barrier height below the conduction band. This suggests that an accumulation layer could form at fields below ~100MV/m, but would dissipate in the field range from 100 to 600MV/m. When an accumulation layer forms, electrons are trapped at the surface and will impinge on the barrier at a high rate so that emission could still be considerable even with transmission probabilities < 10^{-20}.

Table 3. Transmission coefficient through a 0.9eV barrier and image force barrier lowering for electric fields from 100 to 1000MV/m.

Electric Field [MV/m]	Image Force Barrier Lowering [eV]	Transmission Coefficient
100	3.793E-01	3.602E-20
200	5.364E-01	4.342E-08
300	6.570E-01	3.532E-04
400	7.586E-01	2.721E-02
500	8.481E-01	3.382E-01
600	9.291E-01	1.000E+00
700	1.004E+00	1.000E+00
800	1.073E+00	1.000E+00
900	1.138E+00	1.000E+00
1000	1.199E+00	1.000E+00

For practical applications, where the electrode areas are several orders of magnitude larger, the role of field enhancement from isolated irregularities must be considered. Failure may occur due to field enhancing sites at the cathode-oxide interface. With a thin film, the enhancement from these sites may extend to the oxide surface in which case the resultant behavior would be similar to the non-enhanced case for fields β times lower. If the film thickness is large compared to the field enhancing site at the cathode-oxide interface then a different behavior would be expected which would promote the formation of an accumulation layer. Field enhancement at the oxide-vacuum interface would not occur except in the presence of a large accumulation layer.

To estimate the effectiveness of a thin SiO_2 coating, the leakage current measurements of Dumin, et.al., were used. With a 100Å film the leakage currents were below 10^{-9} A/cm^2 with applied voltages up until about 5 volts. The electric field inside the film at that point is 500MV/m. The breakdown strength is

difficult to estimate because there is no hole injection in the vacuum case. With a coated cathode in vacuum, taking the dielectric constant of 3.75 into account, the field in vacuum would be 1875MV/m. At these fields there would clearly be no accumulation layer forming at the SiO_2-vacuum interface.

For large electrode areas a thicker coating will probably be required due to imperfections in the cathode surface. Using the data in Table 2 for fused quartz we can expect a dielectric strength of up to 1000V/mil or ~39MV/m. This corresponds to an electric field in vacuum of 146MV/m. At these fields the presence of an accumulation layer will depend on field enhancement at the metal and trap density inside the film. Based on these calculations a thick SiO_2 coating is viable with breakdown strengths of about 150MV/m or roughly 3 to 5 times that of uncoated cathodes.

Relating to silicon monoxide, coatings of SiO_x with x close to 2 are expected to behave in a similar manner to silicon dioxide and have metal-coating limited emission. As x goes to 1 we expect the band gap to lower increasing the barrier at the coating-vacuum interface. This plus increased leakage current will tend to form an accumulation layer and may lead to coating-vacuum limited emission. However, if the emission for SiO_x for low values of x is metal-coating limited then we expect to observe reduced electron emission due to a higher dielectric constant.

Evaporation of SiO$_x$

Our SiO$_x$ coatings were deposited by thermal evaporation of silicon monoxide in a bell jar evaporator and a baffled boat similar to the one previously described. The evaporation source was 99.99% pure SiO$_1$ which is commercially available from Alfa Aesar, a Johnson Matthey company, Ward Hill, MA. The source came in the form of small black pebble sized pieces of variable size and shape. The baffled boat was the smallest one available with a capacity of two grams. It consists of two separate pieces for loading of the source. SiO$_1$ was loaded in lower portion of the boat and then the upper portion is put into place. The filled boat was then placed in the evaporator.

A bell jar evaporator was used coat the stainless steel cathodes. A schematic of the major components of the evaporator is shown in Fig. 17. The glass bell jar is raised and lowered to access the chamber. The boat is clamped in the center of the chamber. The cathodes are suspended above the boat, slightly off-center, and held in place by a substrate holder and heater. A crystal thickness monitor is placed directly above the boat to monitor and control the deposition.

The vacuum is established with a dry system consisting of sorption roughing pumps and an ion main pump. The three sorption pumps are used on at a time to lower the pressure to ~$4 \cdot 10^{-3}$ torr. The sorption pump valves are then all closed and the ion pump main valve is slowly opened. The evaporation process is started when the pressure drops to 10^{-7} torr or lower.
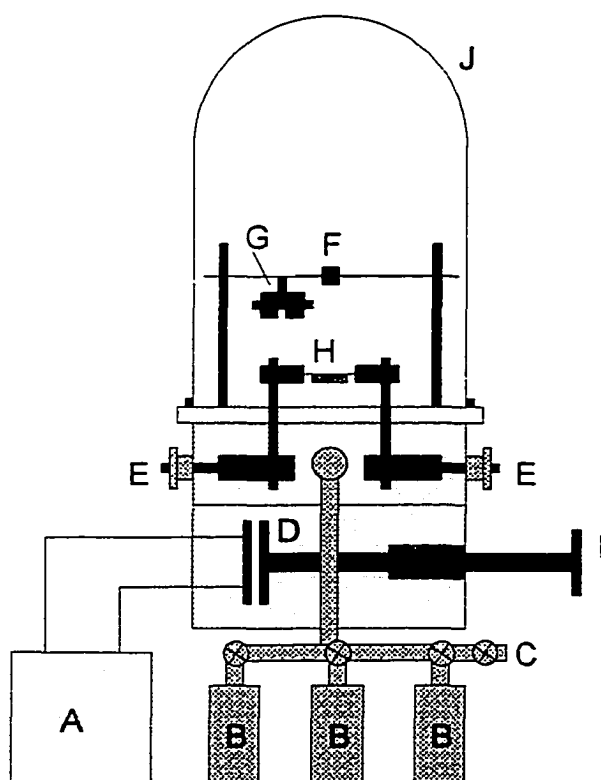
Figure 17. Schematic of the evaporator detailing major components: (A) Ion pump, (B) Sorption pumps, (C) Vent valve, (D) Main valve, (E) Filament power feedthroughs, (F) Thickness monitor, (G) Substrate heater and holder, (H) Boat, (I) Main valve wheel, and (J) Bell jar.

An automatic deposition system, ADS, was used to control the evaporation rate and final film thickness. The inputs to the ADS are a signal from the crystal thickness monitor and front panel settings. The ADS output controls the filament power supply that feeds the high currents required to heat the boat. The heart of the crystal thickness monitor is a quartz crystal. The ADS monitors the resonant frequency of the crystal. During deposition a film is deposited on the exposed surface of the crystal. The frequency of the crystal changes due to the added mass. The ADS calculates film thickness based on the density of the film (supplied via front panel switches) and the added mass.

Controlled deposition of SiO_x was complicated because of the variable density of the SiO_x that is a nonlinear function of deposition rate that in turn

depends on the position of the source relative to the substrate. The thickness monitor data alone is insufficient to determine film thickness or deposition rate. However, with the aid of a SEM to measure film thickness the film density and deposition rate was determined. The mass deposited on the thickness monitor can be determined from the ADS display. Knowing the exposed area of the thickness monitor, the mass deposited on the thickness monitor, and the thickness of the film deposited on the substrate it was possible to calculate the density of the film deposited on the substrate. The deposition rate was calculated simply be dividing film thickness by deposition time. Once the film density at the desired deposition rate was determined, the ADS properly controlled the SiO_x deposition.

CHAPTER V

EXPERIMENTAL SETUP AND PROCEDURES

The experimental setups used in these experiments were designed to yield quantitative scientific data while incorporating techniques that are transferable to actual applications. All cathodes were made from #304 stainless steel, as it is the most common material for high vacuum work. Electrode fabrication, polishing, preparation, and coating methods are all simple and standard methods that can be applied to a wide variety of applications. For scientific purposes, however, we used short electrode spacings and carefully designed electrodes.

Electrode spacing of from 0.1 to 0.3mm was used in these experiments. From the introduction in Chapter 1, gaps spaced less than about 1mm are field-controlled where field emission initiates breakdown at the cathode. Gaps spaced greater than about 1mm are voltage-controlled, where anode interactions lower the breakdown field. By operating with short gaps well in the field-controlled range, anode interactions can be neglected. Field emission current and breakdown voltage of short gaps is determined primarily by the cathode, which is where our coatings have their effect. Also, operating with short gaps allowed us to use relatively low voltages (under 50kV) eliminating may safety concerns including X-ray radiation. Short gaps also enabled the use of relatively small, centimeter scale electrodes so that fabrication of many electrodes is possible. A

small vacuum chamber allowed us to reach operating vacuum pressures quickly (a few hours) thereby reducing total experiment time.

The electrodes were designed in such a way that a relatively large area of the cathode is stressed with a uniform field. Other experimentalists have used either a sphere anode above a planar cathode or a needle-like anode above a planar cathode. These systems have the advantage that several portions of the same cathode can be measured. However, it is well known that with large electrodes the net behavior is controlled by a few defects distributed over the surface. Our electrodes stress the entire available area of the cathode at the same time so that several defect sites are included in the test area. Using this method experimental results can be more easily reproduced and applied to applications.

A main goal in our experiments was to obtain reliable and reproducible results. Testing a large number of cathodes each with a relatively large area increased the reliability. Achieving reproducible results required a great deal of attention to the following areas:

- Electrode Geometry
- Electric Circuit
- Cathode Preparation
- Contamination Control
- Electrode Gap Spacing
- Breakdown and Conditioning Procedures

Electrode Geometry

The electrode geometry was designed to give low field enhancement at the anode and a large uniform field area on the cathode. Although anode effects are negligible with short electrode spacing, a zero field-enhanced anode lessens

the possibility of field ionization of residual gas or the detachment of anode particles at field enhanced sites on the anode. Near zero field enhancement was accomplished with Rogowski profile anodes.

The stainless steel anodes were designed by computer and fabricated using computer-controlled machinery. Stainless steel was used for better vacuum compatibility, strength, and reduced outgassing although the anode material is not considered critical because it is small relative to the vacuum chamber. A computer program was written to generate the coordinates needed by the milling machinery. The program draws Rogowski profiles on the display. The display image is then saved and coordinates are taken from the bit-mapped image. The maximum value of θ was used ($\theta=\pi/2$) to give the most slender possible anode. Only two anodes were fabricated, but they were repolished and cleaned before every experiment.

The constant field area generated under the anodes is ~0.6cm^2. The field on the cathode surface drops off quickly away from the anode although it is substantial over a larger area. If we consider the effective area tested with this configuration to be that over which electric field on the cathode drops to $\frac{1}{2}$ of the maximum value then the effective tested area is approximately 1cm^2.

Because the electric field on the cathode extends beyond the area covered by the anode, the cathode area must be somewhat larger that the anode area. In our experiments a one inch diameter disk cathode was used. The simple shape allowed us to fabricate many cathodes. The one inch diameter is large enough to prevent breakdown at the edge of the cathode and

small enough so that a small mechanical polishing machine could be used. With a larger cathode breakdown to the vacuum chamber walls would also be possible aided by the somewhat sharp edges of the disk cathode. The cathodes have a 0-80 tapped and threaded hole in the center of the opposite surface by which electrical contact is made and the cathode is held in position.

Computer rendered scale images of the experiment flange with this electrode geometry are shown in Figs. 18a,b. Shown in Fig. 18a are the high voltage feedthrough (right), the 4-1/2" conflat flange (center), and the anode and cathode assemblies (left). In Fig. 18b the image is rotated so that the anode assembly is on top and the cathode assembly is on bottom. Note: the cathode is 1" in diameter.

(a)   (b)
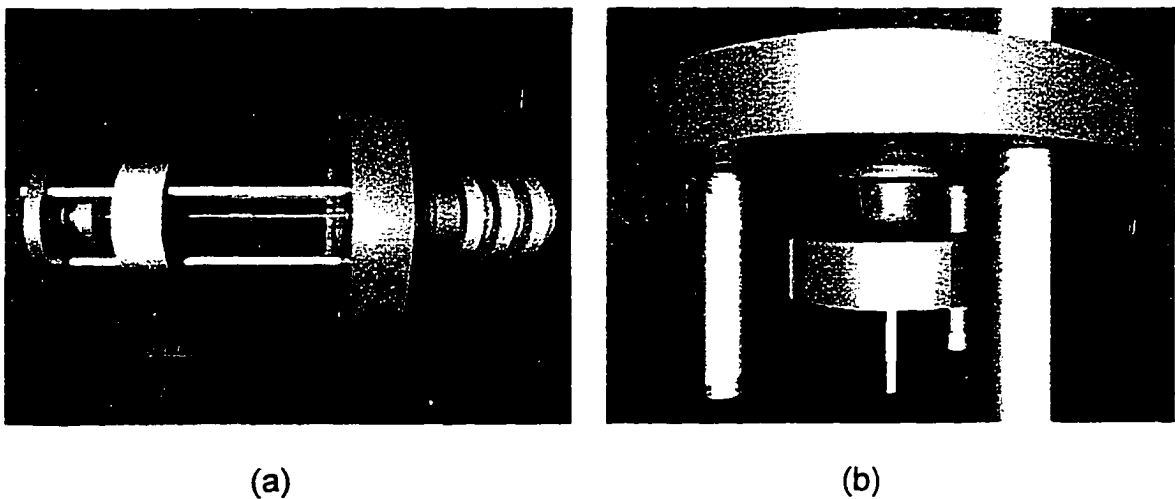
Figure 18. Computer rendered wide angle view of experiment flange (a), and close-up view of anode and cathode (b).

The experiment flange allowed application of high voltages up to 30kV. The high voltage feedthrough is rated at only 25kV but this was exceeded by 5kV

without difficulty (25kV is believed to be a conservative rating). When inserted into the vacuum chamber the anode connection was made with a mechanical spring contact connected to a 5kV feedthrough (The anode voltage is limited to ~100 volts by the circuit).

Electrical Circuit

There were two circuits used in the experiments; a conditioning circuit and a breakdown circuit. The conditioning circuit has high impedance and was used for electrical conditioning of the cathode. The pre-breakdown currents were also measured with the conditioning circuit. The breakdown circuit has a low impedance allowing currents up to 30A.

In both the conditioning and breakdown circuits a relatively large capacitance was charged through a charging resistor ($25M\Omega$) as shown in Fig. 19. The $0.9\mu F$ capacitor was actually a bank of four high-voltage, low inductance capacitors (from Maxwell, Inc.) in parallel. The role of the capacitor and the low series resistance ($1.1K\Omega$) in the breakdown circuit was to provide enough current and energy to decisively indicate breakdown. In conditioning measurements the capacitor acted as a power supply filter which eliminates high frequency transients in the DC voltage.

In the breakdown circuit a current transformer is used to measure the breakdown current. A small resistor was used earlier to measure the current, but the Pearson coil gave a lower inductance, faster rise time, and improved safety since the anode was directly grounded.
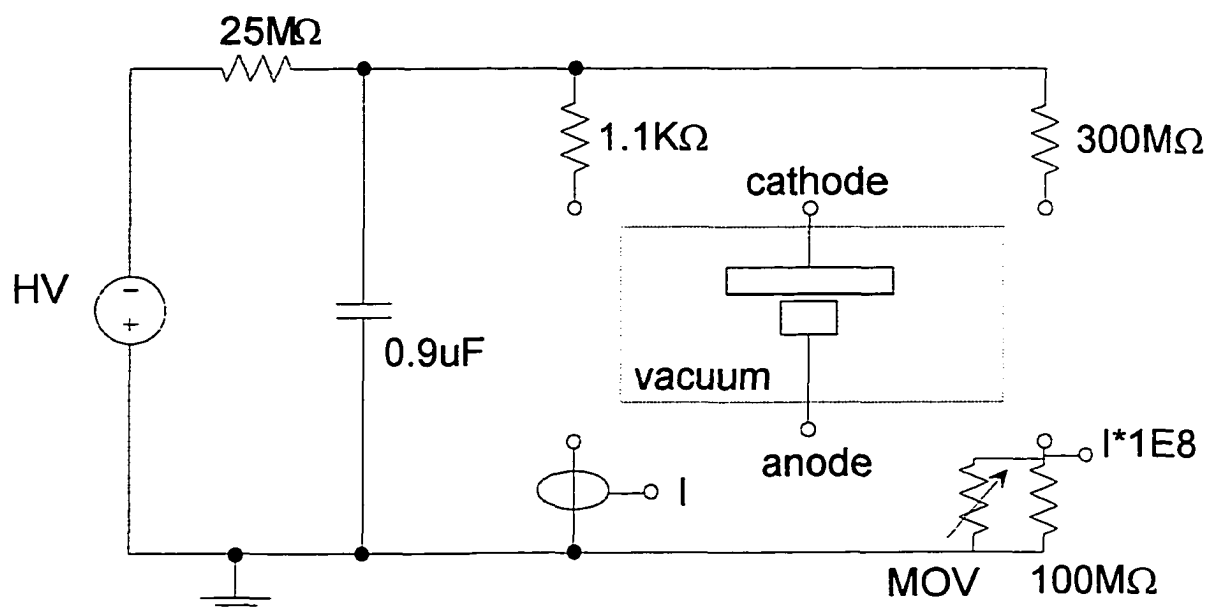
Figure 19. Electric circuits for the conditioning measurements (right) and breakdown measurements (left).

Both preconditioning and post-conditioning currents were measured with the conditioning circuit. This was a somewhat difficult task as current levels can change quickly by several orders of magnitude. Also, it was known that the current is not always entirely stable and can fluctuate randomly about an average level.

The design of our circuit was similar to that used by Hackam and Salman.[71] A large series resistance of 400MΩ (comprised of strings of 50MΩ high voltage resistors) was used to condition the electrodes. This limited the maximum current to the μA range. The current was measured as the voltage across the 100MΩ resistor with an electrometer (the exact resistance was measured with the electrometer). At first we used the electrometer as a current meter, but current spikes easily damaged the electrometer when used this way.

By using the electrometer as a voltage meter, protection was provided with metal-oxide-varistors, MOV's. To protect the electrometer three MOV's were placed in parallel to the 100MΩ CVR (current viewing resistor) and the electrometer. The MOV's limit the maximum voltage to 135 volts and add a capacitance of ~300nF. The added capacitance was useful to the system because it acted to filter high frequency transients allowing us to measure the DC component of the current. This capacitance, however, introduced a slow response time to the system. The time constant depended on the gap current with a maximum value of about ~30sec. With low currents a wait of up to three minutes was required to make an accurate measurement.

The electrometer has large input impedance and high sensitivity. The >100TΩ impedance of the electrometer was required to accurately measure the voltage across the 100MΩ CVR. The electrometer was capable of resolving 10^{-5} volts that allowed us to resolve gap currents as low as 10^{-13} amps. The maximum current reading was limited by the CVR to about 1μA. This circuit then allowed us to measure currents over seven orders of magnitude.

Although the electrometer was theoretically capable of resolving 10^{-14} amps, there were several noise source which limit the capability including:

- Vibration of the electrode gap due to such sources as the turbomolecular pump.
- Triboelectric voltages due to vibration of the cables connected to the electrometer.
- Fluctuations in the HV supply due to line voltage fluctuations.
- Electrical noise from ambient electromagnetic waves.

These noise sources had to be reduced for maximum sensitivity of 10^{-13} A. To reduce vibrations of the electrode gap the experiment cross was separated from

the vacuum pump with a bellows. Using a rigid, air-filled coaxial cable reduced triboelectric voltages. As previously discussed the 0.9μF HV capacitor was used to limit power supply noise. To limit ambient noise the CVR and MOV's were encased in a brass cylinder. Also, the 300MΩ string of resistors was placed in a grounded brass tube connected to the cathode via a high voltage coaxial cable.

In both circuits the voltage was measured at the high voltage capacitor using a 1000 to 1 resistive divider (calibrated with a 1% tolerance 1000X probe) and a DMM with a computer interface for data acquisition. The actual gap voltage could then be calculated since the series resistance is known. In some instances, particularly when a result was in question, an electrostatic voltmeter with essentially infinite input impedance was used to verify the actual voltage on the cathode.

Cathode Preparation

After machining by the Engineering Machine Shop at Old Dominion University, the cathodes were all identically polished and cleaned. The polishing procedure utilized a mechanical polishing machine whose use was facilitated by the flat surface and workable diameter of the cathodes. The final polish was with 1μm diamond paste. The polishing results in a mirror-like finish, but one that could be reproduced on large, curved surfaces as well.

Stainless steel is a hard metal compared with copper, for example, and so mechanical polishing was somewhat difficult and some flaws result. A smoother surface can be achieved using electropolishing. With electropolishing a very fine abrasive is used but the surface is actually polished by applying a voltage in a

chemical bath. With chemicals and the electrical current a chemical reaction occurs on the exposed surface of the steel. This combined with the fine abrasive removes nanometer by nanometer of the surface until a very smooth surface results.

Although electropolishing produces a smoother surface than mechanical polishing, it was believed that better high voltage performance could be achieved via mechanical polishing. A reduced breakdown field with electropolished surfaces could result due to loosely bound grain fragments on the surface. With a very smooth surface it seems likely that the surface will contain many small sections of individual grains. When a high electric field is applied, electrostatic forces could pull such fragments off the electrode. Either the particle itself or field enhancement at the edge of the resultant void could reduce the breakdown field. Mechanical polishing is a scraping technique which scratches the surface with abrasives and so any loosely bound grain fragments would likely be scratched off.

The cathodes came from our machine shop with visible grooves similar in appearance to an old vinyl record from the machining process. Removing the grooves and giving a fine polish required a series of decreasing sized abrasives. The procedure followed in this experiment is given in Table 4.

After polishing, one cathode was take to the SEM to look for imperfections. With the naked eye small pits in the surface were barely visible. The pits had an appearance similar to that of an orange peel. Under the SEM the cathode surface was very smooth with an occasional pit or inclusion. No

Table 4. Polishing procedure for one inch diameter stainless steel cathodes.

Abrasive	Lubricant	Pressure	Speed	Time
SiC paper, 180 grit	Water	60%	4	until smooth
SiC paper, 240 grit	Water	60%	4	~4 minutes
SiC paper, 320 grit	Water	60%	4	~4 minutes
SiC paper, 400 grit	Water	60%	4	~4 minutes
SiC paper, 600 grit	Water	60%	6	~4 minutes
6μm diamond	Metadi Fluid	full	5	~4 minutes
1μm diamond	Metadi Fluid	full	5	~4 minutes

metal protrusions greater than $0.2\mu m$ could be observed. The pits were randomly distributed over the surface with diameter ranging up to about $30\mu m$. There were an estimated 15 pits with size $>10\mu m$ in a $1cm^2$ area. Images of two larger pits taken at a steep angle are shown in Figs. 20 and 21. While the pit shown in Fig. 20 had rounded edges and may not offer a great deal of field enhancement, the pit in Fig. 21 had a sharp edge and could be a likely breakdown site.

Another likely problem site occurs at inclusions. Only a few inclusions $>0.5\mu m$ were observed on the cathode surface. One typical inclusion is shown in Fig. 22. The SEM operator was able to identify the inclusion as insulating based on the contrast changes. From the sharp edges of the inclusion we can deduce that it was likely crystalline in structure. Based on these facts plus an inclusion size of $\sim 1\mu m$ we deduced that the inclusion was actually a piece of the $1\mu m$ diamond abrasive used as the final polish.
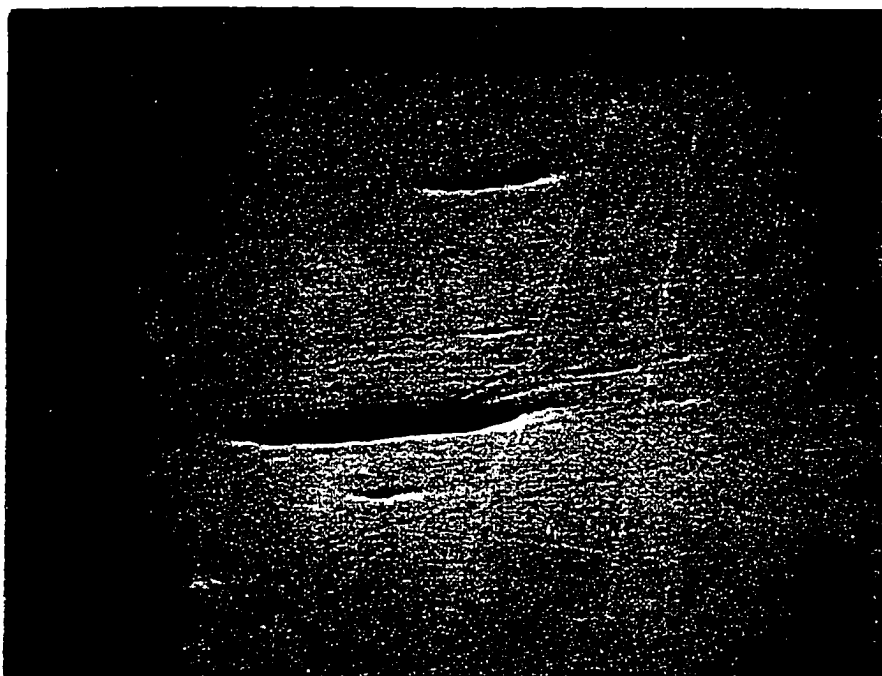
Figure 20. Pit in surface of polished stainless steel cathode with rounded edges.
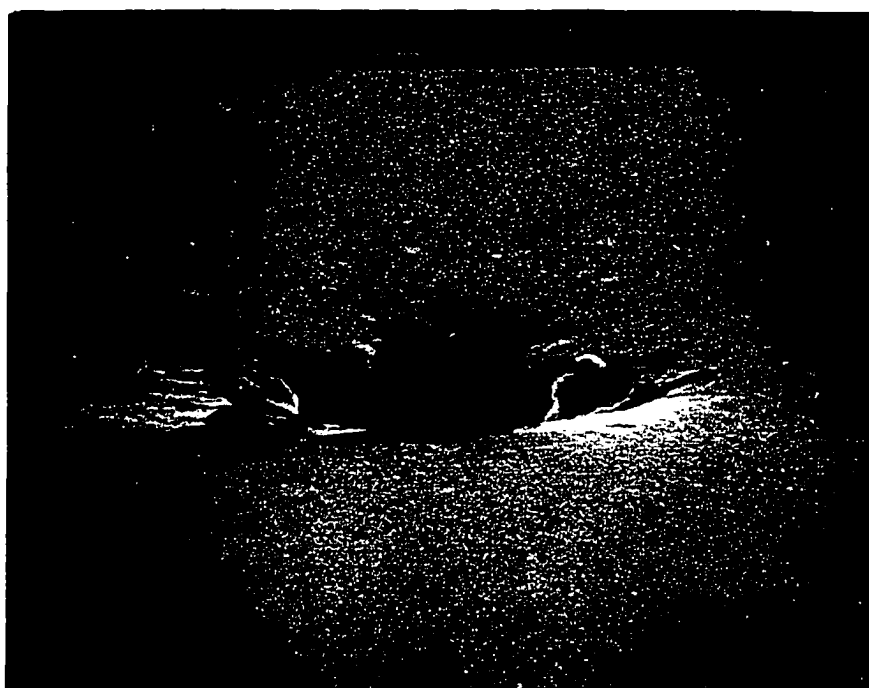
Figure 21. Pit in surface of polished stainless steel cathode with sharp edges.
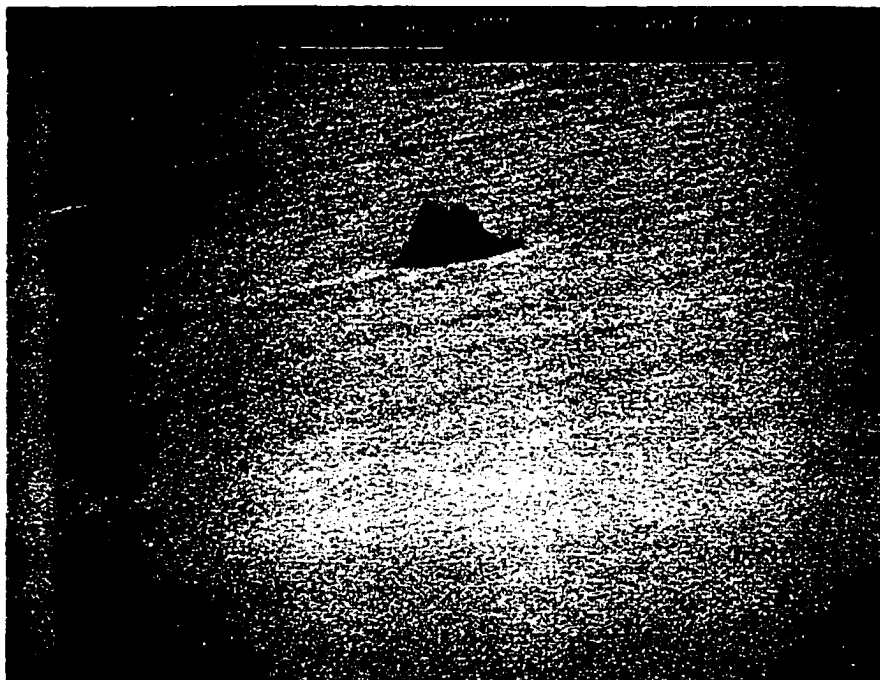
Figure 22. Inclusion of 1μm diamond particle in cathode surface.

Inclusions have been identified as strong field emitters and therefore likely breakdown sites. An insulating inclusion forms a metal-insulator-vacuum triple point that is known to give strong electron emission. Of course, inclusions like this one could be avoided using electropolishing and so there are advantages and disadvantages to both polishing techniques. There may be a relationship between inclusions and pits. It is easy to imagine that a loose diamond particle could become trapped in a pit. Also, if an embedded inclusion is removed during polishing a pit is formed.

After polishing the cathodes were rinsed in ordinary tap water to remove the polishing slurry. Next, the cathodes were ultrasonically cleaned with solvents in the following order: trichloroethylene, acetone, methanol, and distilled water. The final step was a blow dry in either pure nitrogen or argon. Water was useful

as a final solvent because excess drops attached to the cathode could be blown off before drying. This eliminated residue which was observed when either acetone or methanol were used last.

A clean environment was required to prevent the cathodes from becoming contaminated. Without this precaution contamination in the form of small particles that cover the cathode as shown in Fig. 23. Most of the contamination appears only loosely bound to the surface. Many of the contaminant particles appear to be fibers, which are probably insulating. However, some particles were clearly metallic. A closer look at a metallic particle in Fig. 23 is shown in Fig. 24.

Figure 23. High aspect angle view of the edge of a contaminated cathode. Several particles can be observed littering the surface.
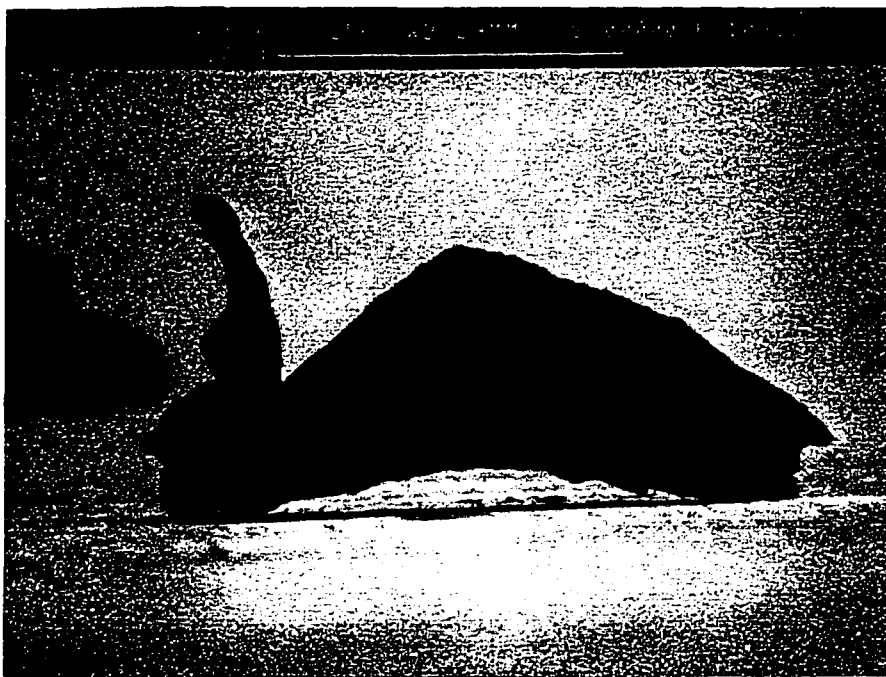
Figure 24. A close-up view of a large (~10μm) metallic contaminant particle above the finely polished stainless steel surface.

Electrode Gap Spacing

A three-step process was used to set the gap as illustrated in Fig. 25. First, the anode and anode holder where lifted above a flat surface using a ceramic spacer. The anode, normally fixed by a set screw, was adjusted vertically to the desired gap spacing using a metal shim with the desired thickness (measured with a micrometer). In the second step the anode assembly was placed on the support rods (not shown) and lowered to the cathode. With the ceramic spacers in place the anode-cathode gap was set and the anode holder was then fixed to the support rods using three set screws. Finally, the ceramic spacers were removed and the process was complete. The
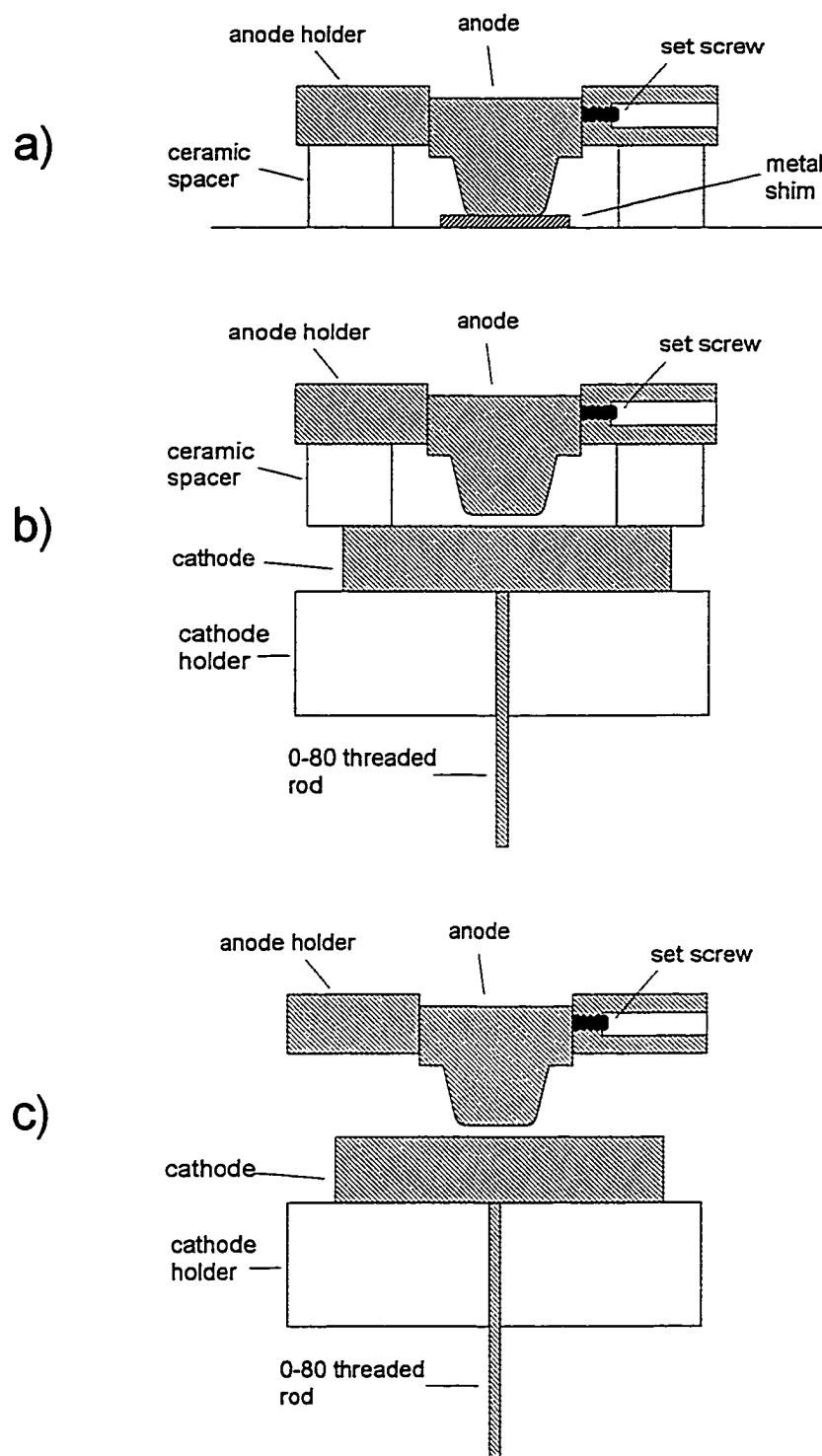
Figure 25. Three-step process for setting the anode-cathode gap spacing while avoiding contact with the cathode surface.

result is a gap equal to the metal shim thickness. The cathodes were handled with latex gloves and only at the outer edge.

To verify gap spacing the capacitance of the gap was measured. Because of the very small capacitance involved this method was only effective for 0.2mm and smaller gaps. With 0.2mm gaps the total accuracy was estimated to be about 5%.

Conditioning and Breakdown Procedures

In order to achieve more reproducible results consistent procedures were followed in the breakdown and conditioning measurements. The combined procedure had four phases. Prior to measurements the electrode gap was set between a refinished anode and a virgin cathode. The experiment flange was connected to the vacuum chamber and evacuated. Measurements began after about four hours when the pressure dropped to ~1 to $2 \cdot 10^{-7}$ torr.

The first phase was raising the voltage for conditioning of the virgin cathode. The voltage was raised in a staircase fashion with steps of ~500V every 3 minutes. Because this was done manually there was some variation in the steps. The first couple steps were sometimes large to speed the procedure. Data was automatically acquired from the DMM recording applied voltage and the electrometer measuring gap current. Data was continuously acquired with one sample every 30 seconds. The voltage was raised until the gap current exceeded 1μA. An example of the voltage staircase used in this step with actual data from a 200μm gap is shown in Fig. 26.

The cathodes were electrically conditioned in the second phase. The voltage was reduced until the current dropped to 1μA or lower. This voltage was then maintained for approximately 30 minutes at which point the cathodes are considered conditioned. Note that with coated samples there was some anomalous behavior to be described later.
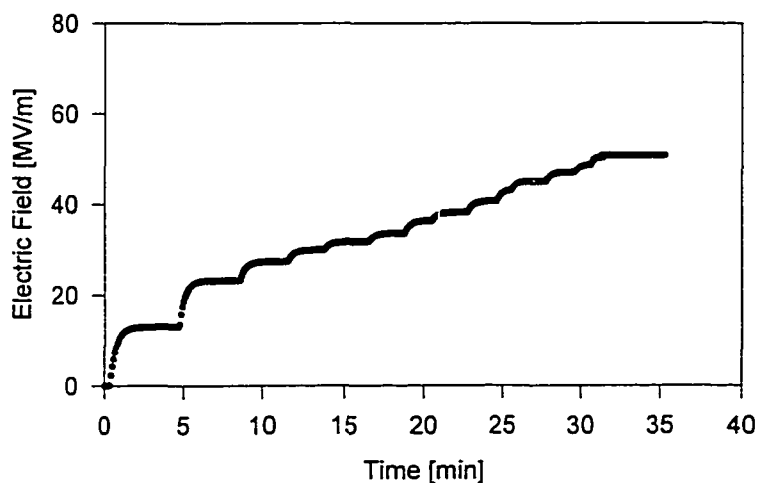
Figure 26. Staircase field (500V/3min) applied to virgin cathodes while raising to the conditioning voltage.

In the third phase (after conditioning) the voltage was reduced in a staircase fashion to take data for Fowler-Nordheim plots. The Fowler-Nordheim plots were used to determine emitter area and field enhancement factor. Because of the non-linearity of field emission the measurable current range of from 10^{-6} down to 10^{-13}A was covered in a small voltage range. Best results were obtained using a downward voltage staircase. With a climbing staircase occasional conditioning type discharges would occur at the higher voltages. After these current spikes a noticeable jump or drop in the current would be observed even as the voltage remained constant. The steps in the downward

staircase were ~250V/3min with the same data acquisition procedure used in phase 1. An example of the voltage staircase is shown in Fig. 27.
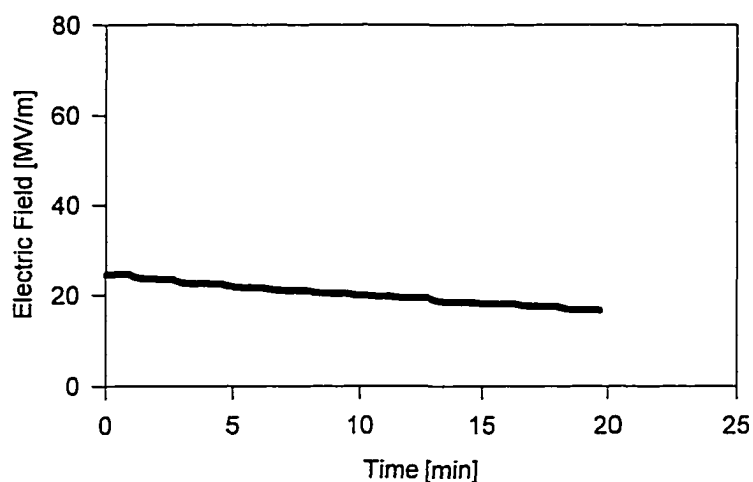
Figure 27. Downward staircase (250V/3min) used to measure Fowler-Nordheim data.

The final phase of an experiment was the breakdown measurement. The electrical circuit was changed to the breakdown circuit described earlier. The voltage was increased at a rate of 500V every minute until breakdown occurred. A different data acquisition program sampled the voltage on the capacitor once per second. The Pearson coil was connected to a 100MHz digital oscilloscope to record the breakdown current pulse. The program monitored the oscilloscope to record any triggers. The point of breakdown was easily identified in all measurements because the following events all occur simultaneously: the capacitor voltage dropped to near zero, the oscilloscope was triggered by a large current pulse, a flash of light was observed between the electrodes through the vacuum viewport, and a slight "click" sound was audible. The breakdown voltage

was taken to be the last high voltage value recorded by the computer. An

example of a voltage staircase from an actual measurement is shown in Fig. 28.
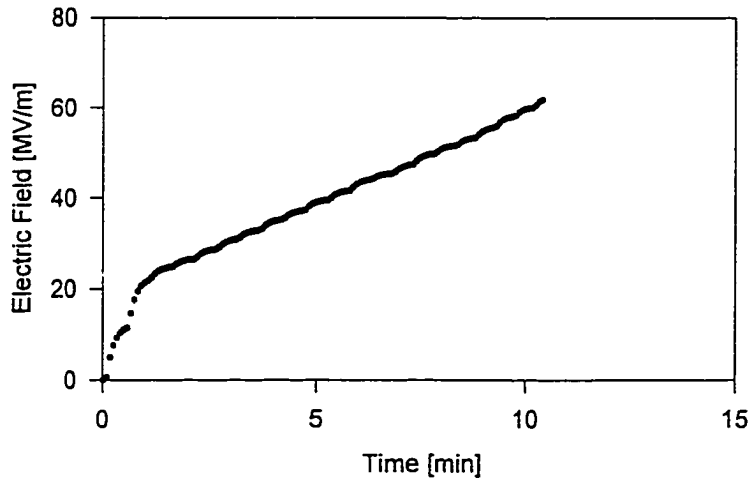
Figure 28. Example of voltage ramp applied to the gap in the breakdown voltage measurement (500V/1min).

CHAPTER VI

ELECTRICAL MEASUREMENTS OF SiO$_x$ COATED CATHODES

Experiments with High-Pressure Water Rinsed Cathodes

In this set of experiments a group of six cathodes were cleaned using a state-of-the-art high-pressure water rinsing system. Each of the six cathodes was identically polished and cleaned with our normal procedure. Next, the cathodes were rinsed with high-pressure water. Ultrapure, 1200psi water was fed to a showerhead inside the cavity being cleaned. The motorized showerhead was rotated and translated through the center of the cavity so that the entire surface was sprayed. This procedure was found to greatly reduce field emission from contamination, which causes loading in the RF cavities.[72] Three of the cathodes were coated with 2μm SiO$_x$ and the others were left uncoated for comparison.

Special caps were created to protect against contamination during transport from preparation facility to experiment. The stainless steel caps created an air tight seal around the edge of the cathode. A screw was used to maintain pressure on the cap-cathode seal. Both the cathodes and the caps were cleaned with the ultrapure water rinsing system.

A. Uncoated Cathodes with High-Pressure Water Rinsing

Current and voltage measurements on the uncoated cathodes were made with the conditioning circuit. Measurements were made while raising the voltage

for the first time and again while lowering the voltage after conditioning. This data is shown Fig. 29. As discussed in chapter 5 each data point in Fig. 29 represents an average of 30 seconds of data with a steady voltage. The results show relatively low field emission and high breakdown fields.

The measurements while raising the voltage on the virgin cathodes showed some interesting features. The current remained, for the most part, below 10^{-11} A until with one voltage step the current rose to the 10^{-6} A range, an event termed "activation". At this point data acquisition was halted to prevent damage to the electrometer. There were at times some current spikes evident in the real-time data, but the peak is reduced because of the average. The occurrence of spikes is responsible for the three high points in sample uncoated #2.

Although others have described similar observations of very low currents until an activation event of some kind occurred, we could find no record of this activation occurring at such high fields, ~50MV/m. In fact, the activation field (Table 5) is only slightly below the breakdown field (measured later).

After electrical conditioning the data was found to follow the Fowler-Nordheim equation as expected. The field enhancement factors and emitter areas were calculated and are listed in Table 5. The typical value for field enhancement in literature for uncoated cathodes is ~200 so our results indicate good polishing and low contamination.

There was deviation from the Fowler-Nordheim equation with low applied fields. The currents (~10^{-11} A) are higher than expected given the behavior at

high fields. This deviation can be readily observed in the Fowler-Nordheim plots (Fig. 34). This excess current at low fields is difficult to explain. Measurement of the electric noise made by setting the gap very large were found to be $\sim 10^{-12}$A or lower. Also, this deviation was not observed with the coated cathodes. One possible explanation is enhanced emission from insulating inclusions. The magnitude of the enhanced emission may be limited to the 10^{-11} A range in a manner similar to the emission from epoxy coated tips as described in Chapter II.

The final step in the experiment was the breakdown measurement. The current was increased until breakdown occurred. The breakdown field ranged from 51 to 61MV/m as listed in Table 5 with an average of 56MV/m. This is higher than the ~40MV/m measured in earlier experiments without contamination control which shows that the contamination control was effective.

Table 5. Measured activation and breakdown electric fields of three uncoated and three SiO_x coated cathodes cleaned with high-pressure ultrapure water at Jefferson Lab.

Sample	Activation Field [MV/m]	Breakdown Field [MV/m]
uncoated #1	58 ±3	61 ±3
uncoated #2	47 ±3	56 ±3
uncoated #3	50 ±3	51 ±3
coated #1	---	100 ±5
coated #2	107 ±5	104 ±5
coated #3	100 ±5	100 ±5
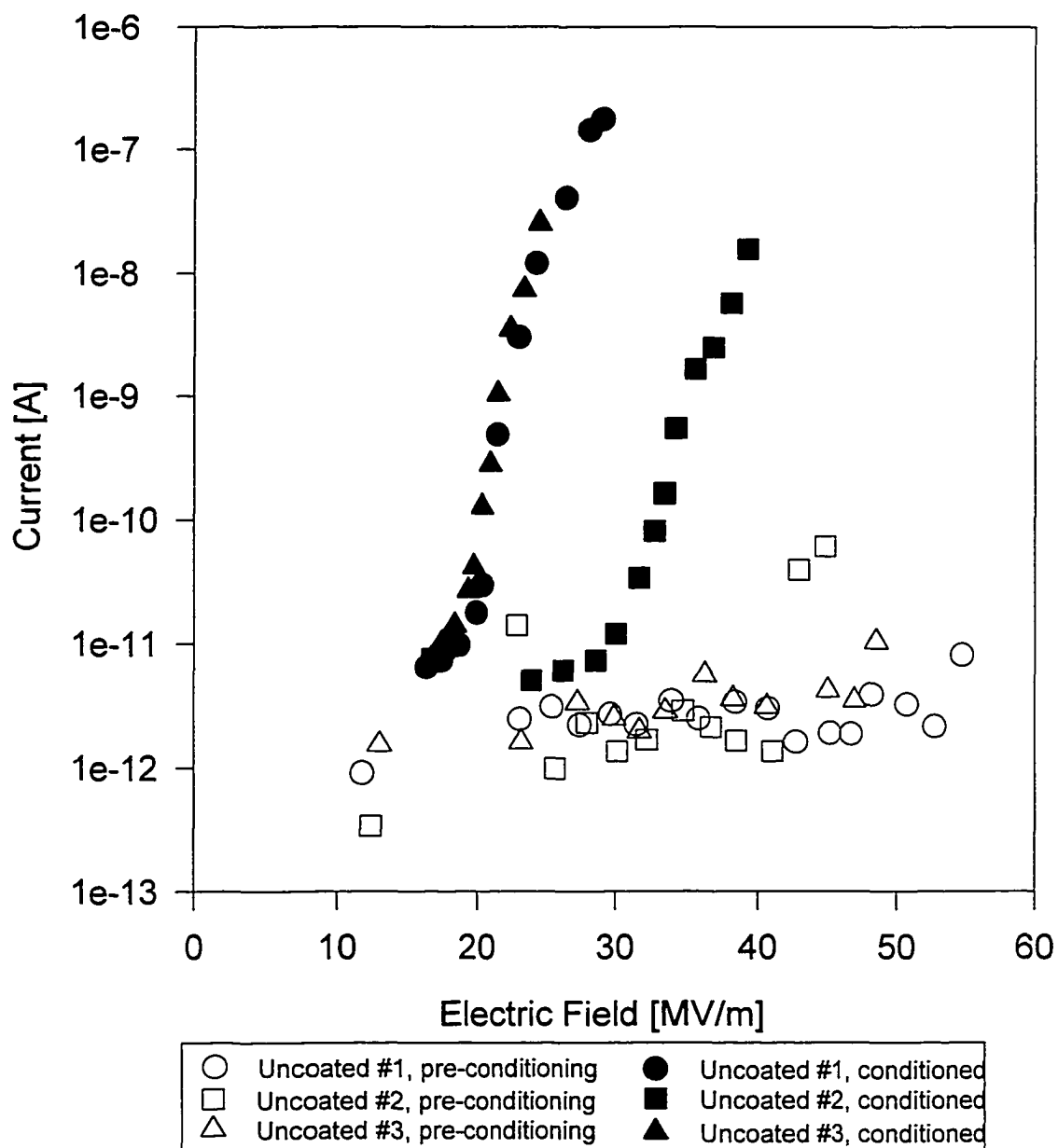
Figure 29. Electrical measurements before and after conditioning on three uncoated cathodes cleaned at Jefferson Lab.

B. Coated Cathodes with High-Pressure Water Rinsing

After coating the other three cathodes with 2µm of SiO$_x$ at 60Å/sec the same electrical measurements were made. The behavior of the samples was

very different to the uncoated samples and the breakdown fields were much higher than in any previous measurements.

In the pre-conditioning measurements the current levels were much larger than the uncoated samples. In all cases, especially in coated#2, the current initially rose very quickly as shown in Fig. 30. Then, at a certain field there would be a current spike after which the current would drop abruptly.

Samples coated#2 and coated#3 achieved very high fields before activation, where the current suddenly exceeded 1μA. (The activation field for sample coated#1 was not recorded due to a circuit fault, voiding data above 70MV/m.) After this discharge, however, the current dropped to its previous level of between 10^{-10} and 10^{-8}A. This did not fit well into our conditioning strategy which was to maintain a current level ~1μA during conditioning. It was decided to leave the field at the setting where it first exceeds 1μA for the same time as used in conditioning the uncoated cathodes. No further current spikes were observed during this conditioning period.

After conditioning, the current followed Fowler-Nordheim down to a current of ~10^{-12}A, the noise limit. At the high fields the current retraces its last path in Fig. 30 indicating that the conditioning discharge had little effect.

The breakdown fields for samples coated #2 and #3 were nearly identical to the activation fields of about 100MV/m. The breakdown field for coated #1 was also 100MV/m.
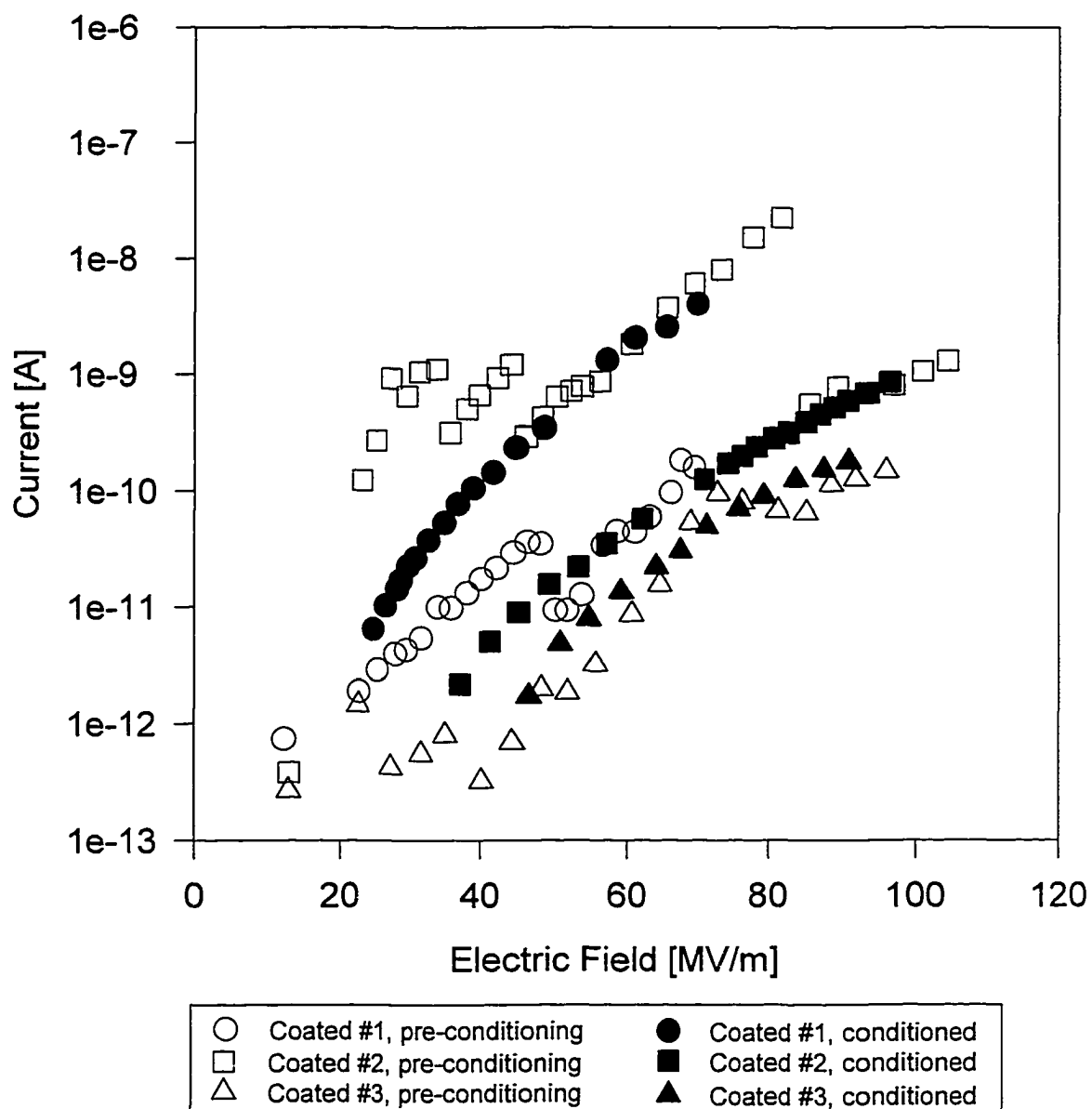
Figure 30. Electrical measurements before and after conditioning on three 2μm SiOₓ coated cathodes cleaned at Jefferson Lab.

The temporal development of breakdown was measured for two uncoated and two uncoated cathodes. In Fig. 31 the waveforms all appeared to be pulses. The rise time of the current is less than 1μs in each case. After tens of μs the discharges terminate. The peak current in each of the pulses is approximately

equal to the breakdown voltage divided by the 1100Ω series resistor indicating very little voltage drop across the gap, consistent with an arc. The uncoated pulses show a decay with the ~1ms RC time constant of the system. The coated waveforms show more complex behavior. One of coated samples has a pulse shape but with a faster decay time. The other coated waveform has an oscillating structure. Due to the pulse shape it appears that the discharge is self-quenching.
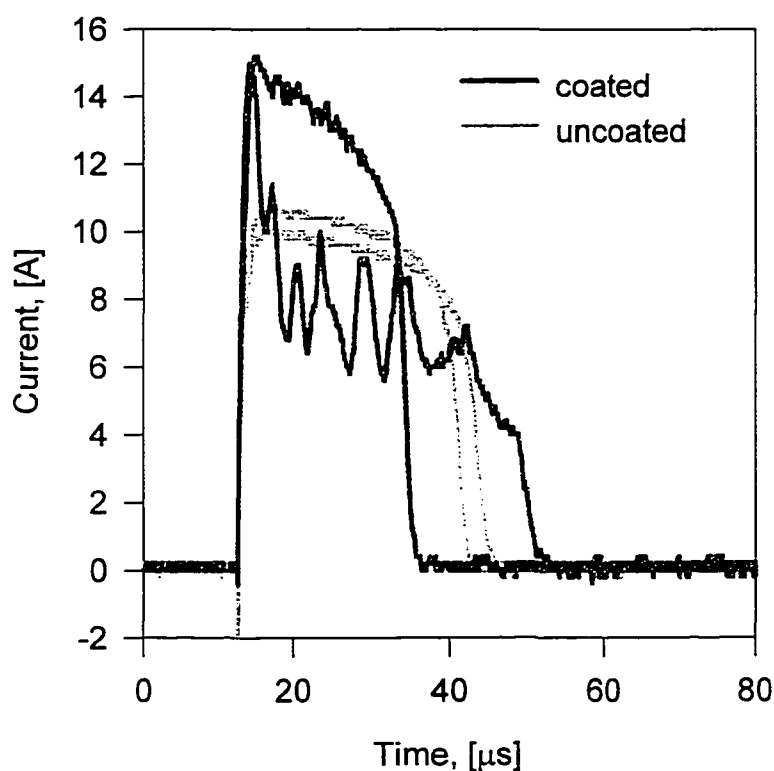
Figure 31. Current waveforms from two coated and two uncoated cathodes during breakdown.

C. Results from High-Pressure Water Rinsed Cathodes

The breakdown fields in the experiment, both for coated and uncoated cathodes, were very high. This is attributed to improved contamination control,

which removes any large particles from the cathode surface. Coated cathodes had a breakdown voltage nearly twice that of the uncoated cathodes as shown in Fig. 32.
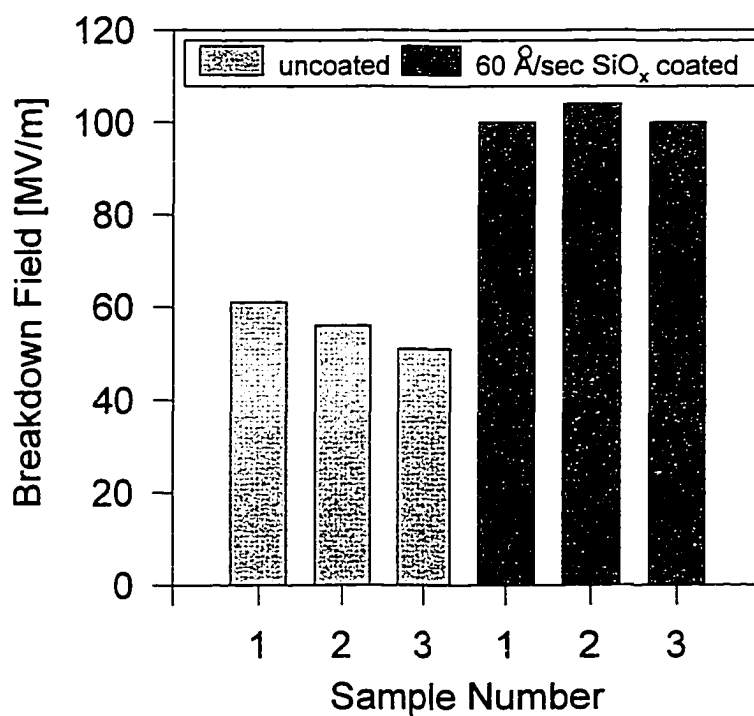
Figure 32. Breakdown voltages for uncoated and SiO$_X$ coated cathodes cleaned with high pressure, ultrapure water at Jefferson Lab.

The field emission currents after conditioning are reduced by two to four orders of magnitude at the highest measured field as shown by direct comparison in Fig. 33. At the breakdown field of uncoated cathodes (~50MV/m) the difference can be estimated to be between three and six orders of magnitude.
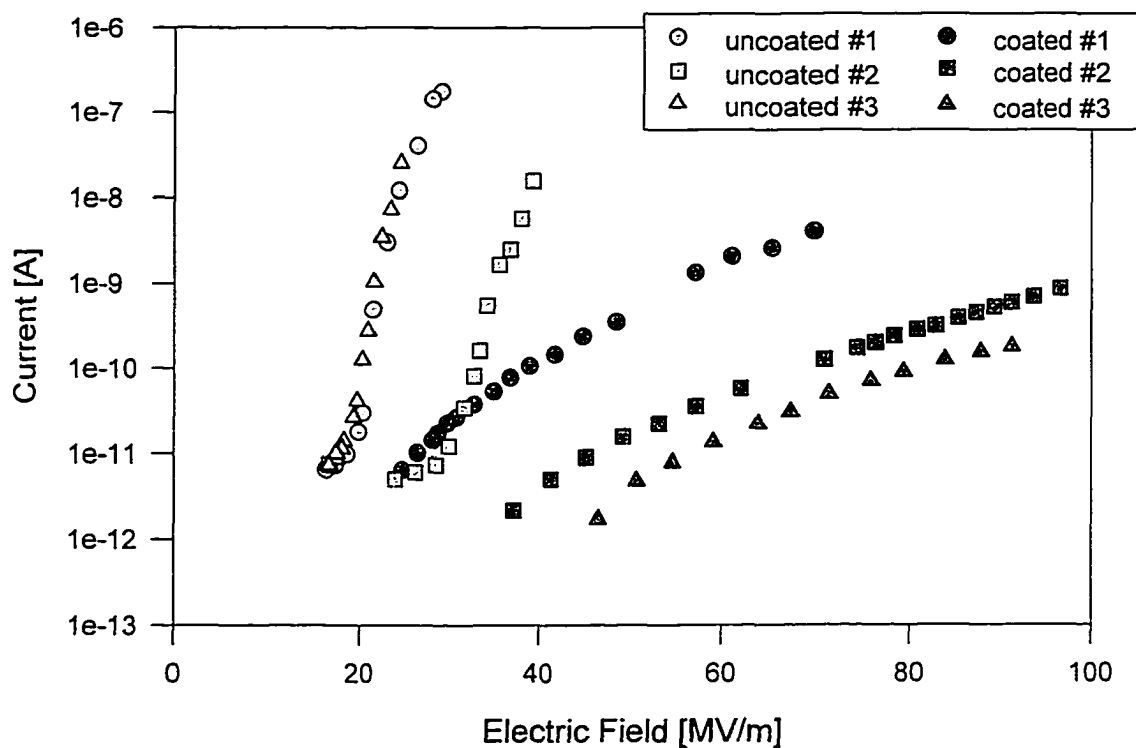
Figure 33. Comparison of the field emission currents of coated and uncoated cathodes after conditioning.

From Fowler-Nordheim plots the field enhancement factor and emitter area were determined. The Fowler-Nordheim plots for all six samples are shown in Fig. 34. The work function of stainless steel, 4.5eV, and the vacuum field were used in both the coated and the uncoated calculations, i.e., the effects of the coating on the Fowler-Nordheim equation were ignored. For the uncoated samples, data points below 10^{-11} A deviated from Fowler-Nordheim as previously discussed. With this exception the data forms straight lines indicating that the Fowler-Nordheim equation governs current flow in both the coated and uncoated cases. From linear regression the slopes and y-intercepts were found from

which the field enhancement factor and effective emitter area were calculated. These results are listed in Table 6.
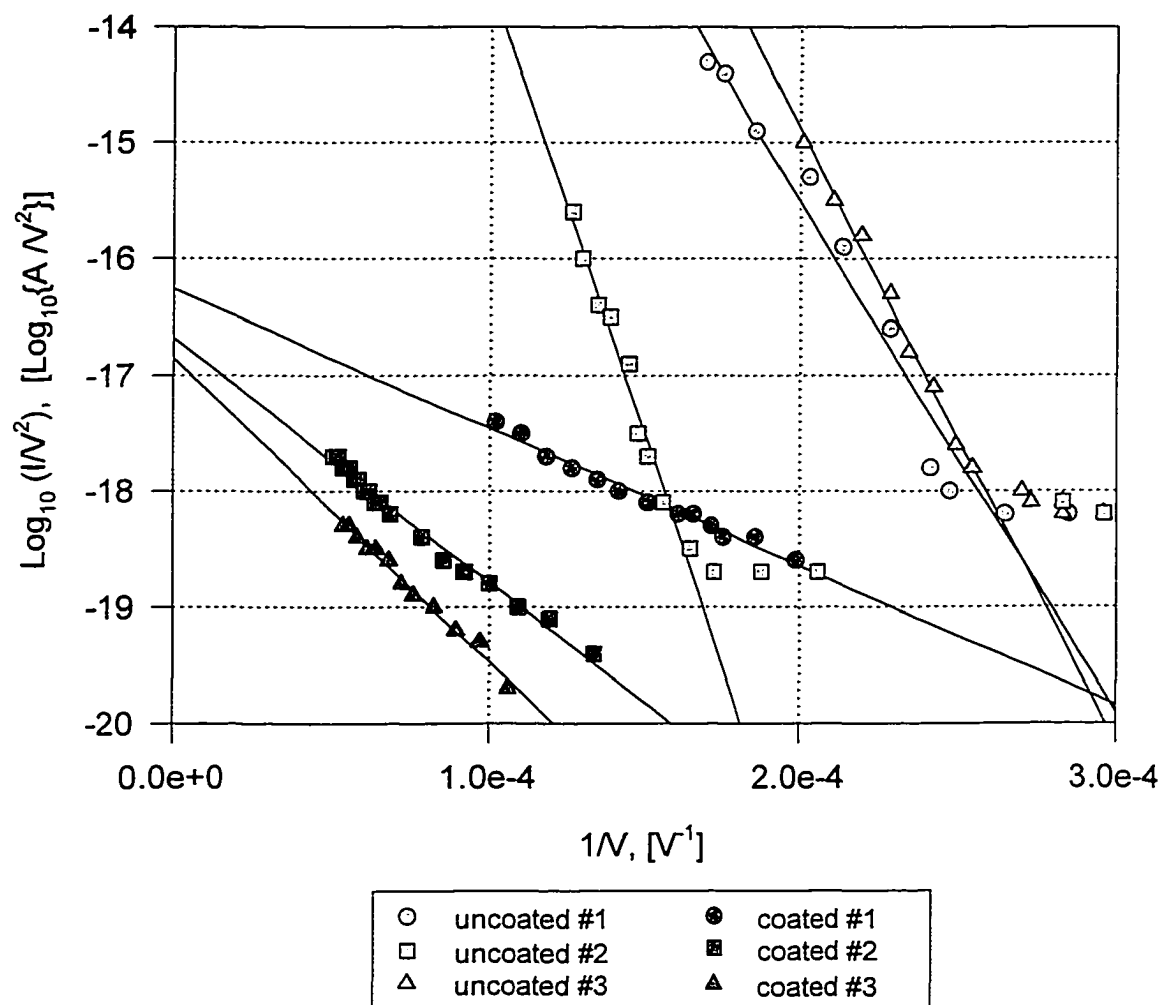
Figure 34. Fowler-Nordheim Plots of three uncoated and three SiO$_x$ coated cathodes.

Table 6. Calculated field enhancement factor and emitter area for uncoated and SiO$_x$ coated cathodes from slopes and y-intercepts of Fowler-Nordheim plots.

Sample	Slope [V·log$_{10}$(A/V^2)]	Field Enhance-ment Factor	Y-Intercept [log$_{10}$(A/V^2)]	Emitter Area [nm^2]	Corre-lation, r^2
uncoated #1	-35131	158	-8.48	1.687	0.960
uncoated #2	-78261	71	-5.83	3455	0.978
uncoated #3	-52996	105	-4.27	57350	0.993
coated #1	-12238	454	-16.17	3.86E-9	0.979
coated #2	-21058	264	-16.69	3.45E-9	0.987
coated #3	-26151	213	-16.84	3.78E-9	0.988

Although the anode damage spots appeared identical for both coated and uncoated electrodes, there were large differences in the cathode damage. The uncoated cathodes showed the typical trail of damage as observed in the preliminary experiment. The coated samples showed virtually no damage. In one sample no damage was visible to the unaided eye, and the other two samples had only a pinhole in the film.

To get a better view of the damage, one of the uncoated samples and the coated sample with no visible damage were taken to the SEM for a closer look. In Figs. 35, 36,and 37 pictures of the damage trail on the uncoated sample with increasing magnification is shown. It is clear that the trail actually consists of a series of pits in the surface with raised, rounded edges. It is probable that molten metal spewed from one pit is sprayed onto the nearby cathode surface. This new debris then has enhanced emission due to both the high temperature and field enhancement. The new spot then vaporizes and the trail continues.

After scanning the surface of the coated cathode the damaged area was located, shown in Fig. 38. There were two pinholes in the film about 300µm

apart. Close-ups of each pinhole are shown in Figs. 39 and 40. Both pinholes are about 15µm in diameter. It appears that the hole stops at the metal surface and the underlying metal was undamaged. The sides of the hole are sloped outward and smooth.
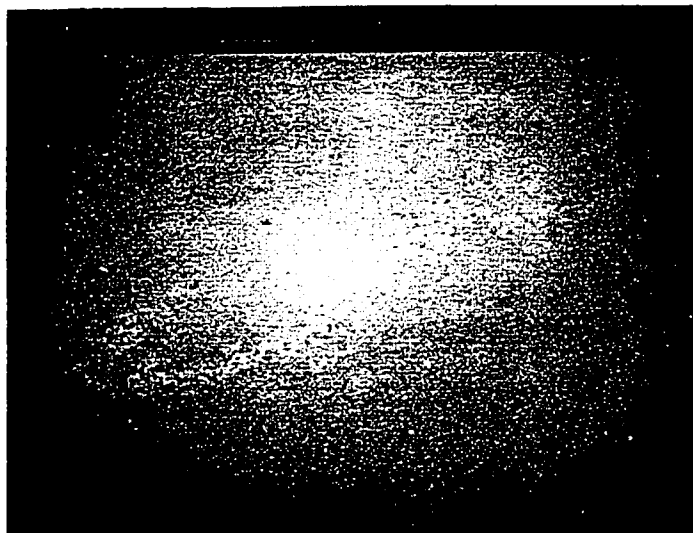
Figure 35. Damage trail on uncoated cathode 27.4X.
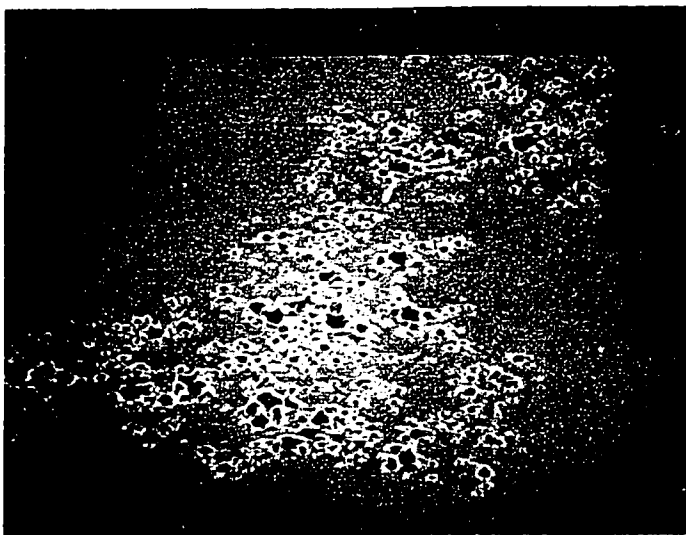
Figure 36. Damage trail on uncoated cathode 241X
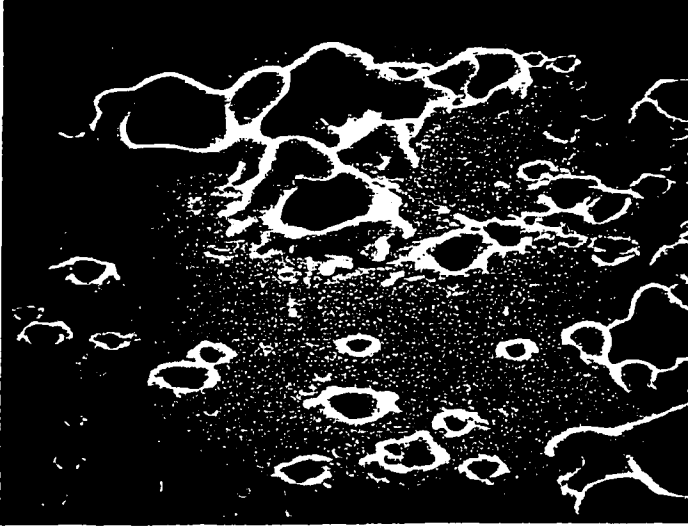
Figure 37. Damage trail on uncoated cathode 2100X

Figure 38. Two pinholes in SiO$_x$ cathode coating after breakdown measurement.

Figure 39. A closer look at the upper pinhole in Fig. 38.
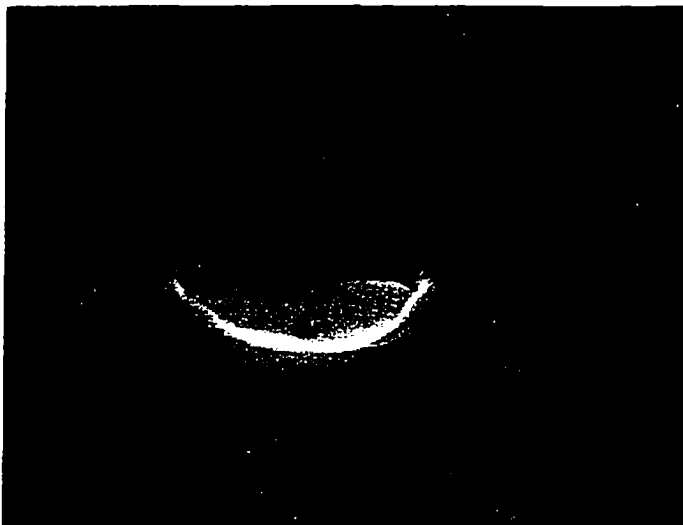
Figure 40. A closer look at the lower pinhole in Fig. 38.

Dependence of Electron Emission and Breakdown on Preparation, Conditioning, History (Prior to Breakdown), Coating, and Annealing of the Sample

In follow-up experiments some variations of the experiment were tested in order to achieve higher breakdown fields, to help explain the nature of the electron emission, to show long-term stability, and to demonstrate effectiveness after high temperature treatment. First, the cathode preparation procedure was changed to give higher breakdown voltages and reduced field emission. Second, the role of conditioning was investigated. Third, the effects of prior breakdown were measured. Next, the effects of coating a known emitter were measured. Finally, we determined the effects of high temperature treatment on field emission and breakdown.

A. Effect of Improved Cathode Preparation

The high breakdown strength of the high pressure, ultra-pure water rinsed cathodes indicates good surface quality. However, higher breakdown voltages

were found using a cleaning procedure involving ultrasonic cleaning in a series of solvents followed by a blow dry as described in Chapter V. The breakdown strength of these samples, both coated and uncoated, exceeded those cleaned with high-pressure ultrapure water rinsing and also exceeded the breakdown strengths quoted in any publications we could find.

The first sample to be discussed, sample#4, was cleaned and left uncoated. This sample was tested in an identical manner the ultra-pure water rinsed samples. An interesting result from this sample in particular was a slow "activation" as shown in Fig. 41. The pre-conditioning current exceeded 1μA at a field of 58.6MV/m.
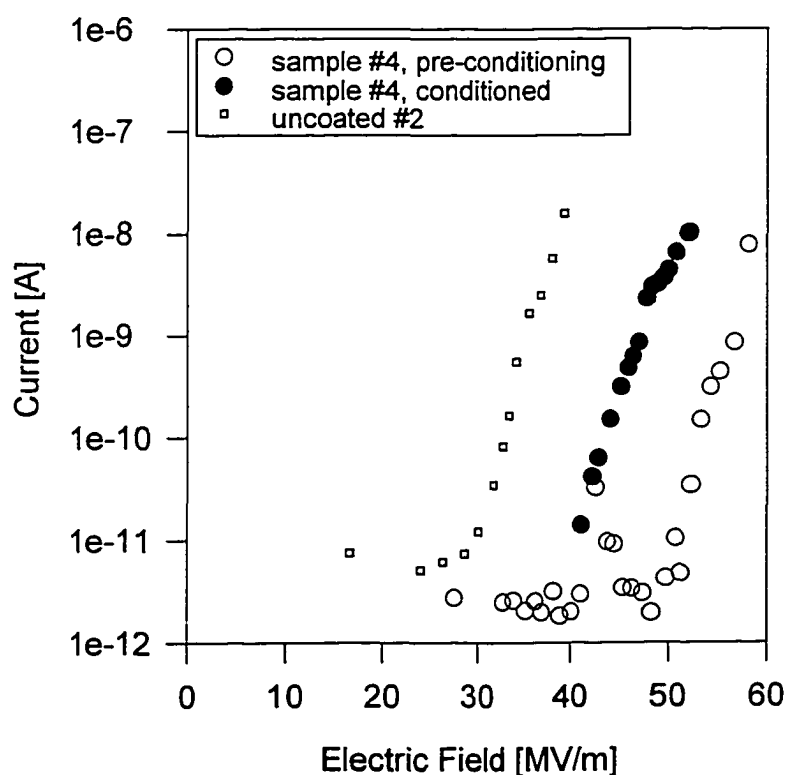
Figure 41. Electrical measurements on sample #4 before and after conditioning along with sample uncoated #2 (high-pressure ultrapure water rinsed) for comparison.

Fowler-Nordheim plots, shown in Fig. 42, indicate that both the pre-conditioning currents (above 50MV/m) and currents after conditioning are due to field emission. There is a change in the emitter area and β after conditioning. Before conditioning, the emitter has an area, A= $1.32 \cdot 10^{12}$ nm^2=1.32 mm^2 and an enhancement factor, β=26. After conditioning, the area is reduced to A=7062 nm^2 but the enhancement doubles to β=52.

The emission level after conditioning is much lower than that of previous measurements. For comparison, the conditioned measurement on the best of the high-pressure ultrapure water rinsed samples, uncoated #2, is also shown in Fig. 41. The breakdown field for sample #4 was 69.2MV/m. This is an almost 15% increase over the best result from the previous measurements with uncoated samples.

B. Effect of Conditioning

The breakdown strength of a second uncoated cathode, sample#9, was measured. The activation field of this cathode was highest we have measured at 65.5MV/m. After conditioning, however, the current was high even at low field as shown in Fig. 43. A Fowler-Nordheim plot of the conditioned current revealed a very high enhancement with β=264 and a small area A=55.9nm^2. The breakdown field of sample#9 was disappointingly low at 27.5MV/m, less than half the activation field.
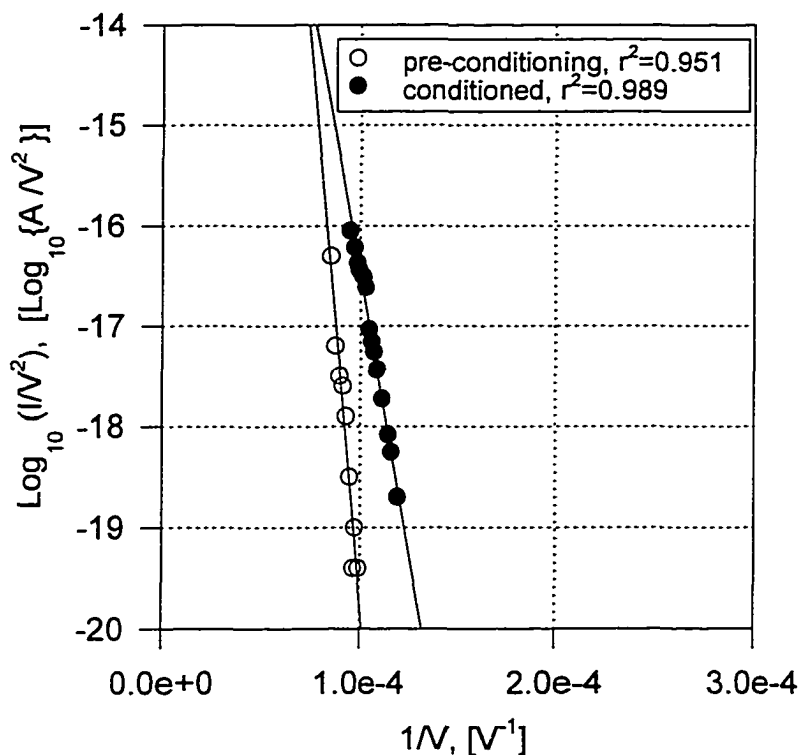
Figure 42. Fowler-Nordheim plots of sample #4 before and after conditioning.

Figure axes: y-axis: Log_{10} (I/V^2), $[\text{Log}_{10}\{A/V^2\}]$ with values -14, -15, -16, -17, -18, -19, -20. x-axis: $1/V$, $[V^{-1}]$ with values 0.0e+0, 1.0e-4, 2.0e-4, 3.0e-4.

Legend:
- ○ pre-conditioning, $r^2=0.951$
- ● conditioned, $r^2=0.989$

This result indicates a limitation of conditioning with well-cleaned surfaces. Although a very large series resistor was used while conditioning, the sample was damaged. It is unclear whether using a larger resistance would be a solution. At the higher voltage at which activation occurred there might have been enough energy stored in even the small capacitance of the gap and the high voltage cable to damage the surface when discharged.

Conditioning may not be necessary with coated electrodes and may actually have adverse effects. Conditioning of a coated electrode by raising the current above 10^{-6} A/cm^2 results in a puncture of the film. There is also damage to the anode during conditioning. An anode spot, small but otherwise very
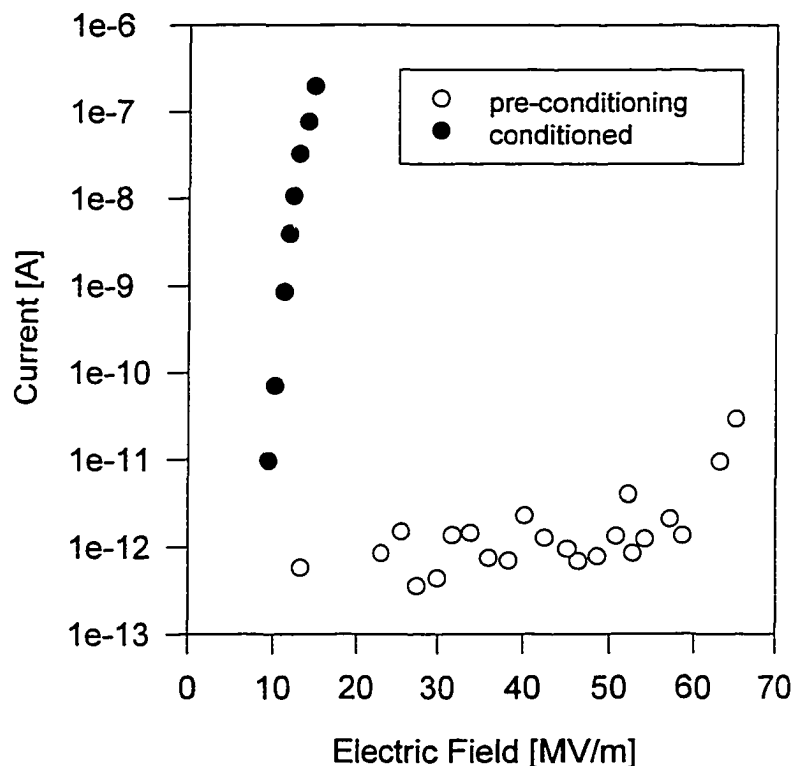
Figure 43. Electrical measurements on sample #9 before and after conditioning.

similar in appearance to the anode spots resulting from breakdown, appears after every discharge in the conditioning circuit. Both coated and uncoated cathodes show small anode spots after conditioning.

A closer look at a typical anode spot from a previous experiment was made with the SEM. As shown in Fig. 44, the spot is round with a diameter of approximately 400μm. At high magnification the center of the anode spot shows extensive damage and appears to have melted and re-solidified leaving micron-sized projections and ridges as shown in Fig. 45.

Sample#2 was used to check the long-term stability of coated cathodes under stress with no conditioning. The field was raised to 80MV/m while observing the current. This field is above the maximum achieved with an
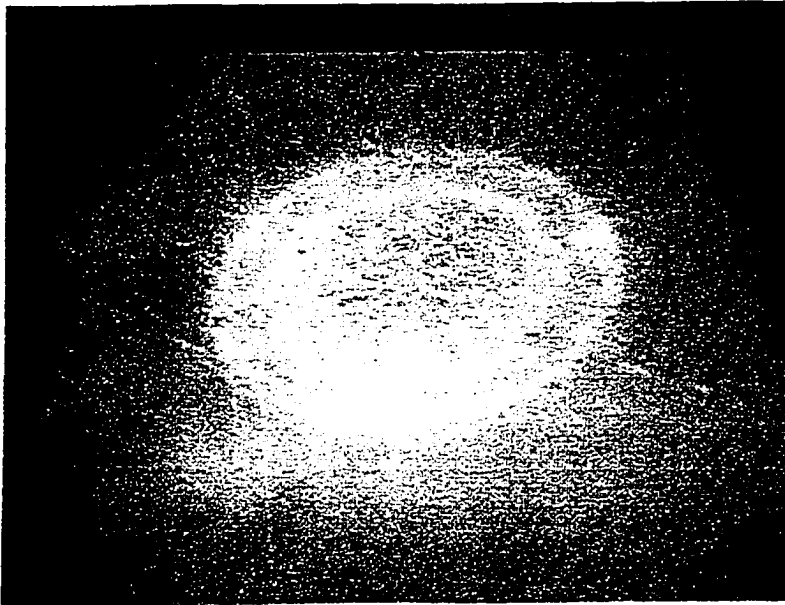
Figure 44. Typical anode spot which results from electrical conditioning.
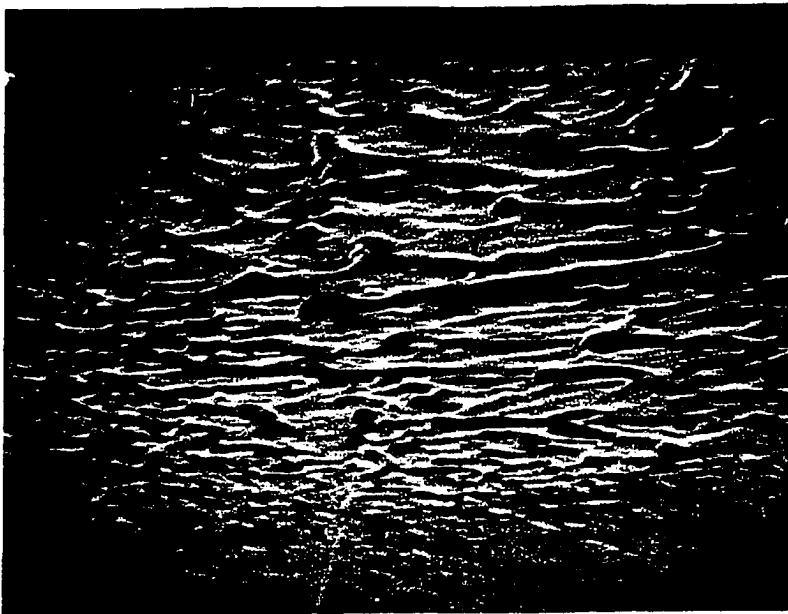
Figure 45. A closer look at the anode spot reveals micron-scale projections and ridges.

uncoated cathode but less than the expected breakdown strength of a coated cathode. The current of ~1nA was monitored while keeping the field constant.

With uncoated cathodes without conditioning the current at high fields is known to be unstable. Activation of an emitter can occur after several minutes,

hours, or days. To ensure that no kind of activation would occur with sample #2, a constant field of 80MV/m was applied for several days while taking current readings once per second.

No discharges were observed after applying a continuous field of 80MV/m for four days. The current remained in the range from 1 to 4nA during the entire period. The first 4½ hours of data are shown in Fig. 46. These results indicate that electrical conditioning is not required for SiO_x coated cathodes. Also, anode and cathode damage is avoided by not conditioning which may substantially improve performance with large gaps.
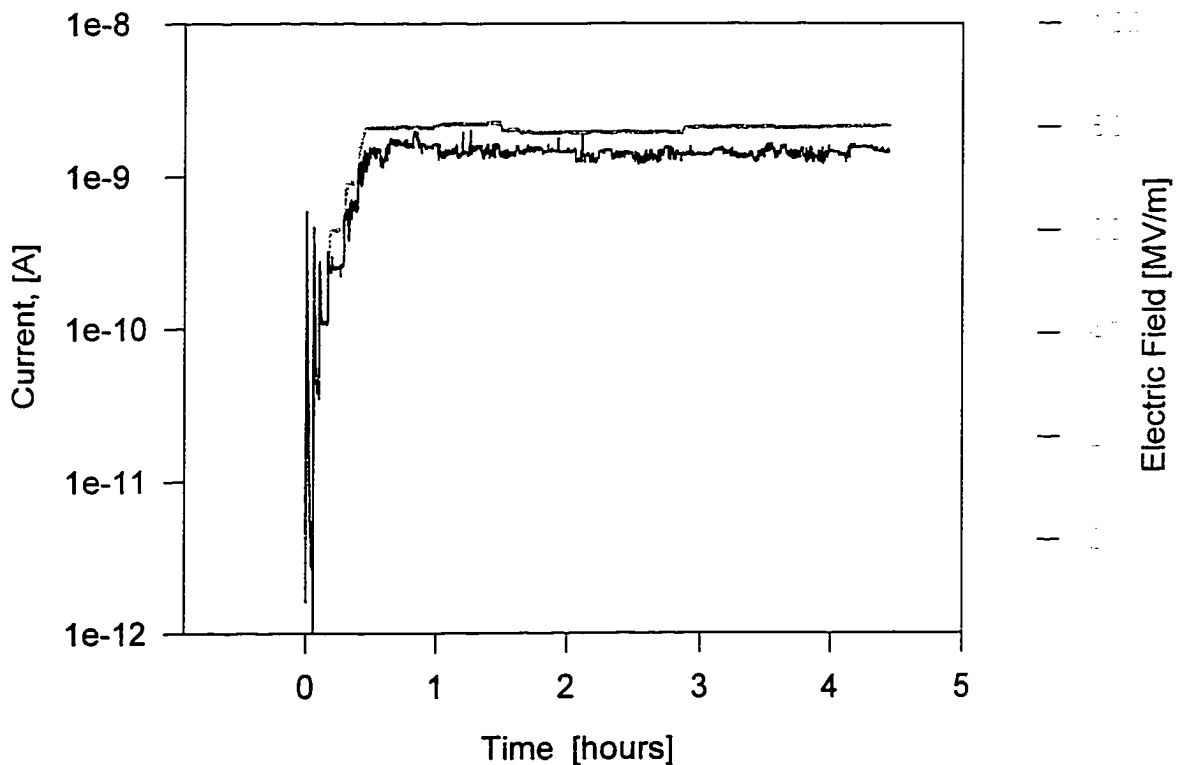
Figure 46. First 4.5 hours of four day, long term, high field test of a non-conditioned, coated cathode.

C. Effect of History (Previous Breakdown)

Sample #12 was cleaned then coated with $2\mu m$ of SiO$_x$ and tested in the usual way except that a $101\mu m$ gap was used. This sample also gave higher breakdown strength, 137MV/m, than the high-pressure ultrapure water rinsed samples. The increased breakdown field after coating cathodes cleaned in our lab from ~70MV/m to ~140MV/m verifies that the effect of the coating is to approximately double the breakdown field. This effect of doubling the breakdown field appears to be independent of the cathode preparation.

The current measurements before and after conditioning, shown in Fig. 47, display the same general behavior as the Jefferson Lab cleaned samples. The limiting of the current to ~10^{-6} A was due to the MOV surge protector. The Fowler-Nordheim plot, shown in Fig. 48, gives the typical large enhancement factor, β=108, and impossibly small area, A=$3.96 \cdot 10^{-4}$ nm^2. There was some deviant behavior observed below for currents below ~10^{-9} A where the slope changes in the Fowler-Nordheim plot. The change is to an even smaller area and higher enhancement. The reason for the shift is not known.
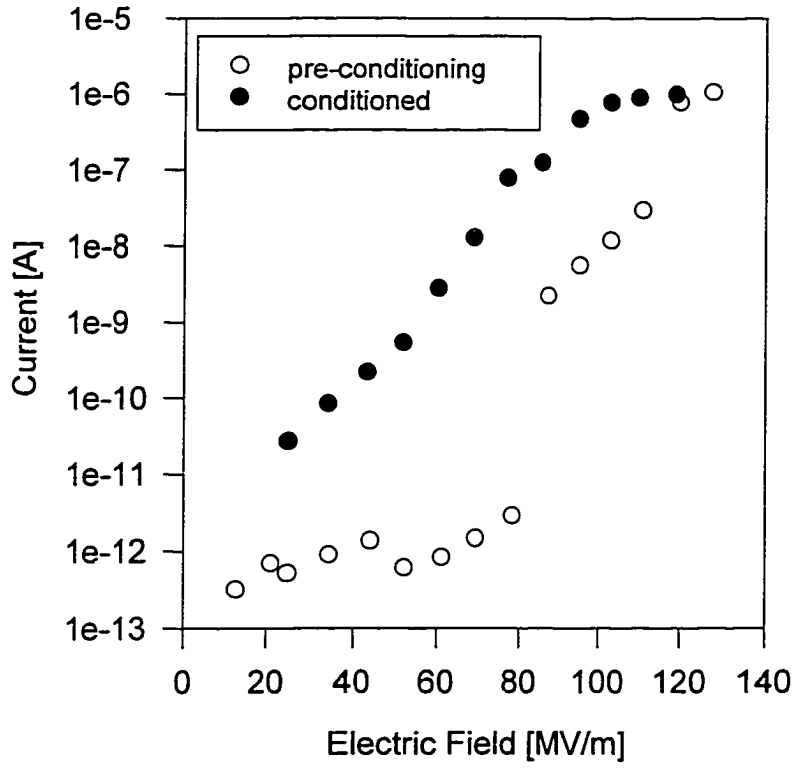
Figure 47. Electrical measurements on sample #12 before and after conditioning.
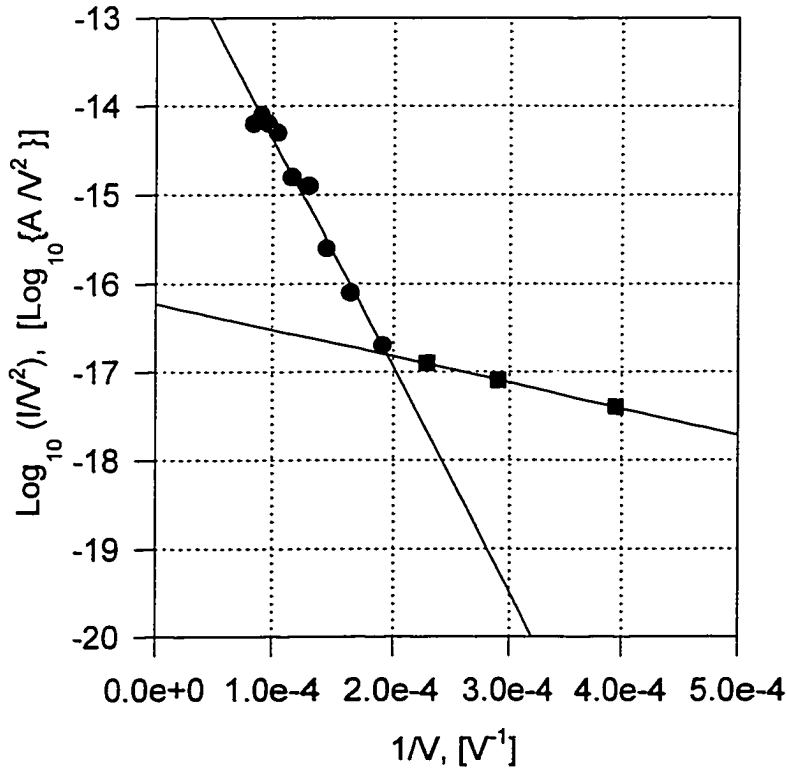
Figure 48. Fowler-Nordheim plot of sample #12.

After the first breakdown measurement, which gave a breakdown field of 137MV/m, we re-measured the breakdown voltage. With uncoated samples the second measurement of the breakdown field is usually no more that ~25% of its original value. The second measurement with sample#12 gave a breakdown field of 100MV/m. This result shows that even after discharging the ~50J of energy stored in the capacitors and conducting more than 10A for several μs the SiO_x coated cathodes can still withstand up to about 75% of the original breakdown voltage. The breakdown measurement was repeated several times in quick succession and each time the voltage was reduced by about 25%. Even after ~10 breakdown events a steady field of ~80MV/m could be restored by slowly raising the applied field. Even after breaking down several times the SiO_x cathode outperforms an uncoated cathode.

D. Effect of Coating

In this experiment the idea was to condition an uncoated cathode, calculate A and β from a Fowler-Nordheim plot, coat with SiO_x, then re-measure A and β. From these measurement we gain insight into the emission mechanism.

The experiment was conducted with sample #13 that was damaged during an attempt to condition using pulsed voltages. A damaged area was clearly visible on the cathode surface. The damage was also evident from the high currents in electrical measurements taken after the damaged area was created which is shown in Fig. 49. The Fowler-Nordheim plot, shown in Fig. 50, of this data yields a large enhancement, β=96, and a small effective area,

$A \approx 0.07 nm^2$. This data suggests that the dominant field emitter is a large, sharp protrusion from the cathode. (Note that the value of A has some uncertainty due to the poor linearity of the data, the actual value may be 10-100 times larger)
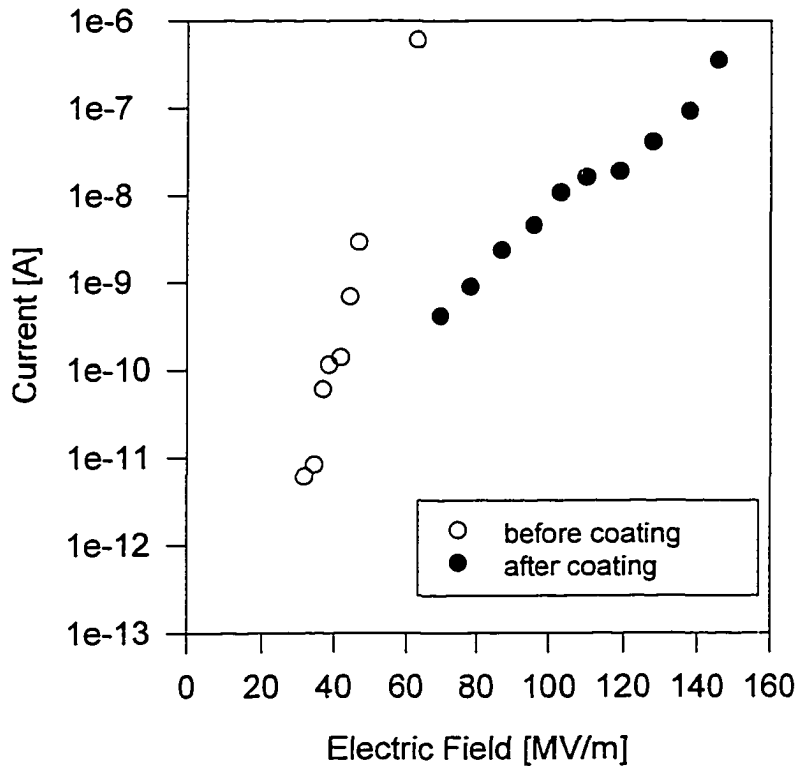
Figure 49. Electrical measurements on sample #13 before and after coating with 2μm SiOx.

Sample #13 was then coated with 2μm of SiOx. Electrical measurements taken while increasing the voltage after coating show a markedly reduced emission as shown in Fig. 49. The activation field of the coated cathode, which is known from previous experiments to be nearly the same as the breakdown field, was 146MV/m which was the highest field achieved in all of our experiments.
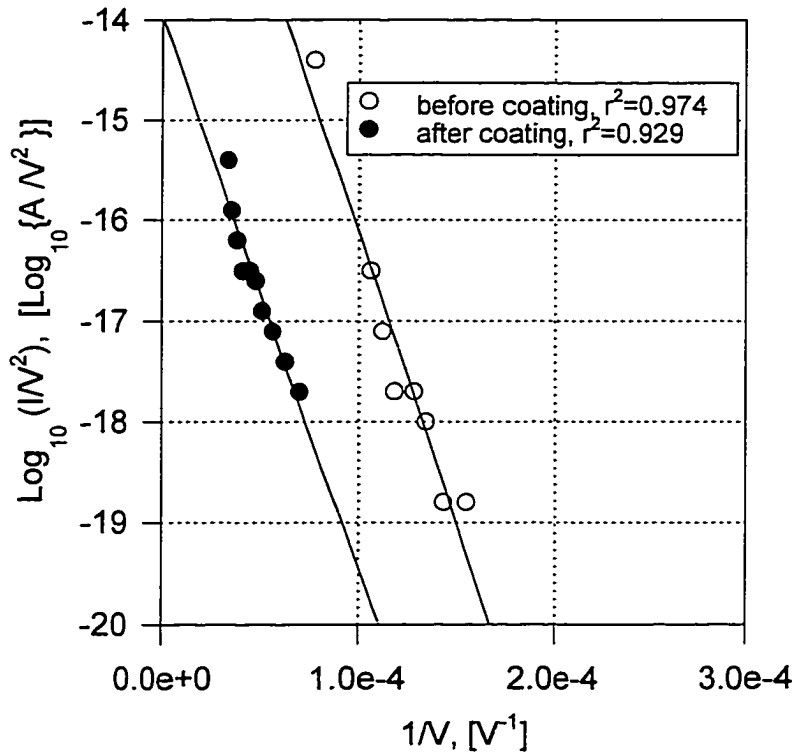
Figure 50. Fowler-Nordheim plots of sample #13 before and after coating.

The Fowler-Nordheim plot of sample#13 before and after coating is shown in Fig. 50. Because a 4mil gap was used in the measurements after coating, the voltage in Fig. 50 was adjusted [multiplied by two] so that a direct comparison with the uncoated measurements with an 8mil gap could be made. The calculated area, $A=1.3 \cdot 10^{-5} nm^2$, is much larger than the high-pressure ultrapure water cleaned samples, but still non-physical. Also, the enhancement factor was much lower, $\beta=102$, than the high-pressure ultrapure water rinsed samples.

Compared with the data before coating, the apparent area is reduced by approximately three orders of magnitude. The field enhancement factor, however, appears almost unchanged as evident from the nearly identical slopes in Fig. 50.

E. Effect of Annealing

In some applications the cathode must be raised to elevated temperatures. To achieve vacuum pressures in the 10^{-10} torr range the vacuum chamber is usually baked at 300°C. Some systems such as the photoelectric electron injector at Jefferson Lab require temperatures up to 600°C. The SiO_x coating can be deposited and annealed at up to 300°C. At higher temperatures the film may crack due to internal stress. Sample #2, undamaged from the previous experiment, was used to test resistance to 600°C temperatures.

The sample was heated in a diffusion oven in air with no gas flow. The heating was done in three steps. First, the sample was raised to 400°C for about 30 minutes then cooled. No damage to the film was observed. Next, the temperature was raised to 500°C for 30 minutes then cooled. There was no cracking of the film but the color of the film had lightened from brown to gold. Finally, the sample was raised to 600°C for 30 minutes. After heat treatments the film appeared undamaged but the color shift from brown to gold indicated some changes in the structure of the film had occurred. The possible reasons for the color shift are oxidation of the film and annealing out of a color center. Oxidizing silicon requires temperatures above 1000°C, so these temperatures are too low for this effect. Annealing of deep centers is then the most likely explanation.

To test the effect of the heat treatment on the electrical properties, the cathode was placed in the conditioning system and the field was raised until breakdown. The current, shown in Fig. 51, was lower than before the heat

treatment. The current at 80MV/m was ~2·10^-10 A, which is ten times lower than the current before the heat treatment. From the Fowler-Nordheim plot in Fig. 52 the area is $2.8 \cdot 10^{-4}$ nm^2 which is typical, but the enhancement, β=70 is lower than other coated samples. Breakdown occurred at a field of 145MV/m, which is one of the highest fields measured.

Heating of the SiO$_x$ coating to 600°C did not damage the film. The only obvious change was a lightening of the color from brown to gold probably due to annealing of traps. The field emission current was lowered by the heat treatment and the breakdown field was one of the highest measured. This experiment suggests that heat treatment may be beneficial for SiO$_x$ cathode coatings.
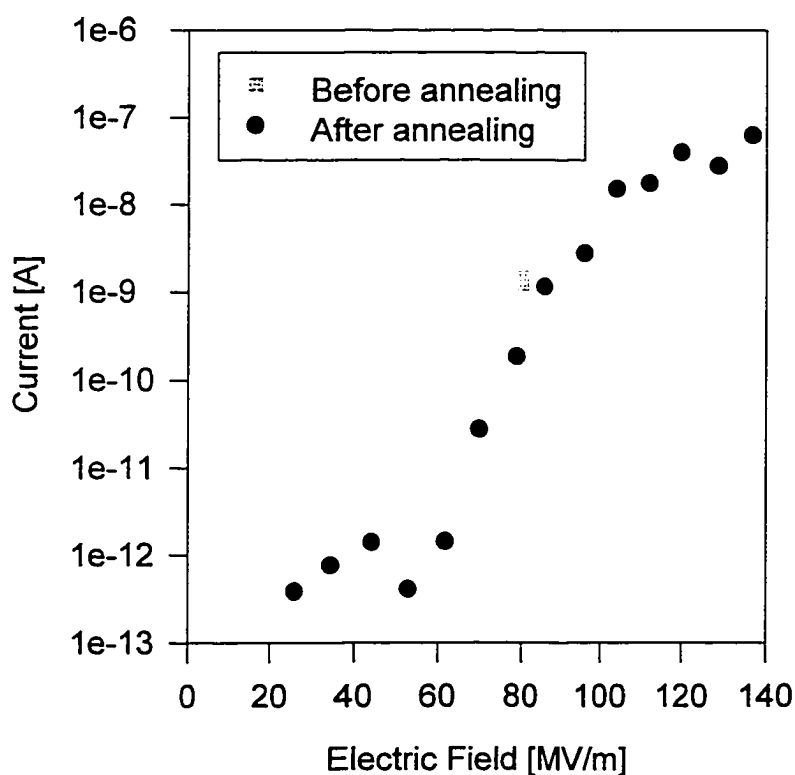
Figure 51. Electrical measurements on sample #2 after annealing to 600°C along with current measured at 80MV/m before annealing.
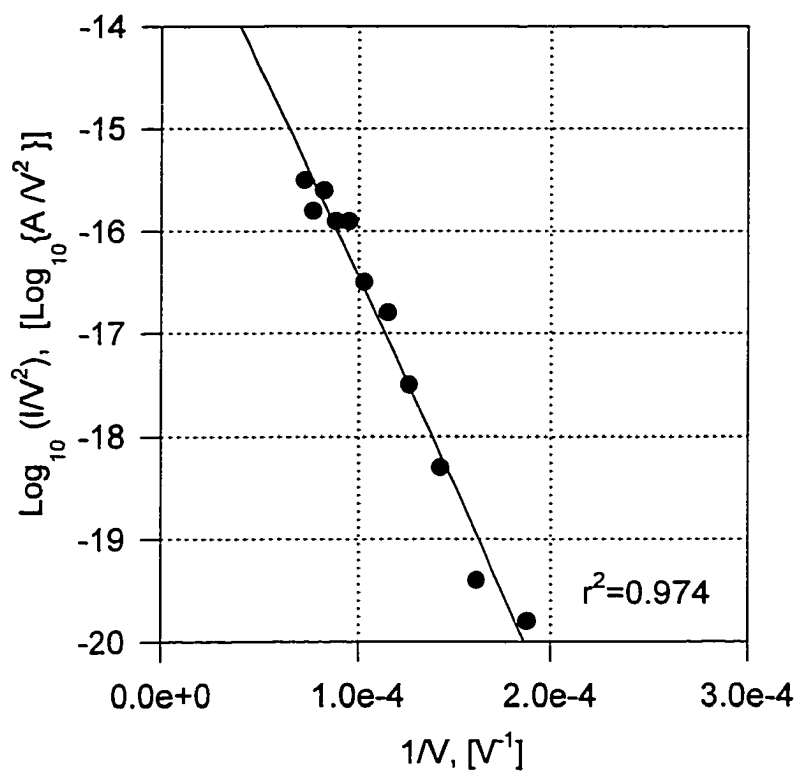
Figure 52. Fowler-Nordheim plots of sample #2 after heat treatment.

The plot shows $Log_{10}(I/V^2)$, $[Log_{10}\{A/V^2\}]$ versus $1/V$, $[V^{-1}]$ with $r^2=0.974$.

CHAPTER VII

ELECTRICAL MEASUREMENTS OF SiO_x PROPERTIES

The variable properties of SiO_x made it desirable to make electrical measurements of the film properties. By creating SiO_x capacitors we were able to determine the dielectric constant, resistivity, breakdown field, and electrical behavior of the film. This information will be useful in analyzing the electron emission from SiO_x coated electrodes in vacuum.

Measurement of Basic Properties of SiO_x Films

Controlled deposition of SiO_x using a thickness monitor is complicated by the variable relationship between the deposition rate and film density. Independent measurement of film thickness is required to determine the film deposition rate. In our research a SEM was used to measure film thickness by scraping away the film along the edge of a cathode disk with a razor. This is not an ideal method since there is some distortion of the SEM image due to charge build-up on the insulator. However, measurements could be made because the films are not perfectly insulating. An example SEM of a scraped edge is shown in Fig. 53. The accuracy using this method is estimated to be $\pm 0.05 \mu m$.

Five coated stainless steel cathode disks were used for electrical measurements of film properties; three samples deposited together at ~20Å/sec (samples #3, #4, and #5), and two samples deposited together at ~60Å/sec (samples #31 and #32). Although the coatings used in the vacuum experiments

Figure 53. SEM image of the scraped edge of a SiO_x film used to measure film thickness showing scraped metal (bottom), edge of the film (middle) and film surface (top).

described in this dissertation were grown at 60Å/sec, the data from the 20Å/sec samples is presented for comparison. The basic material properties determined for each group of films is given in Table 7.

Table 7. Basic material properties from two sets of SiO_x films.

Property	Method	Samples #3,4,5	Samples #31,32
Thickness [μm]	Measured	0.81±0.05	2.29±0.05
Deposition Time [sec]	Measured	338±2	347±2
Capacitance [F/cm²]	Measured	4.48E-9 ±1%	1.97E-9 ±1%
Deposition Rate [Å/sec]	Calculated	24 ±7%	66 ±3%
Dielectric Constant	Calculated	4.1 ±7%	5.1 ±3%

Measurement of the Current-Voltage Characteristics of SiO$_x$ Films

In order to make electrical measurements metal contacts were deposited on the samples. In the case of samples #3, #4, and #5, four aluminum contacts were deposited on each sample forming SiO$_x$ capacitors. Each contact had an area of 0.495cm^2 and a thickness of ~1μm. Sample #31 had seven gold contacts each with an area of 0.178cm^2 and a thickness of 227Å. Sample #32 was tested using water as a contact in order to preserve the sample for measurements in vacuum. (Because of water evaporation this method was abandoned) Later, seven aluminum contacts were placed on sample #32 each with an area of 0.178cm^2 and a thickness of 0.282μm.

The current-voltage characteristics were measured by applying voltage to the substrate and to one of the contacts using a mechanical connection. The measurement is essentially a measurement of the leakage current of the SiO$_x$ capacitors. The current was measured using an electrometer with picoampere resolution. The applied voltage was measured using a DMM. A resistor (1 to 10MΩ) was placed in series to protect the power supply and electrometer in case of breakdown. The voltage across the limiting resistor was later calculated and subtracted from the applied voltage to determine the voltage across the sample. The applied voltage was in the range of from 0 to 100V. The polarity was chosen so that the stainless steel substrate was the cathode and the evaporated contact the anode in order to make comparisons to the vacuum measurements.

Of the 12 capacitors formed on samples #3, 4 and 5 only two on sample #5 gave results. The other 10 capacitors became completely shorted with only

small voltages, ~10volts, applied. The reason for the poor performance of these samples was a combination of contamination and too thin (<1μm) of a SiO$_X$ film. However, the two good capacitors, labeled 5a and 5d, remained highly resistive over the entire voltage range. The current-voltage data from these samples, shown in Fig. 54, show close agreement between the data from samples 5a and 5d with the curves overlapping in the medium and high range of voltage.
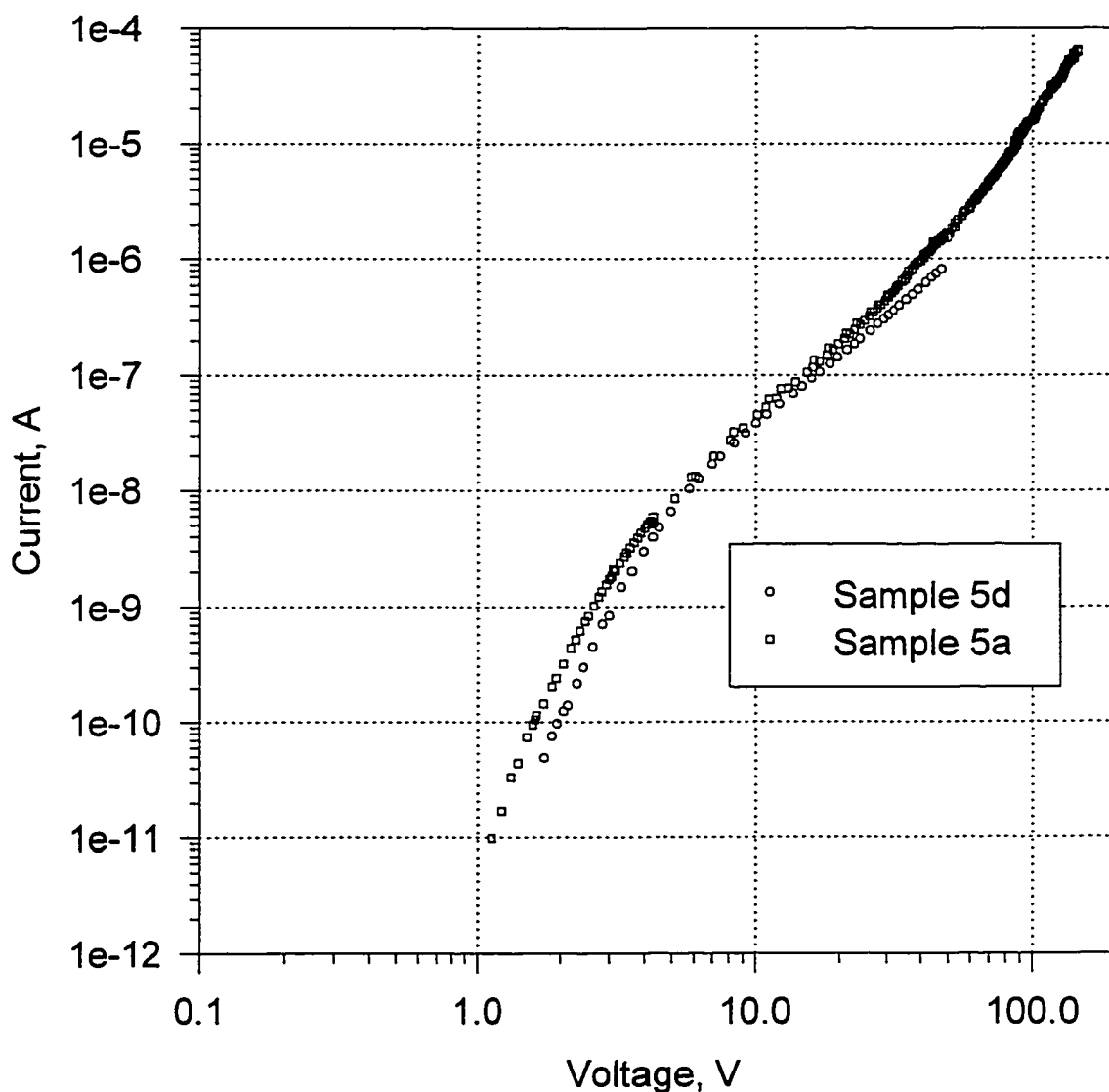
Figure 54. Current-voltage measurements of samples 5a and 5d.

Samples 31 and 32 showed similar behavior as sample 5 when the difference in thickness is taken into account. The data from each of the seven contacts on sample 31 (labeled 31a-g) is shown in Fig. 55. Each of the samples withstood the full range of applied voltage with no sign of breakdown except sample 31b. Sample 31b demonstrated a form of "conditioning" as the breakdown voltage increased with successive breakdown events. The breakdown was marked by a transition into a negative differential conductivity mode typical of a localized high current region or filament. Breakdown events occurred at 7 and 40 volts as shown in Fig. 56. It is assumed that the recovery is due to a high current density in the breakdown region, which caused localized damage to either the contact or the film that, upon cooling, assumed a high resistivity. Also shown in Fig. 56 is the reversed biased I-V curve. The reversed biased results are almost exactly identical to the forward biased curve.

The I-V characteristics of Sample 32 were measured first with a water contact and then after depositing aluminum contacts. A comparison of the data with a water contact and with an aluminum contact is shown in Fig. 57 with a curve from sample 31 included for reference. With the water contact the data was similar to a metal contact up to about 1volt, beyond which the sample appears have shorted. It is likely that another measurement would have
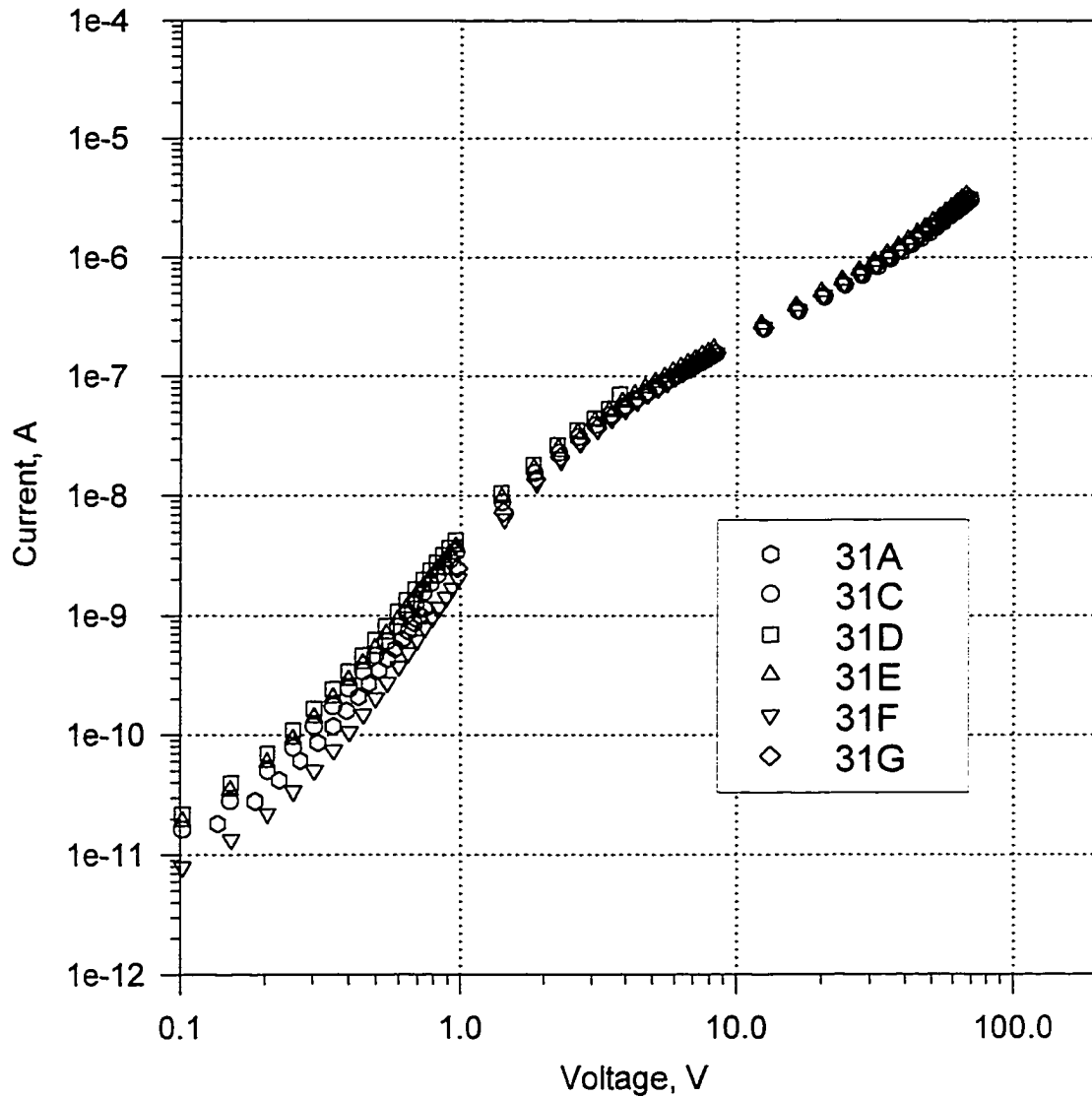
Figure 55. Current-voltage characteristics of samples 31a-g.

produced data similar to that of a metal contact. Unfortunately, this was the only data taken with a water contact. The data for the aluminum contact appears similar to that taken from sample 31 especially at the higher voltages.
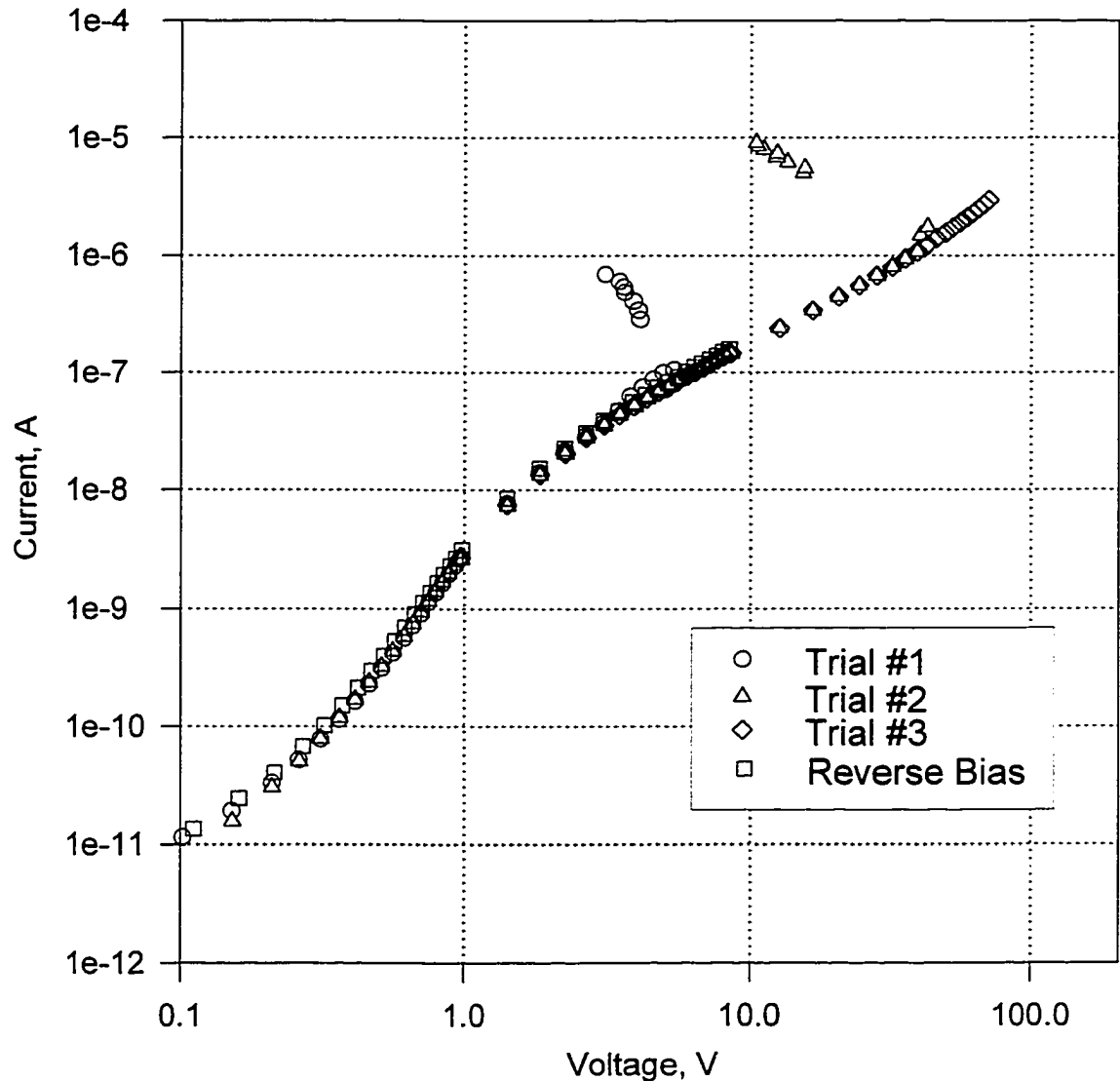
Figure 56. Breakdown and recovery behavior.

Current Vs. Temperature Measurements

To gain more information about the conduction mechanisms in these films the current vs. temperature characteristics were measured. This measurement is useful because many conduction mechanisms have a temperature dependence from which characteristics of the film can be determined. In the

cases of Frenkel-Poole and Schottky emission an arrhenius plot can be used to determine the activation energy or barrier height involved.

A hot plate was used in this measurement to vary the sample temperature. A constant voltage was applied while the temperature was
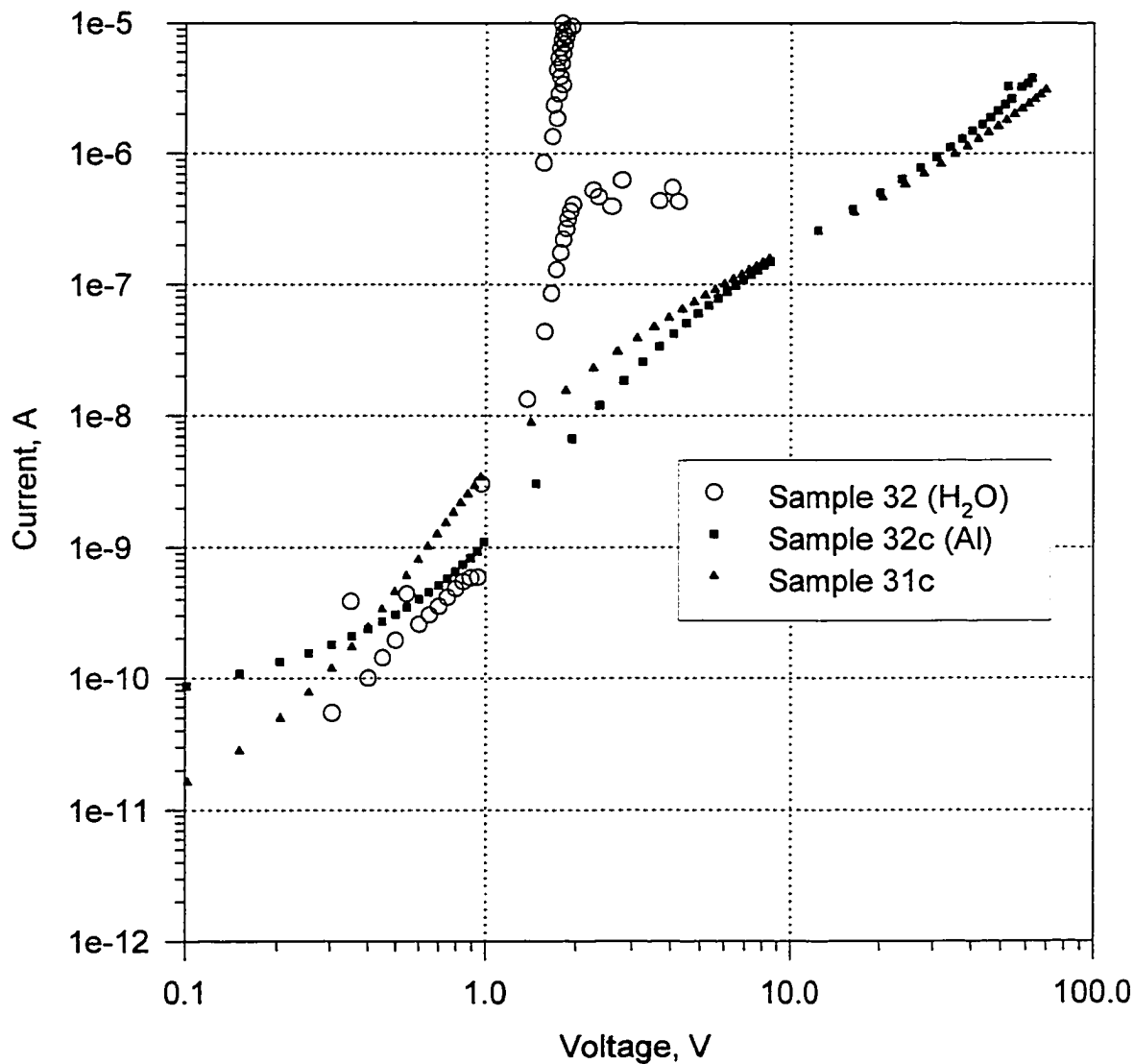
Figure 57. Current-Voltage characteristics of sample 31 with water and aluminum contacts in comparison to sample 32c.

measured with a thermocouple and the current was measured with an electrometer. No series resistance was used so that the voltage on the sample was constant regardless of current. One observation made during this measurement is that conductivity of the SiO_x film changes after being subjected to high temperatures, i.e., the current is lower after a temperature cycle at a fixed voltage. An example measurement is shown in Fig. 58 on sample 32e with 20 volts applied. The room temperature resistivity, however, had little impact on the activation energy. However, because it appears that some change is occurring with the film, the data used for analysis was with decreasing temperature. A more detailed examination of the effects of high temperature was conducted with sample 31 and is described later in this chapter.

Although the thermocouple was placed close to the sample, it was found that data had to be acquired very slowly for accurate temperature measurements. One data point was taken every six seconds by computer. Each temperature cycle lasted several hours during which several thousand data points were acquired.
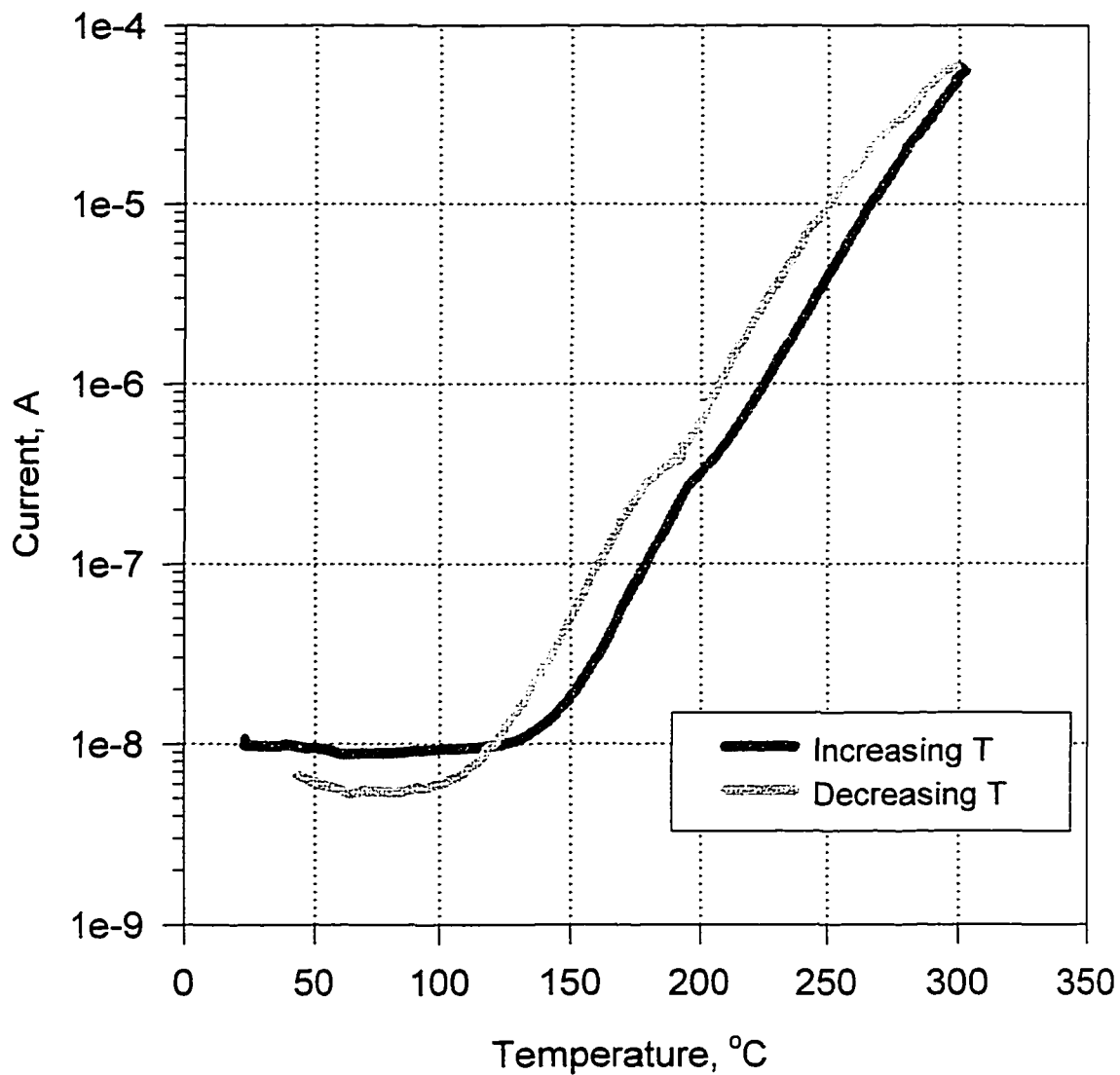
Figure 58. Example of conductivity change during temperature cycle of sample 32e with 20 volts applied.
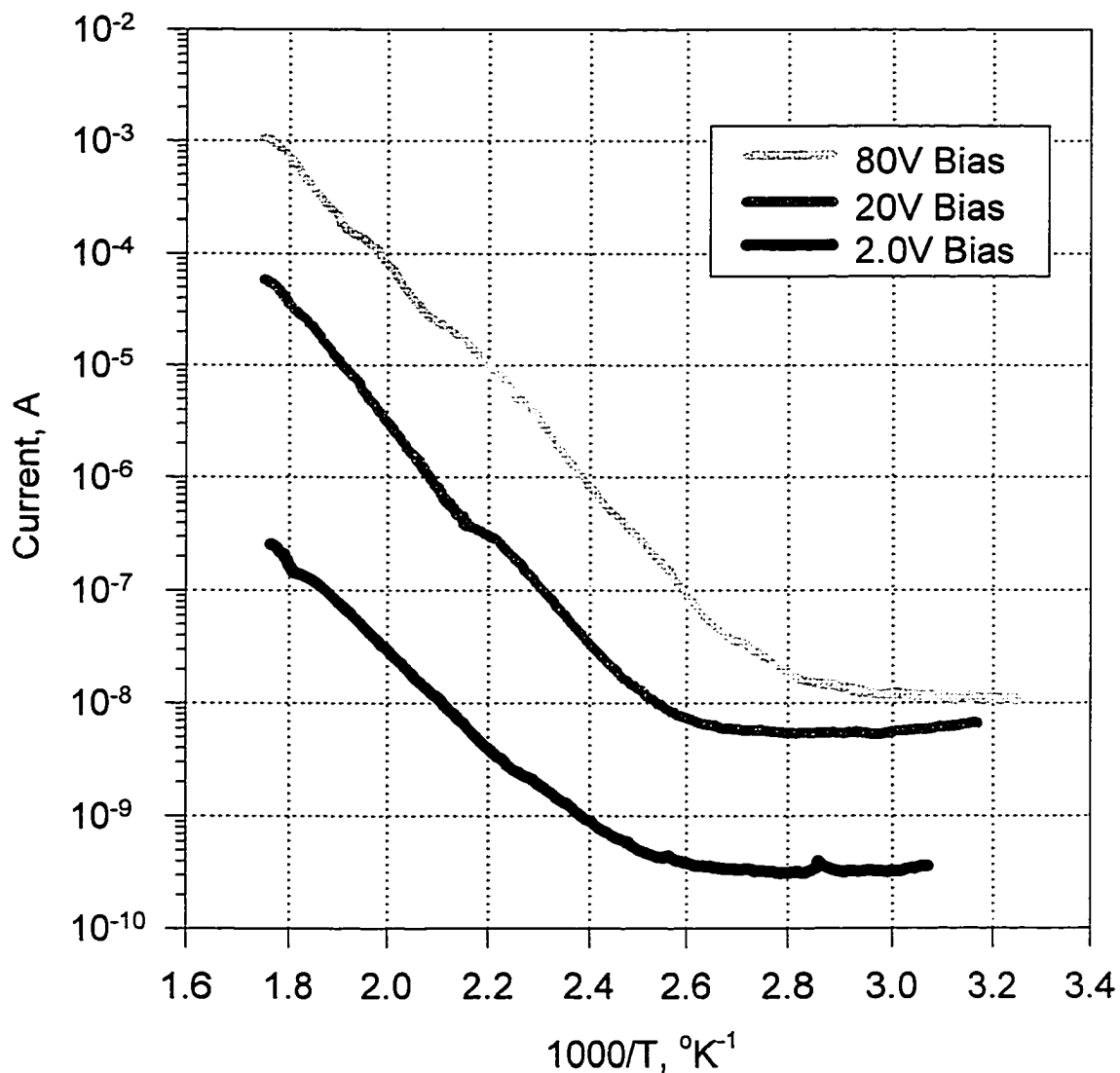
Figure 59. Arrhenius plot of current with sample 32e with bias voltages of 2.0, 20, and 80 volts.

Data was taken for sample 32e with bias voltages of 2.0, 20, and 80 volts as shown in Fig. 59. It is evident that at low temperatures, near room temperature, the sample current is independent of temperature. Between 75 and 125°C, however, the current increases with temperature. The temperature at which this occurs is lower with higher bias voltage. Above 125°C the current

increases in a nearly linear manner when plotted on the Arrhenius plot of Fig. 59. The slopes of the lines are useful for barrier height calculations. Linear regression analysis was used on the linear portion of the data to determine the slopes given in Table 8. While the slopes with biases of 20 and 80 volts are similar, the slope with 2.0 volt bias is lower.

Table 8. Slope of Log[I] Vs. 1000/T for sample 32e.

Bias [volts]	r^2	Slope
2.0	0.998	-3.83
20	0.992	-5.13
80	0.998	-4.75

Effect of Temperatures on SiO$_X$ Film Properties

A change in the room temperature conductivity was noted after sample 32 was raised to 300°C and then cooled as described earlier with respect to Fig. 58. Also, a slight change in the color of sample 32 was noted after heating, the color shifted from brown towards gold. Sample 31d was used to make a detailed study the effects of heat treatment. The I-V characteristics of sample 31d were originally measured from 1 to 10 volts applied. The I-V relationship was re-measured before heating from 10 to 100 volts applied. (Note: a breakdown is observed at 40 volts, however, these breakdowns are self-healing as described earlier with respect to Fig. 56) As shown in Fig. 60 the I-V curves before heating overlap in the region from 1 to 10 volts indicating that no changes in the I-V relationship occurred since the original measurement. Additionally, the capacitance of the sample was re-measured so that any changes in the dielectric

constant of the film could be measured. The capacitance was identical to the original measurement of 373 ± 1pF (using bridge circuit with 1kHz signal).

The sample was then placed on a hot plate, covered, and baked at 350°C for 30 minutes. After allowing the sample to cool slowly to room temperature the I-V curve was re-measured. As shown in Fig. 60 the resistivity of the sample was increased by over an order of magnitude by the heat treatment. Additionally, the I-V curve shows a generally ohmic rather than nonlinear behavior.

Deviations from ohmic behavior were recorded at the extremes of the voltage range. With applied voltages above 70 volts nonlinear increase in current is observed. This current increase may indicate the onset of a filamentary breakdown although the applied voltages were not high enough to demonstrate this conclusively. With voltages below one volt the settling time of the current became less than the three minutes given by the computer between points and many negative current values were measured (not plotted). For this reason data below about one volt should be ignored.

A color change in the film from brown towards gold after heating was noted. Also, the capacitance of sample 31d decreased to 338pF after the heat treatment. The other samples on this substrate, samples 31a-g, also had a lowered capacitance. This change in the capacitance corresponds to a decrease in the dielectric constant of the film from 5.1 before heating to 4.6 after heating to 350°C.
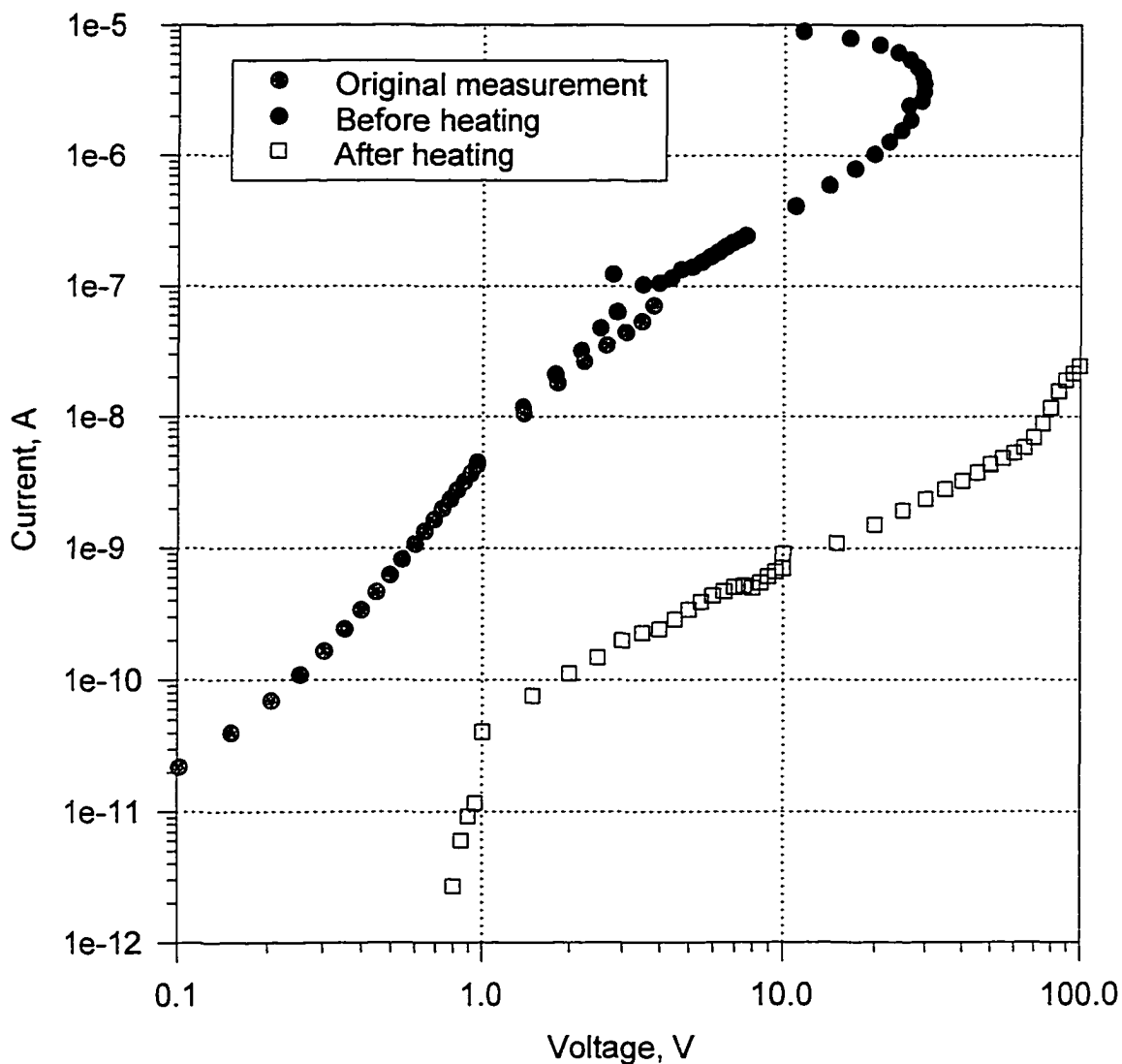
Figure 60. Effect of heat treatment on sample 31d.

Analysis of Electrical Measurements with SiO$_X$ Capacitors

From the electrical measurements with SiO$_X$ capacitors the conduction mechanisms in SiO$_X$ cathode coatings in vacuum can be determined. Samples from three SiO$_X$ films were measured, a film grown at ~20Å/sec and two films grown at ~60Å/sec. These measurements of I and V cannot be directly compared because the film thickness was not constant. However, the

measurements can be compared by plotting in terms of current density, J, and electric field, E, as shown in Fig. 61. Although the general shape of the curves are similar, it is clear that the conductivity of the 20Å/sec sample is much less than that the 60Å/sec sample. This is expected since films with lower deposition rates have properties closer to the insulator, SiO_2.
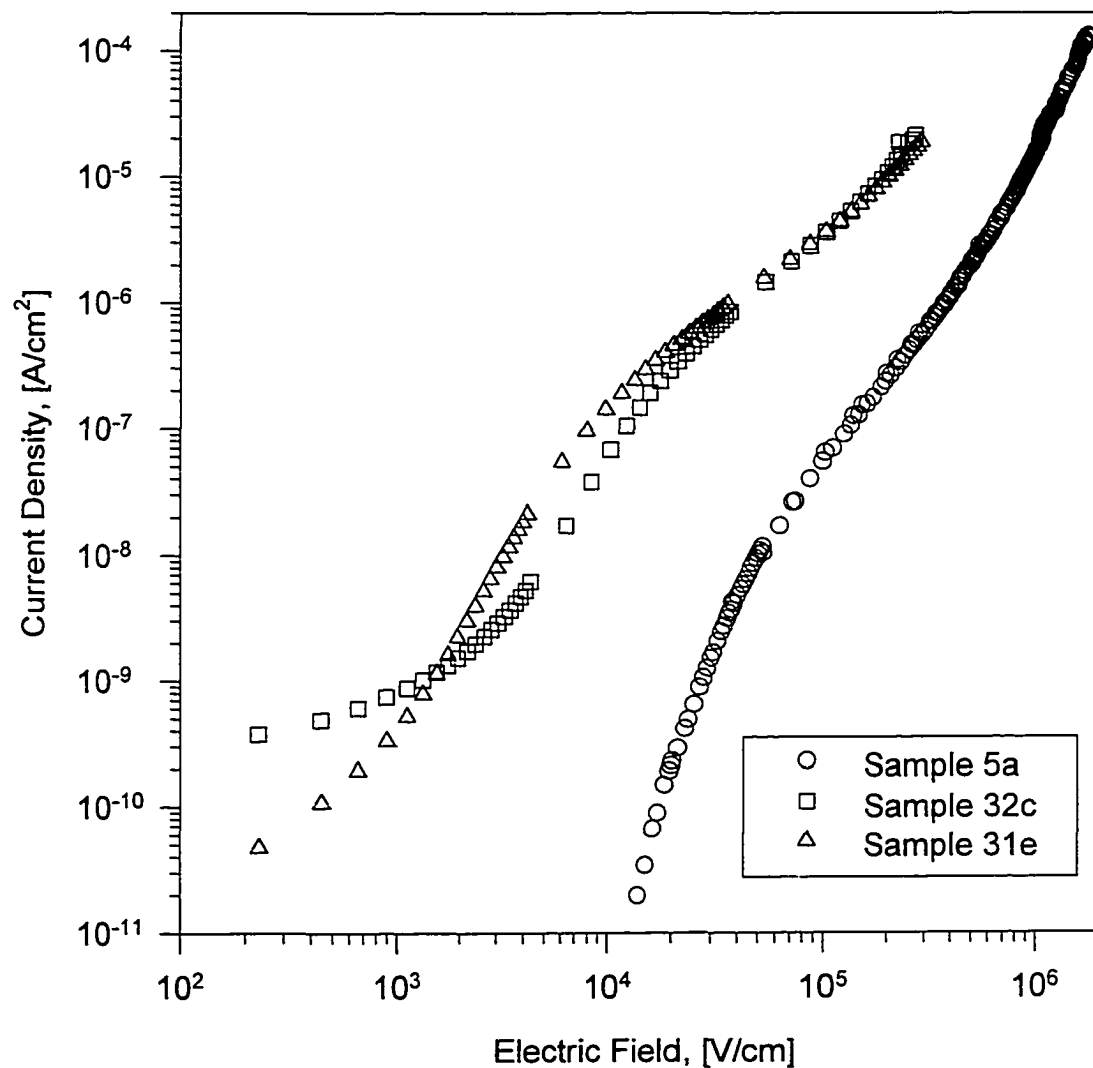
Figure 61. Comparison of J, E relationship for one 20Å/sec SiO_X film (sample 5a) and two films grown at ~60Å/sec (samples 32c and 31e).

The following conduction mechanism are known to be possible in insulating films:[73]

- **Ohmic:** $\quad J \propto \mathscr{E}\exp(-\Delta E/kT)$

- **Space-charge-limited:** $\quad J = \dfrac{8\varepsilon\mu V^2}{9d^3}$

- **Field emission:** $\quad J \propto \mathscr{E}^2 \exp\left(-\dfrac{4\sqrt{2m^*}\,(q\phi_B)^{3/2}}{3q\hbar\mathscr{E}}\right)$

- **Schottky emission:** $\quad J = A^*T^2 \exp\left(\dfrac{-q\left(\phi_B - \sqrt{qE/4\pi\varepsilon}\right)}{kT}\right)$

- **Frenkel-Poole emission:** $\quad J \propto \mathscr{E}\exp\left(\dfrac{-q\left(\phi_B - \sqrt{qE/\pi\varepsilon}\right)}{kT}\right)$

- **Ionic conduction:** $\quad J \propto \dfrac{\mathscr{E}}{T}\exp(-\Delta E/kT)$

Where A^*=effective Richardson constant, ϕ_B=barrier height, $\mathscr{E}$=electric field, ε=dynamic permittivity, m^*=effective mass, d=thickness, ΔE=activation energy, and μ=mobility.

The best correlation with higher voltages was found by fitting the data to Frenkel-Poole emission. Frenkel-Poole emission is field-assisted thermionic emission from trap states within the band gap. Frenkel-Poole emission can be expressed by

$$I = C\,V\exp\left(+2aq\sqrt{V}/kT - q\phi_b/kT\right) \tag{10}$$

where ϕ_b is the barrier height of the trap, $a = \sqrt{q/4\pi\varepsilon d}$, and C is a proportionality constant. Plots of log(I) vs. $\sqrt{V}$ form straight lines. Frenkel-Poole plots for samples 5a, 32c, and 31e are shown in Fig. 62.
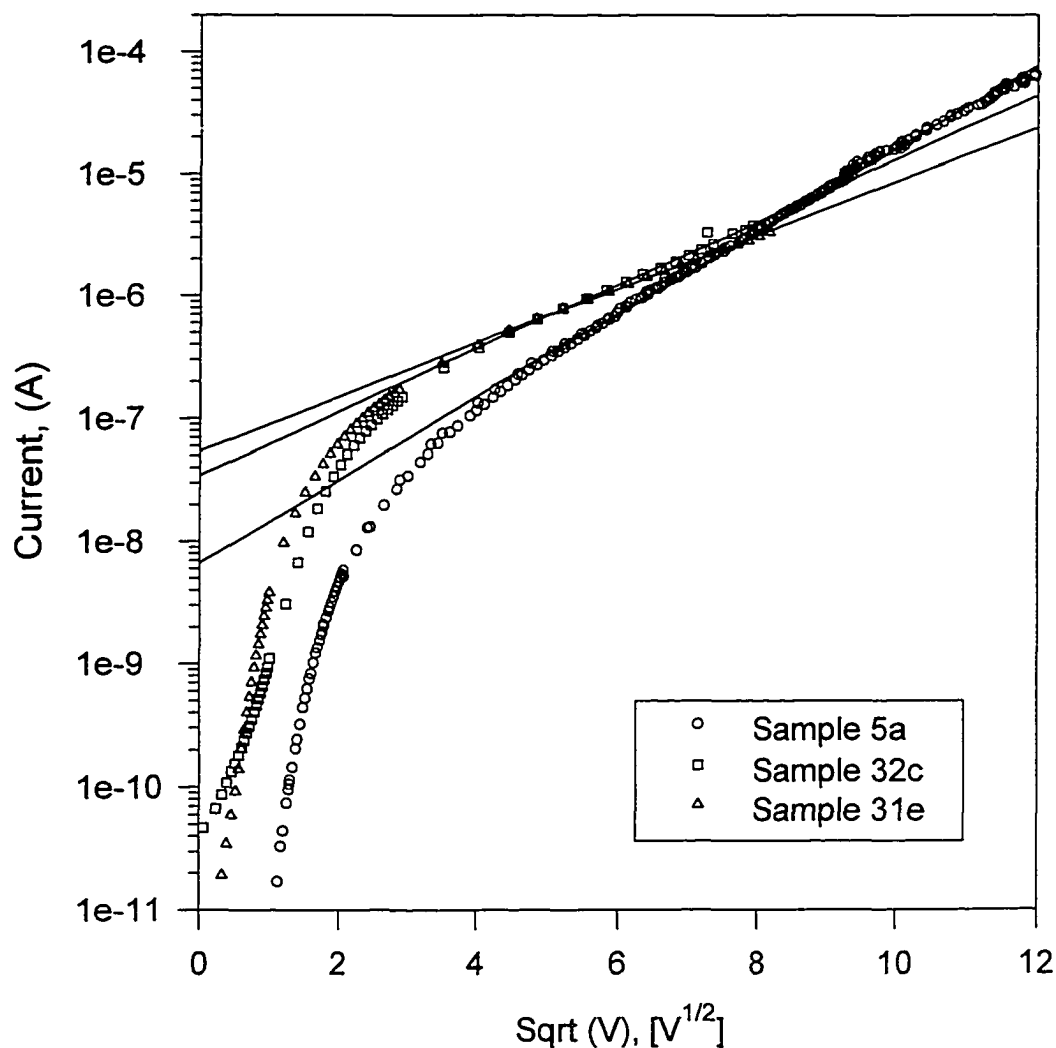
Figure 62. Frenkel-Poole plots of I-V data from samples 5a, 32c, and 31e.

The increase in current with voltage is due to lowering of the barrier for

trap emission. The amount of lowering is determined only by the electric field

and permittivity at the trap location. The dynamic permittivity of the film can be

determined by the slope of the line. However, for completeness, the effects of

field enhancement at the trap location should be considered. Including the effect

of field enhancement, the slope is given by

$$slope = \frac{(\log_{10} e)\, q\sqrt{q\beta/4\pi\varepsilon d}}{kT}$$

(11)

Table 9. Linear regression results from Frenkel-Poole fit.

	Sample 5a	Sample 32c	Sample 31e
Slope	0.338	0.258	0.220
y-intercept	-8.17	-7.46	-7.26
r^2	0.998	0.991	0.999
$\varepsilon_r(\beta=1)$	4.38	2.66	3.66
$\beta(\varepsilon_r=2.1)$	2.1	1.3	1.7

The relative dielectric constant, ε_r, for each sample was calculated using eqn. (11) assuming no field enhancement ($\beta=1$) and the results are given in Table 9. Note that this is the dynamic and not the static dielectric constant. Although no high frequency measurements were made of these films, it is thought that the actual dynamic value of ε_r should be bounded by the dynamic ε_r of SiO_2, ~2.1, and the static ε_r, which was measured experimentally (4.1 for sample 5a and 5.1 for samples 32c, 31e). The calculated values of ε_r in Table 9 are within this range. However, the large difference between samples 32c and 31e is not expected because both samples are from the same batch. Also, since ε_r increases with deposition rate (at least for the static case) one expects ε_r for samples 32c and 31e to be larger than that for sample 5a. To explain these inconsistencies the effects of field enhancement must be considered.

For a given slope, ε_r increases with β. If we assume the lowest expected value of ε_r to be 2.1 then one can calculate the value of β as listed in Table 9. Since these values are relatively small, 1.3 to 2.1, one can conclude that it is bulk traps that are controlling the emission. However, the fact that β is greater than one indicates that some field enhancement is involved. This small increase from one could be averaged effect of field enhanced sites at either electrode surface or the edge of the circular anode contact. One concludes that at higher fields conduction in the SiO_x films is controlled by Frenkel-Poole emission of bulk traps within the film with a small influence from field enhancement.

At low voltages it is clear from Fig. 62 that the data does not follow Frenkel-Poole. The best fit to the low voltage data was with field emission. Fowler-Nordheim plots of the experimental data for samples 5a, 32c, and 31e are shown in Fig. 63. Although a good fit is found for sample 5a at low voltages, the fit for samples 32c and 31e is poor at the lowest voltages, but some linearity is found in the intermediate voltage range. The data acquisition technique may have influenced the data from samples 32c and 31e. The data for sample 5a was acquired manually, while that for samples 32c and 31e was acquired via computer, which may not have allowed enough time for the current to reach steady state at the lowest voltages.

From the slope and intercept of the Fowler-Nordheim plots in Fig. 63 the values of area and β can be determined from eqns. (4) and (5) if Φ is known. As a starting point, it is assumed that Φ equals the work function of the cathode, 4.5eV, as was done in analysis of the coatings in vacuum. As listed in Table 10

the calculated values for β and A when Φ=4.5 are non-physical, just as in the case of the coatings in vacuum. β has values of about 10,000 and the values of A are smaller than an atom. For emission from a metal into SiO_x, however, Φ is reduced by the electron affinity, χ, of the film. Assuming a relatively large χ of 2.5eV the values of β and A were computed for the case of Φ=2.0. Again, although moving in the right direction, β and A are non-physical. The results of the Frenkel-Poole analysis above lead us to consider the possibility of field emission from traps within the bulk of the film.

Assuming field emission from traps within the bulk, the value of β is assumed to have values between 1 and 10. The corresponding values of Φ for β =1 and 10 are between 1.32 and 46.7meV as listed in Table 10. Because this is near or below the thermal energy of 25.9meV traps with these activation energies are likely not to be occupied at room temperature and therefore not a possible current source. One concludes that the source of the field emission current is traps located in a field-enhanced region with β>10.

When considering field emission from traps the calculation of an emitting area, A, is no longer appropriate. The variable A in the field emission equation should be should be replaced with some other factor, which includes the trap density. The low values of A calculated in the capacitor and vacuum measurements are another indication that electron emission is from traps rather than the cathode.
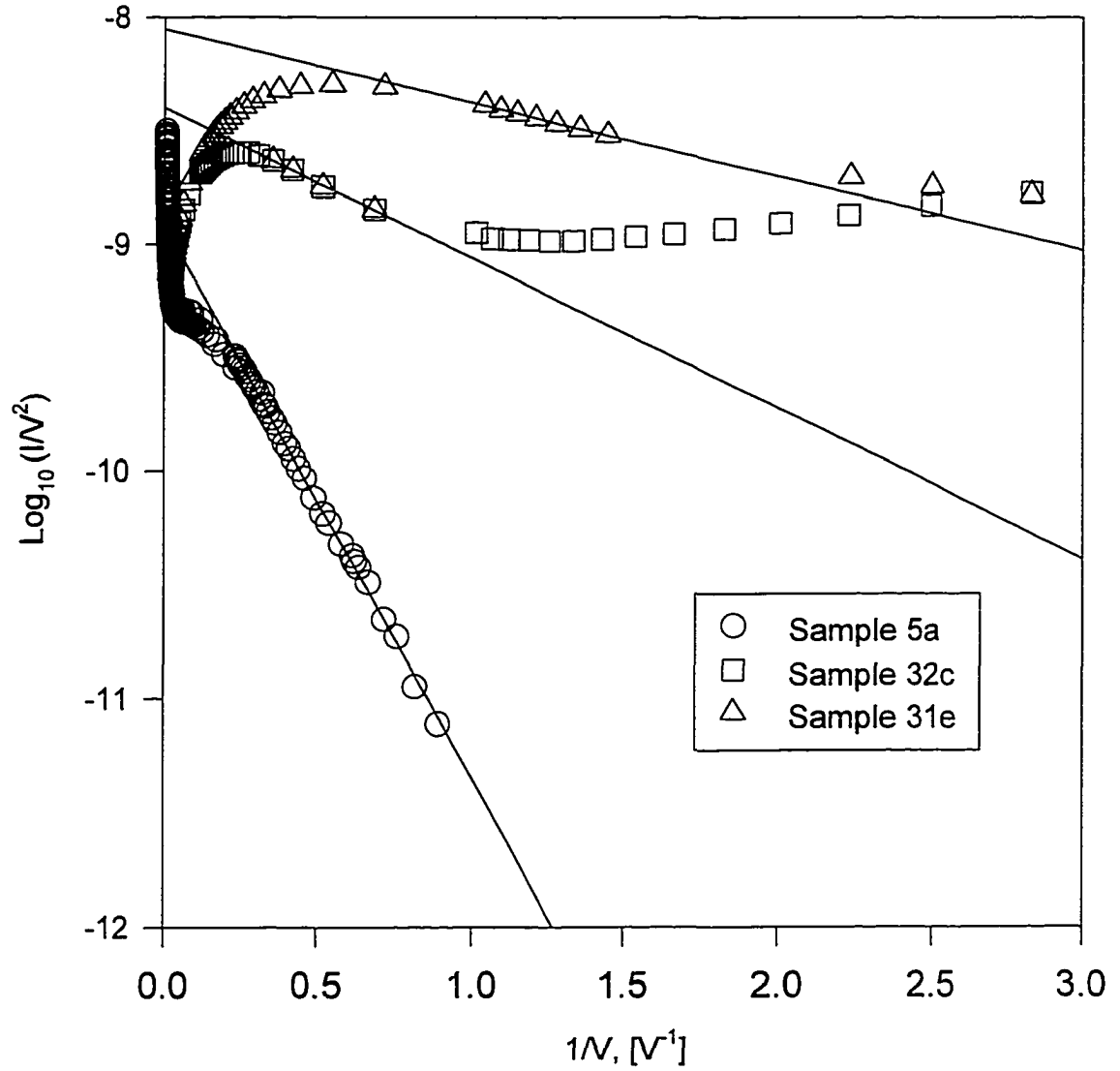
Figure 63. Fowler-Nordheim plots of I-V data from samples 5a, 32c, and 31e.

Table 10. Linear regression results from Fowler-Nordheim fit.

	Sample 5a	Sample 32c	Sample 31e
Slope	-2.43	-0.664	-0.325
y-intercept	-8.92	-8.40	-8.05
r^2	0.999	0.999	0.998
$\Phi^{1.5}/\beta$, [eV$^{1.5}$]	1.01E-3	9.77E-5	4.78E-5
$\beta(\Phi=4.5)$	9.45E+3	9.77E+4	2.00E+5
A($\Phi=4.5$), [nm^2]	2.58E-9	6.39E-10	3.35E-10
$\beta(\Phi=2.0)$	2.80E+3	2.90E+4	5.92E+4
A($\Phi=2.0$), [nm^2]	1.31E-8	3.22E-9	1.73E-9
$\Phi(\beta=1)$, [meV]	10.0	2.12	1.32
$\Phi(\beta=10)$, [meV]	46.7	9.85	6.11

The energy of the traps can be determined from the temperature dependence of Frenkel-Poole emission. Even with low fields, thermionic emission from deep traps can become significant with elevated temperatures. The slope on an Ahhrenius plot of log(I) vs. 1000/T is given by

$$slope = 5.035\left(2a\sqrt{V} - \phi_b\right)$$ (12)

from which the barrier energy of the trap, ϕ_b, can be determined. The value of a is dependent on the choice of ε_r as described earlier.

Calculations of ϕ_b were made from the Arrhenius plot from sample 32c. Slope values from linear regression are listed in Table 11 for the applied voltages of 80, 20, and 2.0 volts. In these calculations the value of ε_r=2.66 from the earlier Frenkel-Poole plot was used. Trap energy of 1.2eV was calculated from both the 80 and 20volt data. A lower value of 0.83eV was calculated for the data with 2.0 volts applied. It is suspected that the low ϕ_b indicates that an applied voltage >2 volts is required for an accurate measurement.

Table 11. Frenkel-Poole analysis of Arrhenius plot sample 32e.

	80 Volt	20 Volt	2.0 Volt
Slope	-4.69	-5.32	-3.96
y-intercept	5.25	5.11	0.353
$2aV^{1/2}$	0.276	0.138	0.044
Φ_B (a=.0154) [eV]	1.21	1.20	0.829

CHAPTER VIII

DISCUSSION OF RESULTS

Electrical Measurements in Vacuum

Preparing six identical cathodes and then coating half of them tested the effectiveness of SiO_x cathode coatings in preventing breakdown. These cathodes were cleaned using high pressure, ultra-pure water rinsing at Jefferson Lab. Three of the cathodes were coated with $2\mu m$ of SiO_x deposited at 60Å/sec. The electrode gap was constructed in such a way as to create a near uniform field in the center of the cathode over an area of $\sim 1cm^2$ with an electrode gap of 0.2mm. The breakdown voltage of each cathode was then measured after electrical conditioning. The results from this experiment and subsequent follow-up experiments are now discussed.

A. Breakdown

The three SiO_x coated cathodes gave breakdown voltages of $\sim 100MV/m$ which is about twice the $\sim 55MV/m$ obtained with the uncoated cathodes. The variation in breakdown voltages was about 10% for the uncoated cathodes and about 5% for the coated cathodes. The high breakdown field indicated that the high pressure, ultrapure water rinse was an effective procedure.

It may be significant that the cathodes with the highest activation field during conditioning also had the highest breakdown field for both coated and uncoated cathodes. The breakdown field was near the activation field for each cathode. It appears that the activation field is an indicator of the surface quality.

SEM microscopy of the post-breakdown cathode surfaces revealed distinct differences between coated and uncoated cathodes. While the uncoated cathodes showed the typical damage trail of pits and bumps (see Figs. 35-37), the coated cathodes showed only small pinholes in the film. In one sample the damage was not visible without magnification. Under the SEM two ~15μm holes were visible in the film (see Figs. 38-40). It is assumed that the two holes are due to the two discharges, one from the conditioning measurement and one from the breakdown measurement, since one large current spike was recorded in each measurement.

The fact that field emission level was nearly unchanged after conditioning suggests that the newly formed hole was not a strong electron source. Additionally, it appeared that breakdown with a coated cathode does not seriously damage the cathode. This sharply contrasts the uncoated cathodes where after breakdown there were deep pits in the surface and the breakdown voltage was thereafter reduced to lower than about 30% of the original value.

The sublimation property of the SiO_x film is believed to be responsible for the lack of widespread damage. With an uncoated cathode (or with a non-sublimating coating) energy must be expended to damage the cathode during breakdown in order to vaporize the metal (or coating) releasing enough gas to maintain the arc. Otherwise the voltage across the gap would be restored and breakdown would be re-initiated. With the SiO_x coated cathodes we observed that the film where the hole is formed appears completely vaporized. Even this small amount of solid is enough when completely sublimated to sustain the arc.

This argument is partially supported by the nearly identically sized holes in Figs. 39 and 40. One hole is believed to be due to a discharge in the conditioning circuit with limited current and the other in the breakdown circuit with substantially increased current. With uncoated cathodes the damage is more extensive in the breakdown circuit because much more gas is required to sustain the arc. With the SiO_x coating the SiO vapor released from the initial puncture site is sufficient to maintain the arc and so only small pinholes are created in the film.

B. Model Concerning "Activation" of Cathode Emitters

The emission from virgin cathodes was negligible in most cases at low fields. Typically, as the electric field is increased a sudden jump in the current by several orders of magnitude occurs. This event is termed "activation". There is presently no explanation for activation. Additionally, there is no explanation for the large enhancement factors found after conditioning. An enhancement factor of 150-500, which is commonly found, requires a protrusion on the order of $5\mu m$ from the surface. However, SEM pictures of virgin mechanically or electropolished samples show no such protrusions.

In most cases activation is a spontaneous event with no increase in current beforehand. However, with sample#4 (discussed in Chapter VI) a steady increase in current was observed before activation. Furthermore, this current followed the Fowler-Nordheim equation, but with a very large area of $1mm^2$ and very low enhancement factor of 26. On a well-polished surface emission is likely from all the defects on the surface such as scratches, pits, inclusions, and grain

boundaries. The combined effective area of all these defects on our $1cm^2$ cathodes may well be on the order of $1mm^2$ as calculated for sample #4. Because these defects project less than $1\mu m$ from the surface, a β of 26 or lower is also possible. Calculated current from $1mm^2$ emitters with β from 10 to 40 is shown in Fig. 64. We see that for large emitting areas with $\beta\sim40$ the current is negligible until a certain field is reached and then rises very quickly as the applied field is increased.

Activation discharges occurs at fields much lower than the critical field for emitters with low β from 10 to 40. The trigger for the activation discharge is not known, however, one possible source is movement of an emitter on the cathode due to electrostatic forces. An emitter that bends to align itself with the electrostatic field thereby increasing β or an emitter that becomes detached from the cathode surface could be the trigger for activation.

After activation, the emitter area is markedly reduced and β is increased with sample#4. The larger β must be due to a newly formed projection from the surface. This is consistent with the work of Sinha, et.al.,[74] who studied the surface of cathodes after breakdown. Sinha observed that projections are formed on the cathode after breakdown. The area around the projection is smooth indicating that it was melted then re-solidified. The projection is believed to be the result of electrostatic forces pulling on the molten metal. The formation of such projections on the surface during activation explains the increased β and lower area.
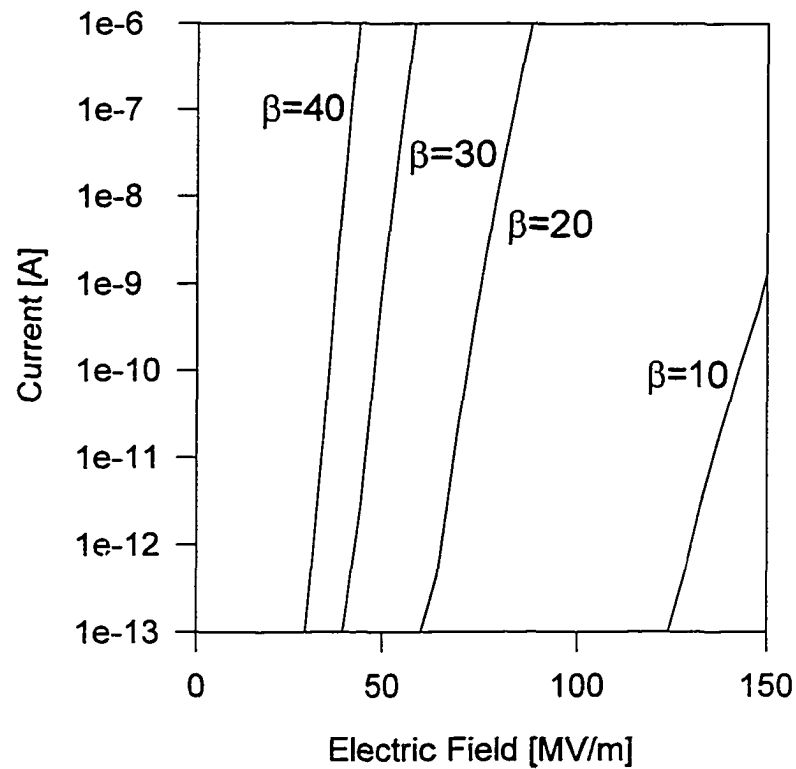
Figure 64. Calculated currents for 1mm² area field emitters with β from 10 to 40.

By observing the anode and cathode after conditioning, small damage spots on the anode and cathode are observed. We conclude that "activation" does not activate an existing emitter. Rather, activation is a small discharge which damages the electrodes and *creates* a localized emitter with large β on the cathode.

C. Conditioning

Anode damage due to the activation discharge during conditioning was observed after conditioning both coated and uncoated cathodes. This sheds new light on the total voltage effect described in the Chapter I. The total voltage is a reduction in the breakdown field of large gaps due to anode interactions.

The anode can release loose particles due to electrostatic stress. As is evident from Fig. 45 in Chapter VI, there are several protrusions in the anode spot. Some of these protrusions appear weakly bound to the surface and may detach with electrostatic force and impact on the cathode with high energy. This would initiate breakdown at lower fields than that determined by the cathode. Conditioning damages the anode and this damage reduces the breakdown voltage through anode interactions. In this way, the total voltage effect is a direct result of conditioning.

This explains why the total voltage effect was not observed with epoxy coated cathodes in the experiment of Jedynak and Towliati.[75] There was no conditioning prior to measurement. The performance with large gaps may not be limited by the total voltage effect when the conditioning step can be skipped.

With SiO_x coated cathodes conditioning is not required to achieve high fields with long-term stability as demonstrated with sample#2. Although the breakdown field of gaps >1mm was not measured, the breakdown voltage in large gaps with coated electrodes may be several times that of an uncoated electrode because conditioning and the coincident anode damage are avoided.

D. Field Emission

Examining the results from the six high-pressure ultrapure water rinsed samples, the field emission currents of coated cathodes after conditioning are reduced by two to four orders of magnitude compared to uncoated cathodes at the highest measured field. At the breakdown field of the uncoated cathodes, ~50MV/m, the difference can be estimated to be between three and six orders of

magnitude. This reduced emission is important with large DC gaps and in RF cavities. In large DC gaps, field emission from the cathode damages the anode and reduces the hold-off voltage. In RF cavities, field emitted electrons absorb RF power and thereby limit the electric field, an effect known as loading.

The Fowler-Nordheim plots for the SiO_x coated cathodes are different than those of the uncoated cathodes. The field enhancement factors calculated from the plots were much higher for the coated cathodes, from 213 to 454, which was the opposite of what one would expect from a coating that reduces emission. Generally, a surface with a high β after conditioning will also have high levels of field emission. Also questionable was the calculated emitter area which is approximately $3.7 \cdot 10^{-9}$ [nm^2] for all three cathodes. This area is much smaller than that of a single atom. Clearly, a different interpretation of the Fowler-Nordheim plots is required for SiO_x coated cathodes. The deviation in these factors for coated metal surfaces can be due to one of the following:

1. Processes at the metal-coating interface
2. Processes at the coating-vacuum interface
3. Charge transport in the coating

The reduction in electron emission and the effects on the calculated values of β and area, A, from each of these three possibilities is discussed in the following sections.

1. Metal-coating limited emission

If emission controlled by the metal-coating interface then the effect of the dielectric constant, ε_r, in the Fowler-Nordheim equation must be considered. We write the corrected Fowler-Nordheim equation:

$$I = \frac{1.541 \cdot 10^{-2} A \left(\dfrac{\beta V}{\varepsilon_r}\right)^2}{(\Phi - \chi)d^2} \exp\left[\frac{-6.831 \cdot 10^9 d(\Phi - \chi)^{3/2}}{\left(\dfrac{\beta V}{\varepsilon_r}\right)}\right] \qquad \text{[A]}$$

where d is the electrode spacing, V is the applied voltage, and β is the field enhancement factor. The corrected Fowler-Nordheim plots are then based on

$$\log_{10}\left(\frac{I}{V^2}\right) = -\log_{10}\left(\frac{(\Phi - \chi)d^2 \varepsilon_r^2}{1.541 \cdot 10^{-2} A\beta}\right) + \frac{-6.831 \cdot 10^9 d\varepsilon_r (\Phi - \chi)^{3/2}}{(\ln 10)\beta V} \qquad (13)$$

Now, by comparing eqns. (13) and (3) we can find expressions from the corrected values of A and β in terms of the uncorrected values in Table 6. We write

$$\beta_{corrected} = \beta\gamma$$

$$A_{corrected} = A\varepsilon_r \qquad (14)$$

where γ is the figure of merit given in eqn. (8). The corrected values of β and A can now be calculated. Using the approximate values; $\varepsilon_r = 6$, $\chi = 1\text{eV}$, and $\Phi = 4.5\text{eV}$, we find that $\gamma = 4.1$. The corrected β now has values ~1000 and the corrected area is increased by a factor of 6. The corrected field enhancement factors are still high and the emitter areas are still smaller than an atom. We can therefore eliminate metal-coating emission as the current limiting mechanism.

2. Coating-vacuum interface limited emission

If emission is controlled by the coating-vacuum interface then the change in work function must be taken into account. If the insulator surface is essentially degenerate n-type, the work function is equal to the electron affinity. Again, we

formulate equations that give us corrected values of β and A based on the uncorrected values. In this case the modifications are given by

$$\beta_{corrected} = \beta\left(\frac{\chi}{\Phi}\right)^{3/2}$$

$$A_{corrected} = A\left(\frac{\Phi}{\chi}\right)^{2}$$

(15)

Using the estimated values χ=1eV and Φ=4.5eV the corrected value of β in this case is 9.5 times lower than the values in Table 6. The corrected areas are about 20 times higher. Even with this correction the calculated areas are several orders of magnitude smaller than an atom, which is still unreasonable.

3. Charge transport limited emission

As this SiO_X coating is expected to have a high density of electron traps, it is assumed that electron trapping and de-trapping plays the dominant role in electron emission from the coated cathode. Electron traps can have several effects on the electron emission from SiO_X coated cathodes. Trapped electrons in the SiO_X bulk reduce the electric field at the cathode. Also, the generation of an accumulation layer of trapped electrons at the coating-vacuum interface is possible. Each of these mechanisms affects the electric field inside the film and the current flow through the film. The results of the charge transport measurements with SiO_X will be used to determine the nature of electron emission from SiO_X coated cathodes.

Charge Transport in SiO$_x$

The previous analysis suggests that deep levels within the SiO$_x$ film control the conductivity of the film. The dominant conduction mechanisms in SiO$_x$ films are found to be field emission at low fields becoming Frenkel-Poole emission at higher fields and high temperatures. Frenkel-Poole emission is emission from trap levels. Both electron and hole traps are possible but measurements by others with SiO$_2$ show that electron conduction is dominant.[76] The regression results indicate a trap located about 1eV from the band edge. The low value of β indicates that these traps reside within the bulk of the film.

The data from sample 5a and the fits from field emission and Frenkel-Poole emission are shown in Fig. 65. The current at low voltages is much less than the Frenkel-Poole fit. This indicates limiting either in the injection or extraction of electrons from the film. Since there is no barrier at the anode to electron flow, a limiting of electron injection is concluded.

At low voltages, where electron injection is limited, the current appears to follow the Fowler-Nordheim equation. Fitting the low voltage data to Fowler-Nordheim yields extremely large values of β (~1000 or more) and non-physical values of area. One explanation for this is trap assisted tunneling. Electrons from the cathode can tunnel directly into traps very near the cathode surface with a Fowler-Nordheim field dependence. The current is low because the number of traps sites is limited, which results in the non-physical values of area from Fowler-Nordheim plots.

In the voltage range from 8 to 80 volts for sample 5a the current is beneath the Fowler-Nordheim fit and follows Frenkel-Poole. The limiting mechanism changes from injection to transport as the traps become filled. The trapped electrons create a space charge that reduces the electric field at the cathode and therefore the field emission current. In the range from 20 volts to 60 volts the difference in voltage between the Frenkel-Poole data and the Fowler-Nordheim fit is a nearly constant ~9 volts. From this voltage and the known values for film thickness and dielectric constant the number of filled traps can be calculated from

$$\Delta V = \frac{qN_t d^2}{2\varepsilon}$$

where N_t is the filled trap density. Assuming that all traps are filled, it is calculated that the trap density is ~10^{16} cm^{-3}.

Above 80 volts for sample 5a the current would once again be injection limited if the low voltage injection mechanism were the only one. However, with high fields trap-assisted tunneling from the cathode directly into the traps responsible for the Frenkel-Poole emission is possible without any field enhancement.
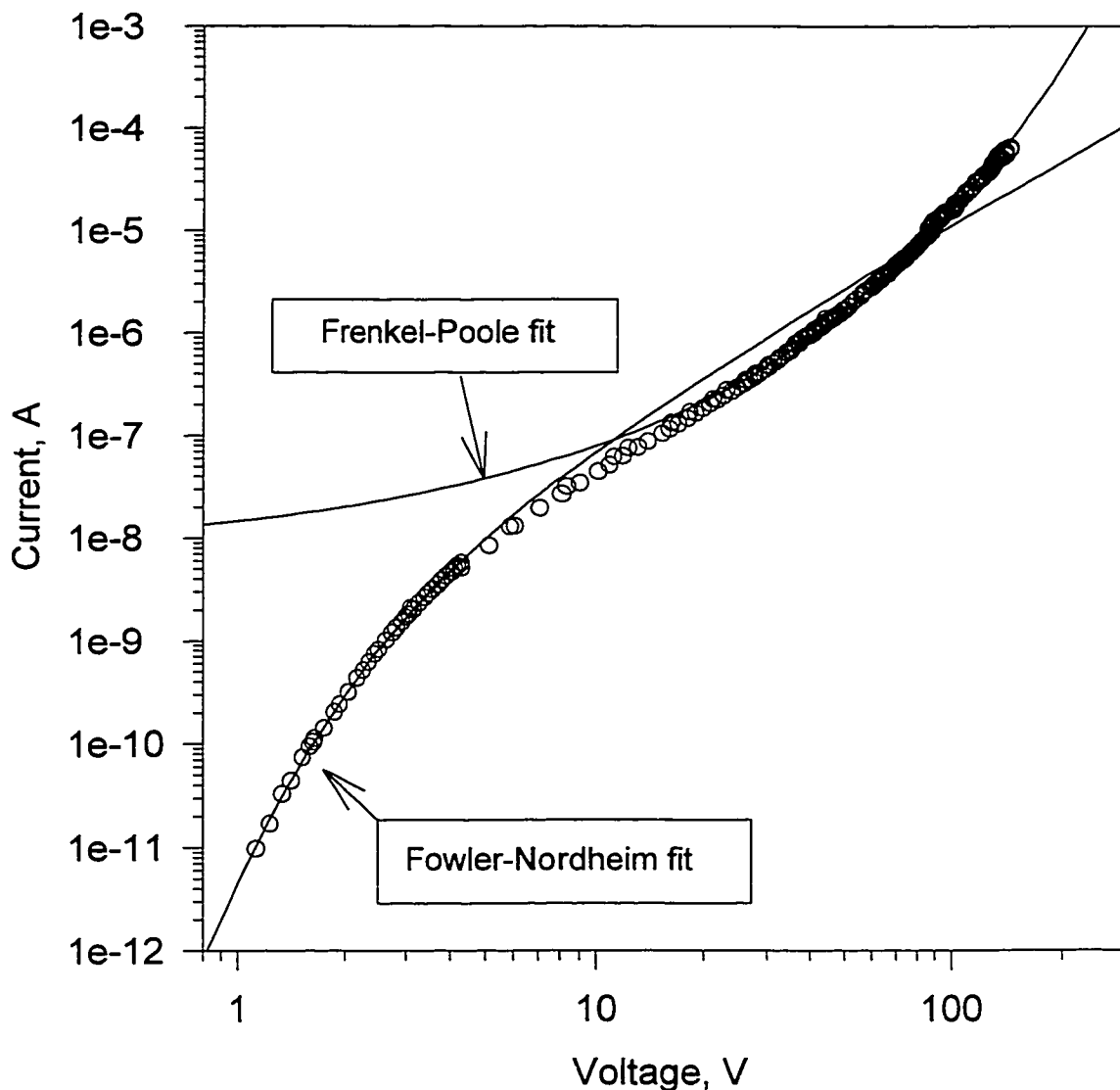
Figure 65. Measured data, Fowler-Nordheim fit, Frenkel-Poole fit, and Fowler-Nordheim estimate for sample 5a.

Comparison of Transport and Vacuum Measurements

In order to directly compare leakage current measurements of SiO_x films to SiO_x cathode coatings in vacuum, the pre-conditioning current of sample 33, which was fabricated in the same batch as samples 31 and 32, was measured. The comparison can be made converting the field data for sample 33 from

current vs. gap voltage into current density vs. field in the SiO$_x$ film. This was done by dividing the applied gap voltage by the gap spacing and also by the dielectric constant of the film (~5.1). The effective tested area of 1cm^2 was used to calculate current density. The resultant J vs. E plot shown in Fig. 66.
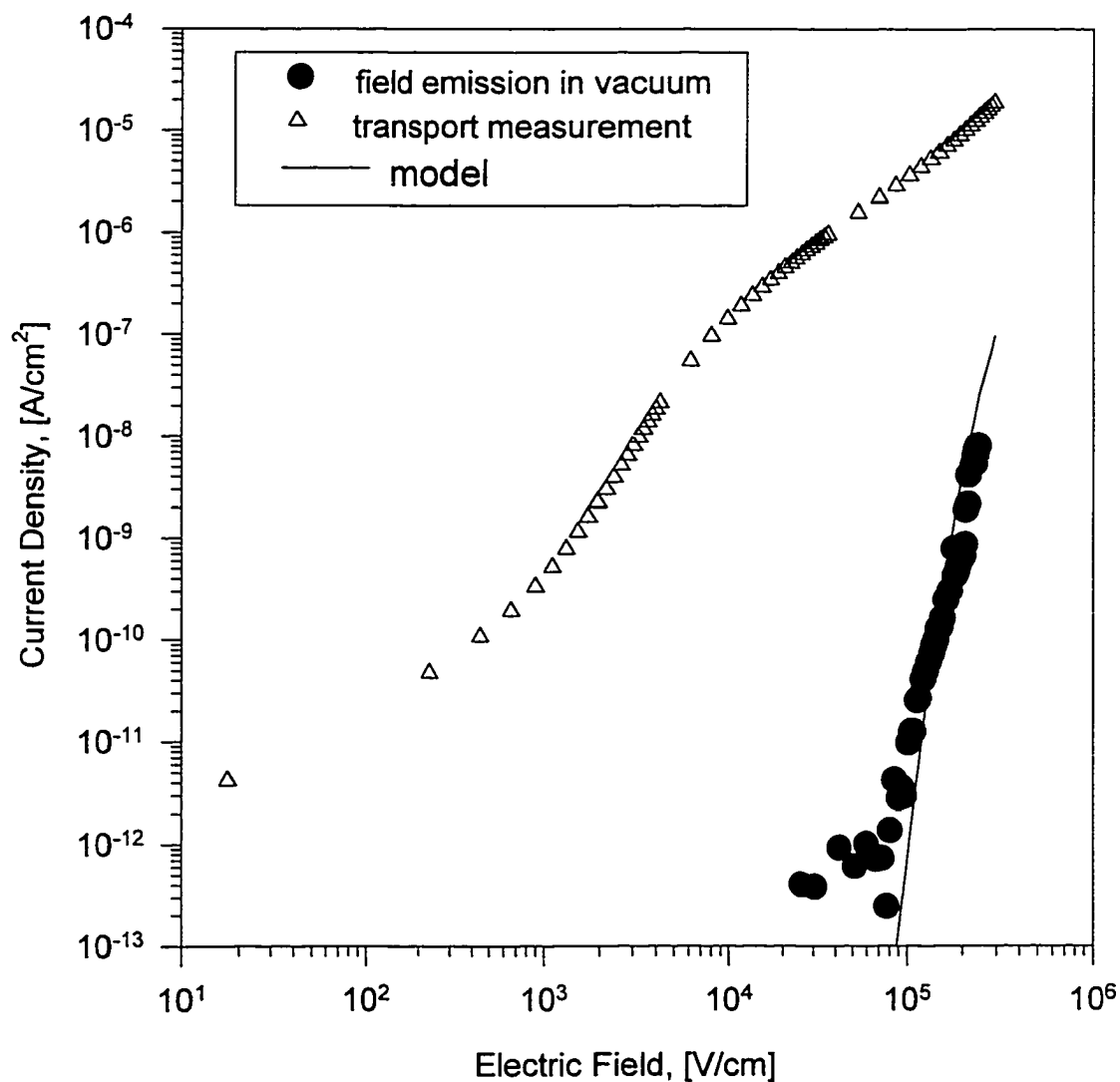
Figure 66. Comparison of field emission measurement in vacuum to transport measurement along with results from a new model for electron emission from SiO$_x$ into vacuum.

The difference between the leakage measurement and the vacuum measurement is the boundary condition at the coating-vacuum interface. In the leakage measurement the positive SiO_x surface is in direct contact with the anode. In this case there is no restriction on electron flow from the film into the anode. However, in the vacuum measurement electrons must overcome a potential barrier of about 2eV at the film surface. If the potential barrier were small enough so that it did not impede electron flow then the curves in Fig. 66 would overlap. If the potential barrier impedes electron flow at the film surface, then electrons accumulate there creating a space charge that reduces the field within the film and therefore the current is reduced. From Fig. 66 it is clear that the current in the vacuum measurement is reduced by several orders of magnitude compared to leakage measurement indicating that an accumulation of electrons exists at the SiO_x surface.

Now, if the barrier were very large then electrons would build up at the surface like in a MOS device until the current dropped to zero. However, because the barrier is ~2eV there is some current flow. From the measurements described in Chapter VI this current follows the Fowler-Nordheim equation for field emission. Fitting the experimental data to the Fowler-Nordheim emission from metal into vacuum results in large β values ~200 and areas too small to be physical. Accounting for a smaller barrier of ~2eV reduces β by a factor of ~5 to more reasonable values. However, the emitting area is still non-physically small.

The non-physical emission area is explained by considering the accumulated charge to reside in a filled trap layer rather than in the conduction

band. Electron emission from SiO$_X$ is then a two step process; emission of the electron from a trap into the conduction band and tunneling from the conduction band into vacuum. With this hypothesis the current density from the SiO$_X$ film can be written

$$J \propto \mathcal{E}PT = \mathcal{E}\exp\left(\frac{-q\left(\phi_B - \sqrt{q\mathcal{E}/\pi\varepsilon}\right)}{kT}\right)\exp\left(\frac{-6.83\cdot10^9\Phi^{3/2}v(y)}{\mathcal{E}\varepsilon}\right) \tag{16}$$

where P is the emission rate from the traps, T is the tunneling probability, ϕ_B is the trap energy, Φ is the conduction band to vacuum level barrier height, E is the electric field in the SiO$_X$ film, and v(y) is the correction factor due to image force barrier lowering. Note that the electric field in vacuum is greater than at the film surface by a factor of the relative dielectric constant. Also, because Φ is only ~2eV the image force correction must be included in the tunneling calculation. A hypothetical band diagram with trap accumulation is shown in Fig. 67.

The expression for current in eqn. 16 can be viewed simply as the Frenkel-Poole current for the electric field at the SiO$_X$ surface multiplied by the tunneling probability from the conduction band into vacuum. From Fig. 66 it is clear that the Frenkel-Poole current at high fields is relatively constant while the current into vacuum changes by several orders of magnitude. This explains the good fit of the data on Fowler-Nordheim plots, i.e., P can be treated as a constant and so $J \propto T$ which is just the Fowler-Nordheim equation. The small areas calculated by the Fowler-Nordheim fit are due to the low density of traps, ~10^{16} cm^{-3}, compared with the number of electrons inside a metal, ~10^{23} cm^{-3}.
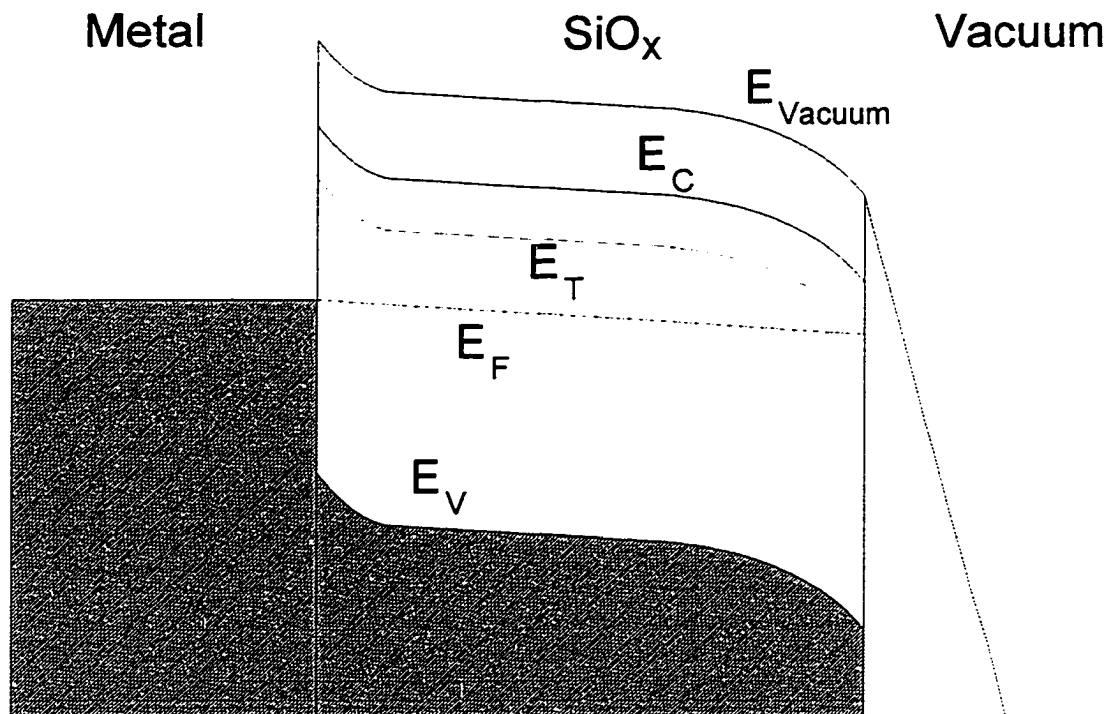
Figure 67. Proposed band diagram of SiO$_X$ coating with trap accumulation.

The hypothesis of a current given by eqn. (16) can be tested with the experimental data in Fig. 66. The Frenkel-Poole current is given by the leakage current measurements. By multiplying this by the tunneling probability a reasonable fit is obtained using $\Phi=2eV$ and ε_r. From earlier Fowler-Nordhiem plots it is know that a relatively small field enhancement is present. The fit, shown as the solid line in Fig. 66, was made using an enhancement factor of 25. Although the fit is not perfect, it is reasonably good considering the simplicity of the calculations.

Figure of Merit for SiO$_X$ Coated Cathodes

It is clear that an accumulation of electrons at the coating-vacuum interface reduces the field inside the SiO$_X$ film. Electron emission is therefore

controlled by the coating-vacuum interface. This is similar to the case of conducting or semiconducting coatings described in Chapter III. The main difference is that with SiO_x coatings the electrons accumulate in the trap levels rather that in the conduction band. Despite this difference the same figure of merit derived for conducting or semiconducting coatings applies, which was given by

$$\gamma = \frac{V_b(coated)}{V_b(uncoated)} = \frac{\beta_m E_{C\,coating}}{\beta_c E_{C\,metal}} \tag{7}$$

From the analysis of sample 33 in the previous section a field enhancement factor of the coating, β=25, was estimated. The breakdown field for sample 33 was ~120MV/m. The critical field for the SiO_x coating is then $E_{C\,coating}$=$3\cdot10^9$ [V/m]. From the values of E_C given in Table 1 for various metals the critical field for SiO_x is about ½ that stainless steel, $E_{C\,metal}$~$6\cdot10^9$ [V/m]. Because SiO_x is thermally insulating one would expect a very low E_C. However, since there are few free electron in SiO_x there is lower current and therefore less heating at a given field compared to metals. Now, uncoated stainless steel cathodes prepared in the same fashion as sample 33 had typical field enhancement factors, β=100, after conditioning. Then, from eqn. (17) it is found that

$$\gamma = \frac{V_b(coated)}{V_b(uncoated)} = \frac{\beta_m E_{C\,coating}}{\beta_c E_{C\,metal}} \approx \frac{100\cdot3\cdot10^9}{25\cdot6\cdot10^9} = 2$$

In this way the improvement in breakdown voltage with SiO_x coating of stainless steel electrons by a factor of about 2 is explained in terms of a figure of merit.

CHAPTER IX

SUMMARY

The breakdown field of uncoated stainless steel electrodes was increased to more than 50MV/m through careful polishing and cleaning procedures. Coating with a ~2μm film of SiO_x was found to increase the breakdown field above 100MV/m. In a few samples the breakdown field was as high as 140MV/m which is believed to be higher than any other reports over a $1cm^2$ area.

It was demonstrated that SiO_x coated cathodes do not require "activation" or conditioning for long-term stability. By eliminating the need for conditioning SiO_x coated cathodes offer the possibility of extending the breakdown voltage of large gaps beyond the normal limitations of the total voltage effect from anode interactions.

The measurements indicate that charge transport in SiO_x is controlled by Frenkel-Poole electron emission from deep traps located ~1eV below the conduction band. Cathode coatings limit electron emission due to the build-up of a space charge from filled electron traps near the coating-vacuum interface. A model for electron emission from SiO_x was developed based on the transport measurements. In the model, electron emission from SiO_x coated cathodes into vacuum is given by the probability of Frenkel-Poole emission from traps in the accumulation layer multiplied by the probability of tunneling from the conduction band into vacuum.

Given coating-vacuum limited emission, the breakdown field of SiO_x coated cathodes can be expressed in term of E_C and β of the coating. The level of electron emission and the thermal conductivity of the coating determine the emission site temperature and therefore the value of E_C. The smoothness of the film surface, influenced by the substrate smoothness and film thickness, determines β.

Based on the trap accumulation layer model of electron emission, the optimal characteristics of a cathode coating can be given as follows:

- Large numbers of electron traps to shield the electric field inside the coating
- Deep traps with low Frenkel-Poole emission rate
- Large electron affinity to reduce the tunneling probability
- High dielectric constant to reduce the field in the accumulation layer
- High thermal conductivity to increase E_C
- Smooth surface to reduce β

Additionally, for UHV applications the film should be bakeable to at least 300°C. For application to RF systems the coating should have a low secondary emission coefficient to prevent multipacting. Ease of application and material costs should also be considered. A material that sublimates, such as SiO_x, appears to increase the robustness of the coating, i.e., the performance after a breakdown.

REFERENCES

1. W.P. Dyke, et al., *Phys. Rev* **91**, p.1043 (1953)

2. D.K. Davies and M.A. Biondi, *J. Appl. Phys.* **48**, p.4229 (1977)

3. H.W. Anderson, *Electr. Eng.* **54**, p.1315 (1935)

4. D.K. Davies and M.A. Biondi, *J. Appl. Phys.* **42**, p.3089 (1971)

5. I.N. Slivkov, *Zh. Tekh. Fiz.*, p.1385 (1968); transl. *Sov. Phys.-Tech. Phys.*, p.13 (1968)

6. A. Maitland, *J. Appl. Phys.* **32**, pp.2399-2407 (1961)

7. F.M. Charbonnier, C.J. Bennette, and L.W. Swanson, *J. Appl. Phys.* **28**, p.627 (1967)

8. C.J. Bennette, L.W. Swanson, and F.M. Charbonnier, *J. Appl. Phys.* **28**, p.634 (1967)

9. W.A. Smith, C.T. Elliot, P.A. Chatterton, and D.L. Pulfrey, *Br. J. Appl. Phys. (J. Phys., D)* **2**, p.1005 (1969)

10. Gomer, Robert, Field Emission and Field Ionization, Harvard University Press, Cambridge MA, p.1 (1961)

11. R.W. Wood, *Phys. Rev.* **5**, 1 (1897)

12. J.E. Lilienfeld, *Phys. Z.* **23**, 506 (1922)

13. W.D. Coolidge, *Am. J. Roentgenol. Radiat. Ther.* **19**, 313 (1928)

14. L.W.Nordheim, *Proc. Roy. Soc. Lond.*, Ser. A **121**, p.626 (1928)

15. A.J. Ahearn, *Phys. Rev.* **50**, p.238 (1936)

16. R.P. Little and W.T. Whitney, *J. Appl. Phys.*, **34** p.2430 (1963)

17. B.M. Cox, *J.Phys.D: Appl. Phys.* **8**, pp.2065-73 (1975)

18. C.S. Athwal and R.V.Latham, *Physica*, **104C**, pp.46-49 (1981)

19. P. Kneisel, "SRF Cavity Technology: Status and Prospects", presented at: Laser Processing Consortium's University Member Workshop, June 23-24, Jefferson Labs, Newport News, VA (1994)

20. R.H. Good and E.W. Müller, *Handbuch der Physik*, **21**, p.176 (1956)

21. J.D. Cobine, Gaseous Conductors, Dover, New York, pp. 177-81.

22. Ibid. 20, pp.181-191

23. R.V. Latham, "Field-Induced electron emission from localized sites on extended-area electrodes", 2nd Workshop on RF Superconductivity, CERN, July 1984.

24. R.Hackam and S.K.Salman, *Proc. IEE* **119** (3), pp. 377-84 (1972)

25. G.A. Farral, "Electrical Breakdown in Vacuum", pp.28-31, from Vacuum Arcs Theory and Applications, J.M. Lafferty ed., John Wiley & Sons, New York (1980)

26. C.J. Bennette, L.W. Swanson, and F.M. Charbonnier, *J. Appl. Phys.* **28**, p.634 (1967)

27. N.B. Rozanova and V.L. Granovskii, *Zh. Tekh. Fiz.* **26**, p.489 (1956); transl. *Sov. Phys. -tech. Phys.* **1**, p.471 (1956)

28. A.S. Pokrovskaya-Soboleva, T.S. Borisova, L.K. Mazurova, and V.M. Stuchenkov, *Sov. Phys.-Tech. Phys.* **17**, p.1047 (1972)

29. Ibid. 19.

30. H.Gruszka and H. Moscicka-Grzesiak, "Conditioning process of electropolished electrodes by field emission current in vacuum," 11th Int. Symp. On Discharges and Electr. Insul. in Vacuum, Berlin, GDR, Sept. 24-28, 1984 pp.33-36

31. C.S. Athwal and R.V. Latham, *J. Phys. D: Appl. Phys.* **17**, pp.1029-43 (1984)

32. R.Hackam and S.K.Salman, *Proc. IEE* **119** (3), p.1947 (1972)

33. R.N. Bloomer and B.M. Cox, *Vacuum* **18**, p.379 (1968)

34. C.M. Cooke, "Residual Pressure and It's Effect on Vacuum Insulation", *Proceedings of the Second International Symposium on Insulation of High Voltages in Vacuum*, Cambridge, Mass, September 1966, p.181

35. L.W.Nordheim, *Proc. Roy. Soc. Lond.*, Ser. A **121**, p.626 (1928)

36. B.M. Cox, *J. Appl. Phys. D: Appl. Phys.* **8**, pp.2065-73, 1975

37. C.S. Athwal and R.V. Latham, *Physica*, **104C**, pp.46-49, 1981

38. N. Pupeter, A. Göhl, T. Habermann, A. Kirshner, E. Mahner, G. Müller, and H. Piel, "Influence of surface roughness and preparation, bulk purity and heat treatment on electron field emission from Nb and Nb_3Sn", 7th Workshop on RF Superconductivity, Saclay, October 17-20, 1995

39. E. Mahner, G. Müller, H.Piel, and N.Pupeter, "Reduced Field Emission of Niobium and Copper Cathodes", 7th International Vacuum Microelectronics Conference, Grenoble, 1994

40. E.Mahner, N. Minatti, H.Piel and N. Pupeter, Applied Surface Science 67, pp.23-28 (1993)

41. L.Jedynak, J.Appl.Phys. 35 (6), pp.1727-33 (1964)

42. L.Jedynak and S.Y. Towliati, J.Vac. Sci. Technol., 11 (1), p.472 (1974)

43. J.G. Trump and R.J. van de Graaff, J. Appl. Phys. 18, p.327 (1947)

44. R.V. Latham and M.S. Mousa, J. Phys.D: Appl.Phys. 19, pp.699-713 (1986)

45. J.N. Smith, Jr., J.Appl.Phys. 59 (1), p.283 (1986)

46. J.N. Smith, Jr., J.Appl.Phys. 60 (4), p.1490 (1986)

47. Ping He and M.K.Sinha, J.App.Phys. 66 (12), pp.6184-86 (1989)

48. W. Opydo, S. Grzybowski, and E. Kuffel, Physica 104C, pp.76-81 (1981)

49. G.J.Sayag, N.T. Viet, H. Bergeret, and A. Septier, J. Physics E: Sci. Inst. 10, pp.176-79, (1977)

50. W.Peter, J.Appl.Phys. 56 (5), p. 1546 (1984)

51. W.Peter, private communication.

52. J. Maserjian and N. Zamani, J. Appl. Phys. 53 (1), pp.559-67 (1982)

53. W.P. Dyke, et al., Phys. Rev. 91, p.1042 (1953)

54. R. Williams, Phys. Rev. A 140 (2), pp.569-75 (1965).

55. J.A. King, ed., Material Handbook for Hybrid Microelectronics, Artech House, Boston, 1988

56. C.D. Clark, P.J. Dean, P.V. Harris, Proc. R. Soc. (Lond.) A (UK), 277, 1964

57. Ibid. 54

58. Z.M. Jarzebski, Oxide Semiconductors, Pergamon Press, Oxford, 1973

59. D.R. Lide ed., CRC Handbook of Chemistry and Physics 76th ed., CRC Press, New York, p.12-122 (1995)

60. S.M. Sze, Physics of Semiconductor Devices 2nd Ed., John Wiley & Sons, New York, 1981, Appendix I.

61. E.H.Blevis, "Silicon Monoxide - Properties and Evaporation Techniques", distributed by the R.D. Mathis, Co.

62. L.I. Maissel and M.H. Francombe, An Introduction to Thin Films, Gordon and Breach, New York, p.248 (1973)

63. Ibid 62.

64. Physics of Semiconductor Devices, 2nd Ed., S.M.Sze, John Wiley&Sons, New York, John Wiley&Sons (1981)

65. "Guide to Deposition Techniques", Kurt Lesker, Inc. catalog or web page www.lesker.com.

66. M.Lenzlinger and E.H.Snow, J.Appl.Phys. 40 (1), pp.278-283 (1969)

67. D.J.Dumin, J.R.Cooper, J.R.Maddux, R.S.Scott, and D.-P.Wong, J.Appl.Phys. 76 (1), pp.319-327 (1994)

68. Scott and Dumin, J. Electrochem. Soc., 142 (2), p. 586 (1995)

69. K.F.Schuegraf and Chenming Hu, J.Appl.Phys. 76 (6), pp.3695-3700 (1994)

70. R.Williams, Phys.Rev.A 140 (2), pp.569-75 (1965)

71. R.Hackam and S.K.Salman, Proc. IEE, 119 (3), pp.377-84 (1972)

72. Peter Kniesel, private communication.

73. Physics of Semiconductor Devices, 2nd Ed., S.M.Sze, John Wiley&Sons, New York1981 John Wiley&Sons., pp.402-407

74. M.K.Sinha, Yee-Gee Ku, and Randall P. Johnson, J.Appl.Phys. 52 (2), pp.699-705 (1981)

75. Jedynak and Towliati, J. Vac. Sci. Technol., 11 (1), p.472 (1974)

76. Ibid 70.

77. W. Schottky, Z. tech. Physik 14, 63 (1923)

78. D.R. Lide ed., CRC Handbook of Chemistry and Physics 76th ed., CRC Press, New York, p.12-122 (1995)

79. Kittel, Charles, Introduction to Solid State Physics 7th ed., John Wiley & Sons, Inc., New York, p.143-151, 1996

80. Fowler, R.H., and Nordheim, L., Roy. Soc. Proc. 119, 173 (1928)

81. Ibid. 79.

82. R.H.Good Jr. And Erwin W. Müller, "Field Emission", Encyclopedia of Physics, vol. 21, pp.176-231, (1956)

83. L.W.Nordheim, *Proc. Roy. Soc. Lond.*, Ser. A **121**, p.626 (1928)

84. R.E.Burgess, H.Kroemer and J.M. Houston, *Phys. Rev.* **90**, p.515 (1953)

85. S.M. Selby ed., CRC Standard Mathematical Tables 19th ed., CRC Press, Cleveland, pp.535-37 (1971)

86. P.J. Davis and P. Rabinowitz, Methods of Numerical Integration, Academic Press, New York, p.48 (1975)

87. Ibid. 82. p.187

APPENDIX A

THE FOWLER-NORDHEIM EQUATION

The equations used today to describe field emission are virtually identical to those used by Fowler and Nordheim in 1928. The only essential differences are the use of the WKB approximation described here and the inclusion of a field enhancement factor described in the introduction. In this short derivation of the Fowler-Nordheim equation we describe basic electron emission processes, the shape of the potential barrier including the image force, the WKB approximation, and finally the calculation of the Fowler-Nordheim equation.

Electron Emission

With an applied electric field the vacuum level is bent down from the cathode as shown in Fig. 68a. Measuring energy from the bottom of the potential well and distance from the cathode surface, the vacuum level is described in simplest terms by

$$V(x) = E_{VAC} = E_F + \Phi - \mathcal{E}ex \tag{18}$$

The forms of emission can now be discussed. Once an electron leaves the cathode it is accelerated towards the anode by the field and contributes to current, but it must first overcome the potential barrier. There are two basic ways this is accomplished:

1) <u>Emission over the barrier.</u> Electrons gain enough energy through heating (thermionic emission), photon absorption (photoemission), or particle

interactions (e.g., secondary emission) to be lifted to an energy level higher than the barrier.

2) Emission through the barrier. This is the basis of *field emission*. When large fields are applied the barrier width shrinks allowing electrons to tunnel through the barrier.
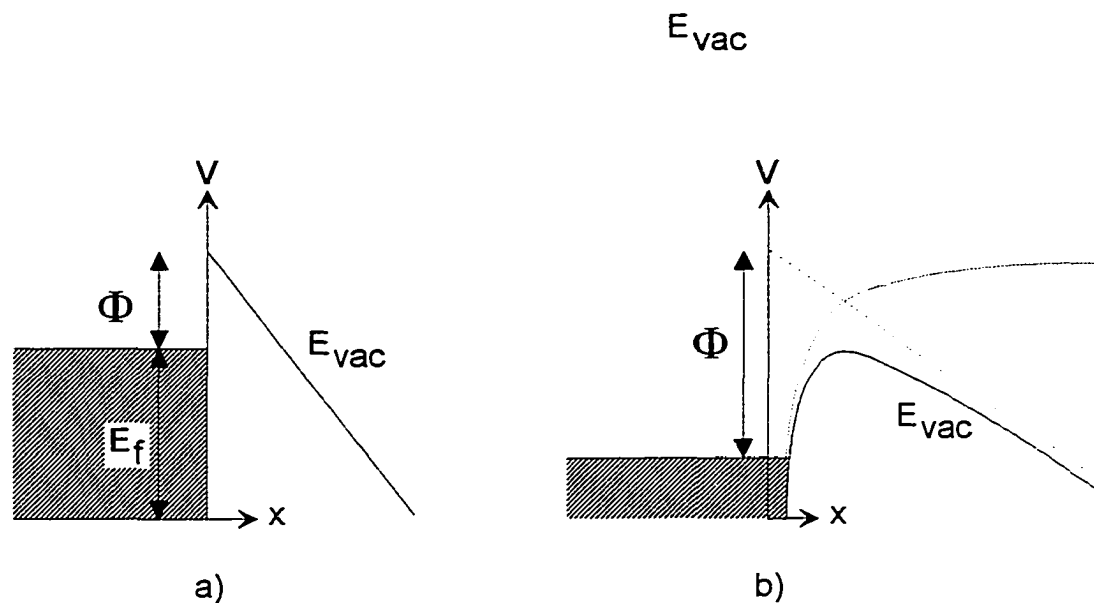

Figure 68. (a) Bending of vacuum level at cathode with applied field. (b) Effect of image charge on vacuum level.

The exact shape of potential barrier is important to both forms of emission. A closer look reveals that the "image force" modifies the shape near the surface. It is well known from electromagnetics that a charged particle is attracted to a conductor by the image force, so termed because the force can be calculated as that between the particle and an "image" particle with opposite

charge located an equal distance inside the conductor. Adding the image force, the barrier becomes

$$V(x) = E_F + \Phi - \bold{E}ex - \frac{e^2}{16\pi\varepsilon_0 x}$$

(19)

At high fields the image force as shown in Fig. 68b reduces the effective barrier height and width. The image force has a strong influence on emission over the barrier. This is known as the Schottky[77] effect. The image force has less of an effect on emission through the barrier, but should be included in precise calculations.

Work Function

With the source of tunneling electrons defined, the potential barrier and tunneling probability as a function of electron energy need to be investigated. As shown in Fig. 68a,b the shape of the potential barrier in relation to the E_F is primarily determined by the applied electric field and the work function, Φ. At 0°K the work function is the minimum energy required to liberate an electron from the metal into vacuum.

For metals, Φ is measured to have values between 2 and 5eV. However, Φ is found to vary with surface conditions. Therefore, Φ is said to be composed of two components; an intrinsic component unique to the particular metal, and an extrinsic component which depends on surface conditions including the crystal structure, smoothness, and adsorbed gas layers. Apparently, no one has yet been able to accurately calculate from basic principles the intrinsic portion of the work function for all materials, however, there are models to explain the extrinsic

portion. Fortunately, it is straightforward to measure Φ using either the photoelectric effect or thermionic emission. . Measured values of Φ for some common metals are listed in Table 13 for polycrystalline specimens.

Table 12. Measured values of the work function, Φ, and calculated values of the Fermi energy of some common metals.

Element	Work Function (eV)[78]	Fermi Energy (eV)[79]
Ag	4.26	5.48
Al	4.28	11.63
Au	5.1	5.51
Cs	2.14	1.58
Cu	4.65	7.00
Li	2.9	4.72
Pb	4.25	9.37
Sn	4.42	10.03

To explain how Φ should vary with surface crystal structure or smoothness it is necessary to consider that the electron wavefunctions of a metal atom on the surface extend as small but finite distance into the vacuum. Considering, for a moment, the surface to be perfectly smooth there is then a net negative charge above the metal surface and a net positive charge below as illustrated in Fig. 69a. This results in an electric field that acts to impede electrons from leaving the surface. So, for a perfectly smooth surface the net effect is a deepening of the potential well and hence an increase in Φ. A rough surface, on the other hand, gives the opposite result. As shown in Fig. 69b the electron wavefunctions tend to be smooth in spite of roughness in the surface leaving a net positive charge above the metal. This model shows why the

closely packed surface of a metal gives a higher Φ than that of a loosely packed or roughened surface.

Adsorbed gas layers also play an important role in determining Φ. Metal atoms at the surface of the crystal have incomplete bonding known as dangling bonds. Gas molecules sometimes quickly attach to dangling bonds. There is some charge transfer resulting in a dipole whose electric field modifies the work function.
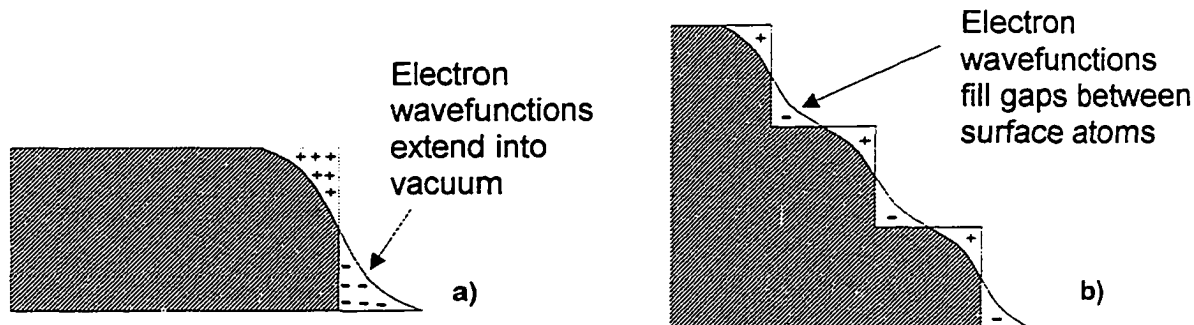
Figure 69. Charge redistribution at the surface of a metal which is (a) perfectly smooth (Φ is increased) and (b) rough (Φ is decreased).

WKB Approximation

Transmission through the triangular-like barrier, which keeps electrons inside the metal, is more complicated to calculate than a simple rectangular barrier. The first step is to calculate the wavefunctions inside and outside the metal. Of course, the wavefunction inside the metal is that of a free particle. Fowler and Nordheim were the first to calculate the field emission current.[80] In their first paper on the subject, the triangular barrier (Fig. 68a) was used

neglecting the image force. The wavefunctions outside the metal were found by solving the Schrödinger equation

$$\frac{\partial^2 \varphi}{\partial x^2} + \frac{2m}{\hbar^2}(E - E_F - \Phi + Ex)\varphi = 0$$

The solutions of which are Bessel functions of order $\frac{1}{3}$. Calculations of the transmission using this approach were the first to match experiment in form.

With the image force is included the Schrödinger equation is now

$$\frac{\partial^2 \varphi}{\partial x^2} + \frac{2m}{\hbar^2}\left(E - E_F - \Phi + Ex + \frac{e^2}{16\pi\varepsilon_0 x}\right)\varphi = 0$$

Calculating the wavefunctions outside the metal exactly becomes more difficult. Instead, an approximation known as the Wentzel-Kramer-Brillouin (WKB) method is used. Kittel[81] gives a detailed formulation of the WKB approximation. The basic foundation of the WKB approximation is to assume that the wavefunction varies slowly compared to the potential. The WKB approximation is most valid for large values of $|E - V|$ and small dV/dx. For application to transmission problems it is also approximated that the transmission coefficient, T, is given by

$$T \cong \left[\frac{\varphi(x_2)}{\varphi(x_1)}\right]^2 \tag{20}$$

where x_1 and x_2 are the beginning and end points of the barrier. In a simple rectangular barrier with constant potential the wavefunctions inside the barrier decay with rate, $\kappa = \sqrt{2m(V - E)/\hbar^2}$ times distance. In a small distance, dx, then it is approximated that

$$\frac{\varphi(x+dx)}{\varphi(x)} = e^{-\kappa x}$$

Integrating over the barrier gives

$$\frac{\varphi(x_2)}{\varphi(x_1)} = \exp\left(-\int_{x_1}^{x_2} \kappa\, dx\right)$$

Finally, from (3) we have the WKB approximation for transmission

$$T = \exp\left(-2\int_{x_1}^{x_2} \kappa\, dx\right) \tag{21}$$

This result can be compared to the exact result with a rectangular barrier and large values of κa. Transmission through a rectangular barrier is given by

$$T \cong \frac{16E}{V} e^{-4\kappa a}$$

whereas the WKB transmission is

$$T = e^{-4\kappa a}$$

which is seen to be a good approximation (considering the amount of work which it avoids).

Derivation of the Fowler-Nordheim Equation

The tunneling current density is the electron charge times the electron flow which is found by integrating the number of electrons having a particular energy times the probabili$_{J = e\int N(W)T(W)dW}$s given by

$$J = e\int_{0}^{\infty} N(W)T(W)dW \tag{22}$$

where N(W) is the density of electrons in terms of W and T(W) is the probability of transmission through the barrier. N(W) was calculated using the Sommerfeld model with no further approximation. T(W) is more difficult to obtain and various

degrees of approximation are used to obtain a closed form solution. This derivation of the Fowler-Nordheim equation follows closely that of Good and Müller.[82] Note that in earlier text the symbol, F, is often used for electric field and also that energy is sometimes measured from the vacuum level of the metal instead of from the bottom of the potential well as it is here. Also, earlier text use electrostatic units where the MKS system is used here. From the WKB approximation [eqn. (21)] we write

$$T(W) = \exp\left(-2\int_{x_1}^{x_2}\sqrt{\frac{2m}{\hbar^2}[V(x)-W]}\,dx\right)$$

Substituting V(x) with the potential in eqn. (19) which includes the image force as shown in Fig. 70 we have

$$-\ln(T) = -2\int_{x_1}^{x_2}\sqrt{\frac{8m}{\hbar^2}\left[E_F+\Phi-W-eEx-\frac{e^2}{16\pi\varepsilon_0 x}\right]}\,dx \tag{23}$$

where now x_1 and x_2 are the zeros of the radicand marking the positions where tunneling begins and ends. Evaluating the roots of [V(x)-W] one finds

$$x_1,x_2 = \frac{E_F+\Phi-W}{2eE}\left(1\mp\sqrt{1-\frac{e^3E}{4\pi\varepsilon_0(E_F+\Phi-W)^2}}\right)$$

The integral in eqn. (23) was first calculated by Nordheim[83] and later improved by Burgess, Kroemer, and Houston.[84] Evaluation of the integral begins by making a change in variables

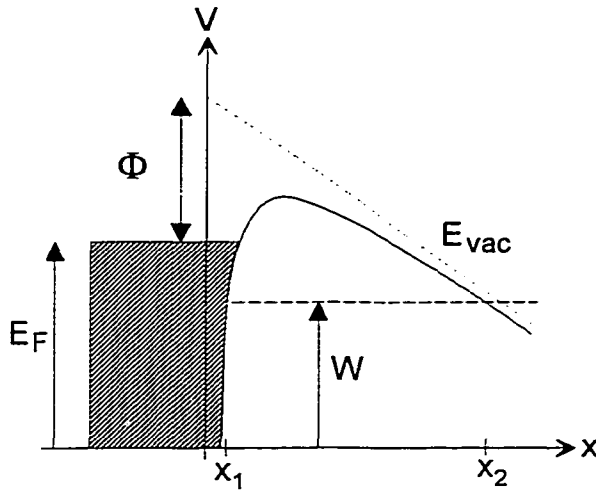$$y = \frac{\sqrt{e^3E/4\pi\varepsilon_0}}{E_F+\Phi-W} \tag{24}$$

Figure 70. Potential barrier at cathode surface under high field including the image force. Electrons tunnel through the barrier from points x_1 to x_2.

and the integration variable,

$$\xi = \frac{2eE}{E_F + \Phi - W} x$$

so that

$$-\ln(T) = \frac{\sqrt{m(E_F + \Phi - W)^3}}{\hbar eE} \int_{1-\sqrt{1-y^2}}^{1+\sqrt{1-y^2}} \sqrt{-\xi^2 + 2\xi - y^2} \, \frac{d\xi}{\sqrt{\xi}}$$

(Note: The numerator of y in eqn. (24) equals the barrier lowering due the image force while the denominator is the barrier height without image affects so that y is actually the ratio of the image lowering to the non-lowered barrier height.) With another substitution, $\eta = \sqrt{\xi}$, the integral becomes a standard elliptical integral

$$-\ln(T) = \frac{2\sqrt{m(E_F + \Phi - W)^3}}{\hbar eE} \int_b^a \sqrt{(a^2 - \eta^2)(\eta^2 - b^2)} \, d\eta$$

where

$$a = \sqrt{1 + \sqrt{1 - y^2}} \qquad b = \sqrt{1 - \sqrt{1 - y^2}}$$

From elliptical integration tables it is found that

$$-\ln(T) = \frac{4a\sqrt{m(E_F + \Phi - W)^3}}{3\hbar eE}\left[\frac{(a^2 + b^2)}{2}E(k) - b^2 K(k)\right]$$

where

$$k^2 = \frac{a^2 + b^2}{a^2}$$

and K and E are the complete elliptic integrals of the first and second kinds given

by

$$K(k) = \int_0^{\pi/2} \frac{d\varphi}{\sqrt{1 - k^2 \sin^2 \varphi}}$$

$$E(k) = \int_0^{\pi/2} \sqrt{1 - k^2 \sin^2 \varphi}\ d\varphi$$

Values for K and E are tabulated[85] or they can be numerically calculated using

Simpson's rule.[86] The final form of the transmission coefficient can now be

written

$$T = e^{\frac{-4\sqrt{2m(E_F + \Phi - W)^3}}{3\hbar eE}v(y)} \tag{25}$$

where

$$v(y) = 2^{-\frac{1}{2}}\sqrt{1 + \sqrt{1 - y^2}}\left[E(k) - \left(1 - \sqrt{1 - y^2}\right)K(k)\right]$$

$$k^2 = \frac{2\sqrt{1 - y^2}}{1 + \sqrt{1 - y^2}}$$

and y was given in eqn. (24). If one were to compare the result in eqn. (25) and

the result ignoring the image force it is clear that v(y) is the correction factor for

the image force.

The equation for the field emission current can now be constructed from

equations (5), (6) and (9). We have

$$J = \frac{4\pi m e}{h^3} \int_0^\infty kT \ln\left(1 + e^{-\frac{W-E_F}{kT}}\right) e^{\frac{-4\sqrt{2m\left(E_F+\Phi-W\right)^3}}{3\hbar e E}v(y)} dW \qquad (26)$$

This integral can be greatly simplified by considering the usual case of low temperatures. At normal temperatures there are few electrons above the Fermi level and so tunneling occurs very near the Fermi energy. The first simplification is in the density term in eqn. (26). Taking the limit as T → 0 we find

$$kT \ln\left(1 + e^{-\frac{W-E_F}{kT}}\right) = 0 \qquad \text{for} \quad W > E_F$$

$$= E_F - W \quad \text{for} \quad W < E_F \qquad (27)$$

Next, with the transmission term we approximate the exponent as the first two term in a Taylor series centered on W=E_F. One finds that

$$\frac{-4\sqrt{2m\left(E_F+\Phi-W\right)^3}}{3\hbar e E} v\left(\frac{\sqrt{e^3 E/4\pi\varepsilon_0}}{E_F+\Phi-W}\right) \approx -c + \frac{W-E_F}{d} \qquad (28)$$

where

$$c = \frac{4\sqrt{2m\Phi^3}}{3\hbar e E} v\left(\frac{\sqrt{e^3 E/4\pi\varepsilon_o}}{\Phi}\right)$$

$$d = \frac{\hbar e E}{2\sqrt{2m\Phi} t\left(\frac{\sqrt{e^3 E/4\pi\varepsilon_o}}{\Phi}\right)}$$

$$t(y) = v(y) - \frac{2}{3} y \frac{dv(y)}{dy}$$

The effect of the image force are now expressed in the functions v(y) and t(y) values of which are tabulated. Some values for v(y) and t(y) from Good and

Müller[87] are given in Table 14. Both functions are slow varying and are often treated as constants. Substituting eqns. (27) and (28) back into eqn. (26) the integral becomes

$$J = \frac{4\pi m e}{h^3} \int_{-\infty}^{E_F} (E_F - W) e^{-c+\frac{W-E_F}{d}} dW = \frac{4\pi m e d^2}{h^3} e^{-c} \qquad (29)$$

The lower limit of integration can be replaced with -∞ for ease of integration since the contribution to the integral for energies far from E_F is negligible. Substituting for the values of the physical constants in (13) one obtains the final result

$$J = \frac{1.541 \cdot 10^{-2} E^2}{\Phi t^2(y')} \exp\left[\frac{-6.831 \cdot 10^9 \Phi^{3/2} v(y')}{E}\right] \qquad [A/m^2]$$

$$\qquad (30)$$

$$y' = \frac{3.795 \cdot 10^{-5} \sqrt{E}}{\Phi}$$

where E is in units of V/m and Φ is now in units of eV.

Table 13. Values of the functions v(y) and t(y).

y	v(y)	t(y)	y	v(y)	t(y)
0	1.0000	1.0000	0.55	0.6351	1.0502
0.05	0.9948	1.0011	0.60	0.5768	1.0565
0.10	0.9817	1.0036	0.65	0.5152	1.0631
0.15	0.9622	1.0070	0.70	0.4504	1.0697
0.20	0.9370	1.0111	0.75	0.3825	1.0765
0.25	0.9068	1.0157	0.80	0.3117	1.0832
0.30	0.8718	1.0207	0.85	0.2379	1.0900
0.35	0.8323	1.0262	0.90	0.1613	1.0969
0.40	0.7888	1.0319	0.95	0.0820	1.1037
0.45	0.7413	1.0378	1.00	0	1.1107
0.50	0.6900	1.0439			

APPENDIX B

DERIVATION OF THE ROGOWSKI PROFILE

A Rogowski profile electrode has a cross-section that is an equipotential surface between two parallel plates. While the potential between the plates is a straight line, it is the potential at the edge of the plates that defines the special shape. Derivation of the Rogowski profile is made fairly straightforward with the use of conformal mapping using complex math. First, we simplify the problem by considering one plate above an infinite ground plane with spacing, a, which yields identical solutions to two plates at a distance, 2a. Next, we place the 2-D structure on the complex plane, Z where z=(x+iy), and search for a transformation which yields simple solutions in the transformed plane, W where w=(u+iv). Since it is well known that in the center of the plate the equipotential lines are parallel with equal spacing (as in an ideal capacitor), we need only the solution at the edge of the plate (fringe field). Placing the edge of the plate at $(x = -a/\pi, \quad y = a)$ and the ground plane at y=0 the transform

$$ Z = \frac{a}{\pi}\left(W - Log(W)\right) \tag{31} $$

maps the ground plane onto the positive u-axis and the upper plate onto the negative u-axis. Therefore, the entire half-plane, y>0, is mapped onto the half plane, v>0, as illustrated in Fig. 71.
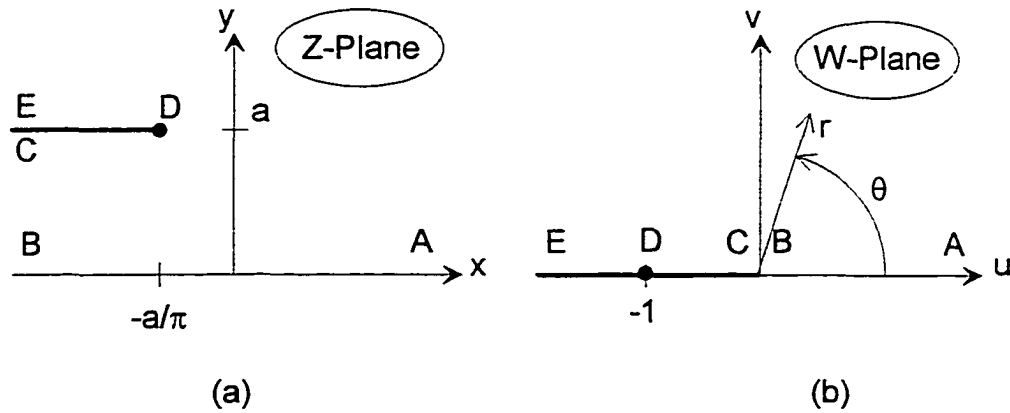
Figure 71. Conformal mapping of a plate (EDC) above a ground plane (x-axis) in the Z-plane (a) to the W-Plane where the plate is the negative u-axis and the ground plane is the positive u-axis (b).

Solutions for the potential in the W-plane are trivial. The potential on the positive u-axis is $V=0$ and the potential on the negative u-axis is $V=V_0$. Therefore, equipotential surfaces in the W-plane are straight lines emanating from the origin which can be expressed as

$$u = r\cos(\theta)$$
$$v = r\sin(\theta)$$

$$(32)$$

where θ is the angle made with the u-axis and r is the radial distance from the origin. Note that since lines made with a constant θ are equipotential, lines of force will be perpendicular. As a result, lines of force extending from the top plate to the ground plane are semicircles with radius, r, in the W-plane. Transforming eqn. (32) back into the Z-plane using (3) one finds

$$x = \frac{a}{\pi}\left[r\cos(\theta) + \ln(r)\right]$$
$$y = \frac{a}{\pi}\left[r\sin(\theta) + \theta\right]$$

$$(33)$$

Finally, the equipotential lines in the Z-plane are formed by fixing θ in eqn. (33)

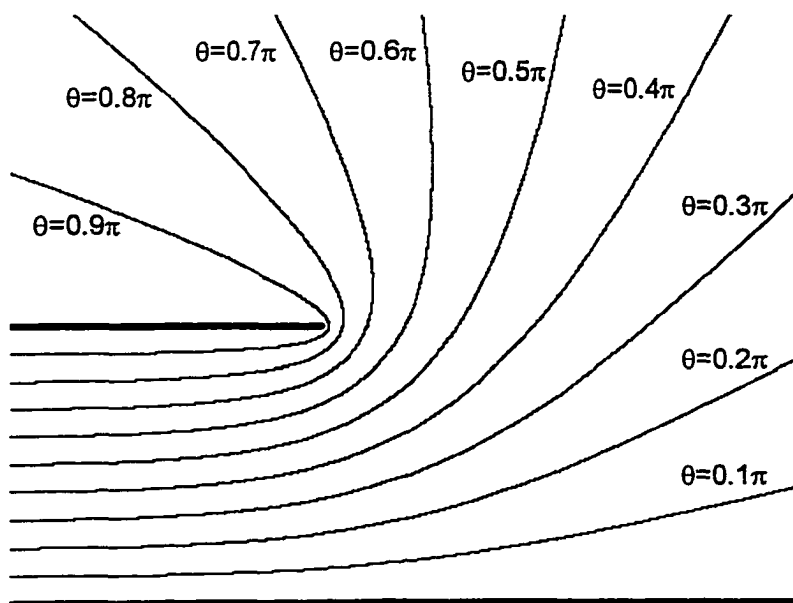and varying r. Equipotential lines for θ=0.1π to 0.9π are shown in Fig. 72.

θ=0.7π θ=0.6π θ=0.5π θ=0.4π

θ=0.8π

θ=0.9π

θ=0.3π

θ=0.2π

θ=0.1π

Figure 72. Equipotential lines at the edge of a plate above a ground plane.

From Fig. 72 we see that for θ>0.5π there is a narrowing of the line spacing near

the edge of the plate. Since the electric field is proportional to the distance

between the equipotential lines there is field enhancement near the plate's edge.

However, for θ≤0.5π the distance between equipotential lines increases

monotonously. Therefore, the electric field is nowhere greater than in the center

of the plate. For a Rogowski profile electrode we simply construct electrodes

with edges like that in Fig. 72 with a shape given by eqn. 33 with θ≤0.5π.

VITA

Raymond Jack Allen III was born in Oakland, California on October 20, 1966. After high school he enlisted in the United States Navy for three years. During this time he was stationed aboard the battleship USS Iowa. Following an honorable discharge from the United States Navy, Raymond Jack Allen III attended college at Old Dominion University, Norfolk, Virginia. He received his BSEE in 1992 and his MSEE in 1994, both from Old Dominion University.
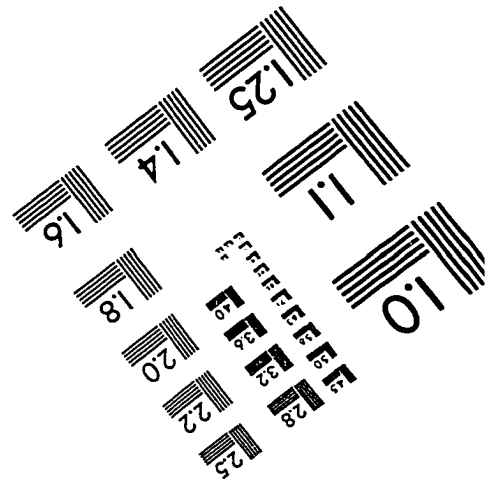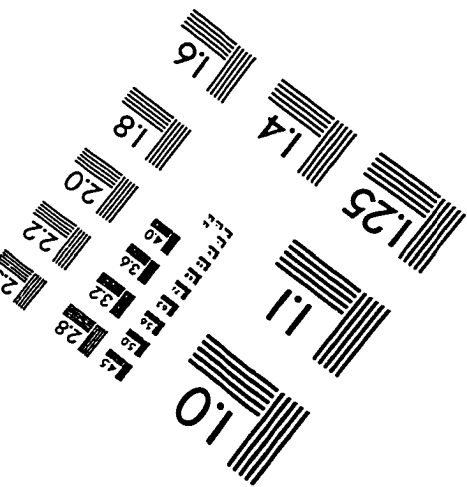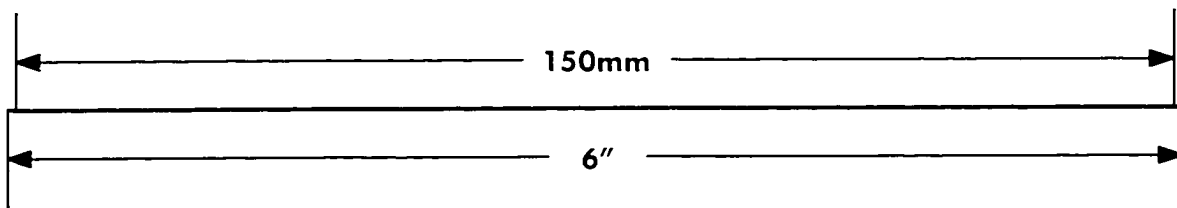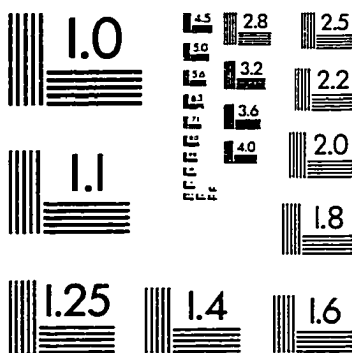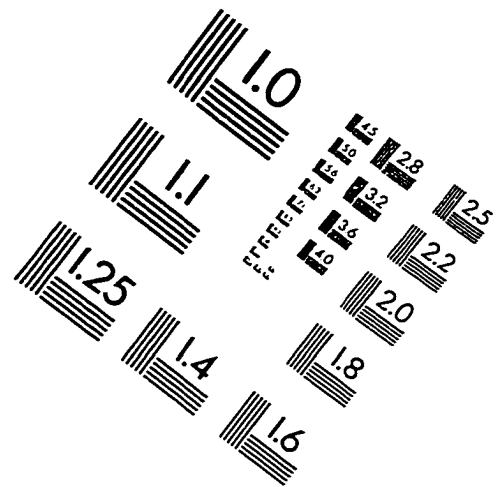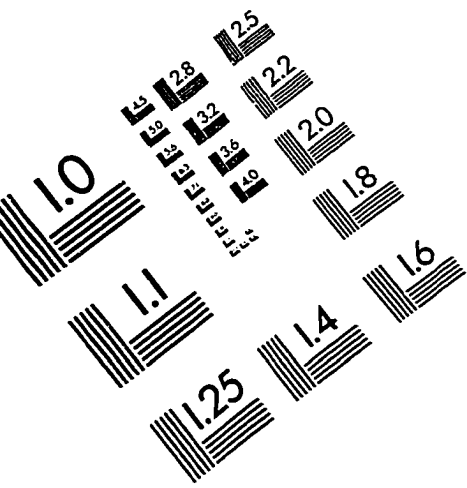
Affiliations:
      IEEE (Institute of Electrical and Electronic Engineers)
      Tau Beta Pi (Engineering Honor Society)

Department Address:
      Old Dominion University
      Department of Electrical and Computer Engineering
      Norfolk, Virginia 23529

IMAGE EVALUATION
TEST TARGET (QA-3)

1.0
1.1
1.25
1.4
1.6
1.8
2.0
2.2
2.5
2.8
3.2
3.6
4.0
4.5

150mm

6"